Interfacing a Transient Stability Model to a Real-Time Electromagnetic Transient Simulation Using Dynamic Phasors

By:
Konara Mudiyanselage Harshani
Koushalya Konara

A thesis submitted to the Faculty of Graduate Studies in partial fulfilment of the requirements for the degree of Doctor of Philosophy

Department of Electrical and Computer Engineering
University of Manitoba
Winnipeg

Abstract

This thesis presents a method to perform real-time Electromagnetic Transient (EMT) simulations for a large power system. The real-time EMT simulation can become prohibitively expensive for large power systems. A solution to this is to divide the system into an internal system where all details are important and an external system (the rest of the system) where only the electromechanical behaviour is important. This thesis presents a co-simulation model consisting of an EMT model and a Transient Stability (TS) model. The internal system is modelled using the EMT model and the external system is modelled using the TS model. The interface between the two models is a portion of the network ("buffer zone") modelled using Dynamic Phasors (DP), which is less detailed than the EMT simulation approach, but more detailed than the TS model. The intermediate buffer zone modelled in DP enables smooth integration of EMT model and the TS model. The challenges of interfacing a DP model to an EMT model and a DP model to a TS model are discussed. A data prediction method is used to overcome the time-step delay between the EMT model and the DP model. The TS model uses a relatively larger integration time-step than the DP model and the DP-TS boundary voltages are updated at every DP time-step in the buffer. A novel voltage source type synchronous machine model is proposed in this thesis to interface to a DP model.

The EMT-TS co-simulation model is implemented in a real-time platform and it is validated using a complete EMT simulation. The New England & New York 68 bus system is used as the test system to validate the co-simulation model. The results of the co-simulation model show a good agreement with the EMT simulation results under the disturbance applied in the internal system.

Use of Copyrighted Material

I would like to acknowledge the use of the following publications in the preparation of this thesis. I'm the main author of these publications.

©2018 IEEE. Reprinted, with permission, from H. Konara, U. D. Annakkage and C. Karawita, "Stability Criterion for Interfacing a Transient Stability Model to a Dynamic Phasor Model", IEEE/PES Transmission and Distribution Conference and Exposition (T&D), Denver, April/2018.

In reference to IEEE copyrighted material which is used with permission in this thesis, the IEEE does not endorse any of University of Manitoba's products or services. Internal or personal use of this material is permitted. If interested in reprinting/republishing IEEE copyrighted material for advertising or promotional purposes or for creating new collective works for resale or redistribution, please go to http://www.ieee.org/publications˙standards/publications/rights/rights˙link.html to learn how to obtain a License from RightsLink.

©2018 IPST. Reprinted, with permission, from IPST, "Novel Voltage Source Type Synchronous Machine Model for Nodal Analysis Based Simulations", The International Conference on Power Systems Transients (IPST), Perpignan, June/2019.

Acknowledgements

Firstly, I would like to express my sincere gratitude to my advisor Prof. U. D. Annakkage for the continuous support for my PhD degree. It has been an honour and a privilege to work under him. I could not have imagined having a better advisor and mentor for my graduate studies.

I'm very much thankful to my co-advisor Dr. Chandana Karawita for his support. I would also like to thank the internal committee members Prof. Shaahin Filizadeh and Prof. R. Jayaraman for giving feedback to the PhD work. I thank the external examiner Prof. R. Iravani for reading my thesis and providing me with valuable suggestions regarding the thesis.

I would like to thank the University of Manitoba and Natural Sciences and Engineering Research Council (NSERC) Canada for funding this research. I like to thank RTDS Technologies for showing their interest in the research project and providing hardware and software support.

I like to thank Prof. Aniruddha Gole, Prof. Athula Rajapakse and Prof. Carl Ho for the invaluable knowledge they shared during the course work. I thank my research group mates for the interesting discussions and for the support. I thank my graduate advisor Amy Dario for her support.

I would like to thank all my friends in Winnipeg for their support during these years. A special thank goes to Annakkage family for their caring and concern.

A special thank goes to my husband Sampath Liyanage, for his support and patience during my graduate studies. I thank my sister Anupama Konara and my brother-in-law Ruslan, for encouraging me to pursue a graduate degree and their support during these years. I would like to extend my deepest gratitude to my parents. Without their encouragement, I would not have a chance to achieve this much. I would also like to thank my brother for constantly reminding me what I should accomplish.

Contents

List of Tables

List of Figures

Abbreviations

EMT	**E**lectro **M**agnetic **T**ransient
TS	**T**ransient **S**tability
DP	**D**ynamic **P**hasor
RTDS	**R**eal **T**ime **D**igital **S**imulator
IEEE	**I**nstitution of **E**lectrical and **E**lectronic **E**ngineers
FDNE	**F**requency **D**ependant **N**etwork **E**quivalent
TLNE	**T**wo **L**ayer **N**etwork **E**quivalent
VBR	**V**oltage **B**ehind **R**eactance
VS	**V**oltage **S**ource
SMIB	**S**ingle **M**achine **I**nfinite **B**us
RI	**R**eal **I**maginary
FFT	**F**ast **F**ourier **T**ransform
NYPS	**N**ew **Y**ork **P**ower **S**ystem
NETS	**N**ew **E**ngland **T**est **S**ystem
HVDC	**H**igh **V**oltage **D**irect **C**urrent
LCC	**L**ine **C**ommutated **C**onverter
PSS	**P**ower **S**ystem **S**tabilizer
THD	**T**otal **H**armonic **D**istortion
PI	**P**roportional **I**ntegral

Symbols

t	Time
Δt	Time-step
V, I	Phasor voltage and current
v, i	Instantaneous voltage and current
R, I	Real and imaginary components
d, q	Direct and quadrature components
X	Reactance
T	Time constant
RL	Resistor and inductor
RC	Resistor and capacitor
P, Q	Active and reactive power
f_0	Fundamental frequency
ω_c	Angular speed corresponding to carrier frequency
ω_0	Angular speed corresponding to Fundamental frequency
A	System matrix of a state space model
B	Input matrix of a state space model
H, K_D	Inertia constant and damping coefficient of synchronous machine
h_t	Time-step of transient stability model
h_s	Time-step of electromagnetic transient and dynamic phasor model
K_p, T_I	Proportional and integral gains of a PI-controller

Chapter 1

Introduction

1.1 Background

The time span of typical power system dynamics can vary from microseconds to days as shown in Fig. 1.1 [1]. Power systems transients are mainly divided into two categories: electromagnetic transients, and electromechanical transients. Electromechanical transients result from the interaction between mechanical energy stored in the rotating machines and the stored energy in the network. The right side of Fig. 1.1 shows some examples for electromechanical transients. They have a large time span and relatively low frequencies in their oscillations. Electromagnetic transients result from the interactions between the magnetic field caused by inductors and the electric field of the capacitors. The frequencies of electromagnetic transients are relatively high compared to electromechanical oscillations. The left-hand side of Fig. 1.1 shows some typical electromagnetic transients. As it can be seen from the Fig. 1.1 the frequency spectrum of dynamics in a power system varies in a large range. It is challenging to model the entire frequency spectrum of the system without burdening the user with the cost of a fast processor. Hence,

different case-specific assumptions are made in different simulation programs to simplify the problem. Mainly, there are three types of simulation programs cov-

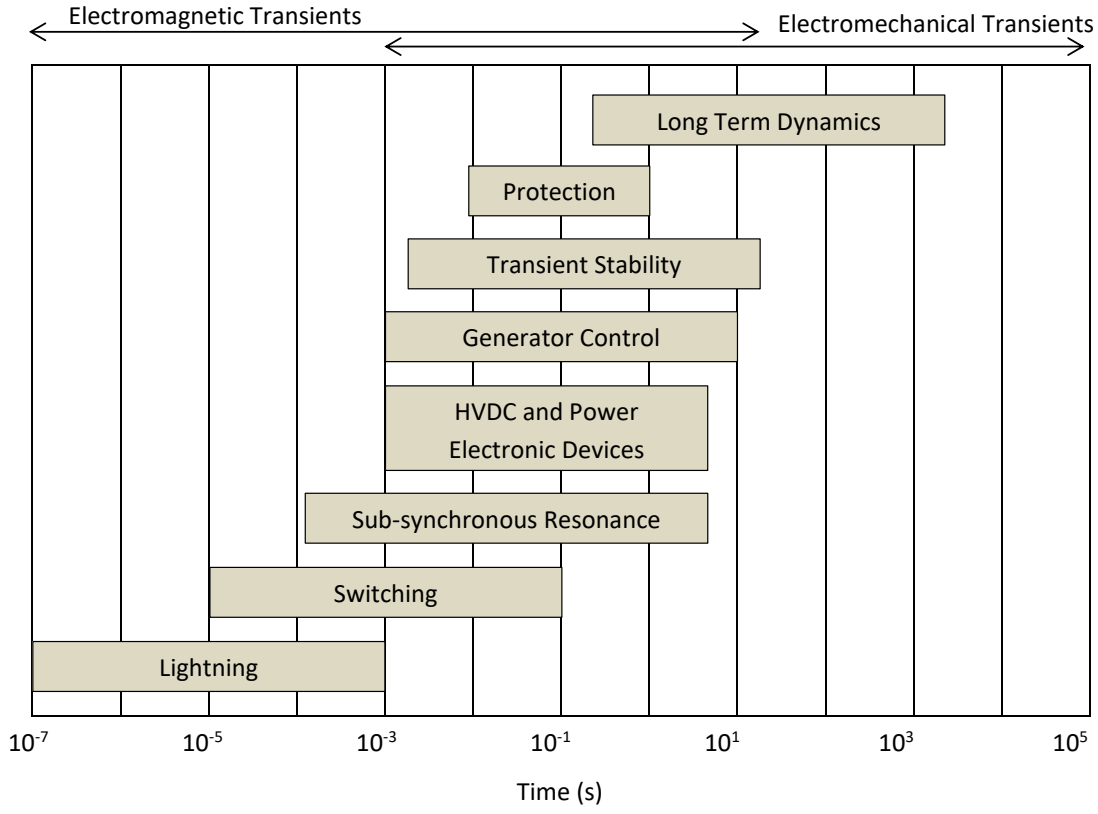

FIGURE 1.1: Time span of typical power system transients

ering different ranges of frequencies [2]: (a) steady-state response analysis, (b) quasi-steady state analysis, and (c) electromagnetic transient analysis.

In the steady-state response analysis, the steady-state algebraic equations are used to analyse the power flow of power systems. It involves representing the sinusoidal currents and voltages by a phasor, i.e. a constant magnitude and a phase angle. Hence, the power system variables are expressed as complex numbers. Time-varying sinusoidal signals are constants at steady-state when the rotational term is removed from the signals. This can be considered as demodulation of the signal from the carrier signal of 60 Hz [3]. As an example, a sinusoidal signal

$V = V_m sin(\omega_0 t - \theta)$ transforms to the phasor $V_m \angle \theta$ in steady-state, where V_m is the voltage magnitude, θ is the angle, ω_0 is the angular speed and t is the time.

The same phasors used in steady-state response analysis are used to model the system in the quasi-steady-state analysis. However, the electromechanical oscillations in the system are modelled using differential equations. The stationary assumption is extended for a quasi-stationary condition where it allows the system voltages and currents to vary slowly. The voltages and currents are updated by solving the algebraic equations in discrete steps. This type of power system modelling is used in Transient Stability (TS) simulations. The frequency bandwidth of a transient stability study falls into a range of 0 Hz to about 5 Hz. Therefore, the time-step of the quasi-steady-state approach can be relatively large and it can vary in the range of 1 ms to 10 ms depending on the problem. Due to the relatively large time step used, transient stability models are fast enough to model large power systems containing hundreds of generators [4], [5]. In the quasi-stationary assumption, the electromagnetic transients in the network and the machines are not captured. It only considers power transfer at the system frequency [6]. Since the electrical variables of the system such as currents and voltages are considered as slowly varying phasors it can only model the system by removing network transients. However, during a transient, the power system will undergo the entire spectrum of frequencies. As an example, the disturbance may start as a fast electromagnetic transient and it can decay leaving only a slow transient that takes longer to decay. When the initial high-frequency transients are of interest, a program that is capable of capturing the entire frequency span is required.

The Electromagnetic Transient (EMT) studies can accurately model the power system and depict the dynamics over a wide band of frequencies. It works with instantaneous time-domain values and it follows the trajectories of the states

of the system. EMT simulation programs need a very small time-step (e.g. 50 μs) to capture system level transients of the power system. Even smaller time-steps such as 2 μs, are required if power electronic converters are involved. Therefore, electromagnetic simulation programs are slow to study phenomena around the base frequency and they are computationally demanding [6]. Typically, EMT studies are not used in studying electromechanical oscillations for many reasons such as: (a) simulation time required for TS studies can be relatively large (e.g. 10s or even larger depending on the transient) and an EMT simulation needs a correspondingly large amount of computational power to simulate an electromechanical transient event with a small time-step like 50 μs, (b) transient stability studies are typically done for large power systems and EMT program are computationally demanding for this purpose.

A comparison of the typical applications of EMT and TS studies are summarized in Table 1.1.

TABLE 1.1: Typical applications of EMT and TS simulations

Type of study	**TS**	**EMT**
System planning, station design, power flow analysis, short circuit analysis, protection system setting design	✓	
Transient stability analysis for system planning, calculating stability limits	✓	
Long term voltage stability	✓	
Fast transient studies: Lightning, Temporary Over Voltages (TOV) studies, breaker Transient Recovery Voltage (TRV) studies		✓
Sub synchronous resonance studies		✓
Harmonic resonance		✓
System planning studies for HVDC, wind integration		✓
Protection and control system design for HVDC, FACTS etc.		✓
Hardware-In-Loop (HIL) and Controller HIL testing		✓

Dynamic Phasors (DP) were introduced in the mid $90's$ as an attempt to overcome the limitations imposed by the quasi-stationary assumption made in transient stability studies [7], [3]. Dynamic phasors are suitable for analysing electromechanical oscillations and most of the typical electromagnetic oscillations. Reference [6] has extended the applicability of dynamic phasors for different cases by making it suitable for unbalanced systems as well. Similar to phasor models, in dynamic phasors, currents and voltages are multiplied by $e^{-j\omega_0 t}$ to remove their time-varying sinusoidal characteristics at the base frequency [6]. Hence, in dynamic phasors, the magnitude and angle are represented by a constant in steady-state. However, during a transient, it is allowed to change over time according to

differential equations [3].

The main difference between dynamic phasor models and transient stability models is the way they model the network. The dynamic phasors represent the currents and voltages in the system as state variables [3] whereas in TS models, they are treated as algebraic equations. Hence, the bandwidth of the dynamic phasor-type simulations is higher compared to a TS model. Table 1.2 summarizes the differences between the two simulation models.

TABLE 1.2: Comparison of TS and DP models

	Transient Stability model	**Dynamic Phasor model**
Network model	Constant admittance	Uses differential equations to model inductor currents and capacitor voltages
Dynamics	Electromechanical only. Electrical states are ignored	Electromechanical & electromagnetic
Frequency bandwidth	Less than 5 Hz	Up to kHz range
Computational burden	Low	Higher than TS

Recently, dynamic phasors have been used in parallel with electromechanical simulations to accommodate high frequency switching components [8], [9]. Reference [8] shows that dynamic phasors significantly improve the accuracy of electromechanical simulations when there are power electronic devices in the system. Another advantage of dynamic phasors is its ability to change the level of complexity of the model. The level of complexity can be altered by selecting the number of harmonics [10] and also by adding sequence components in an unbalanced situation [11], [12]. The dynamic phasor model implemented in [8], which

is demonstrated for fundamental frequency, is extended to include higher-order harmonics in [10], [13], [14] and [15].

The demand for real-time EMT simulation of the power system has increased over time. There are many advantages of real-time simulations. One of these advantages is that it enables the closed-loop testing of physical devices, such as converter controllers and protection devices, in real-time. In real-time simulations, the solution of the EMT model is updated at every time-step in real-time. The simulation time-step of $50\mu s$ is equal to $50\mu s$ in a real world clock. When the size of the power system becomes larger, it is hard to solve the network solution using a single processor. Therefore, the power system is usually divided into subsystems and multiple network solutions are simulated in different processors. The subsystems are divided in places where there is a long transmission line. The natural delay in a travelling wave of the transmission line is used to account for the data transfer delay between subsystems. Splitting the network to subsystems using transmission lines is possible when the travelling time of the transmission line is equal to or greater than the simulation time-step. Due to this delay across the transmission line, each subsystem is decoupled from each other at any given time-step. Using this property, the subsystems of the power system can be simulated in parallel. When it is required to simulate a large power system, many powerful processors will be required. Therefore, if the entire power system is simulated using real time simulators, the cost of hardware can be prohibitive to many utilities, manufacturers, universities and consultants. Real Time Digital Simulator (RTDS) is one of the commercially available real-time simulators. The largest power system in the world that runs in real-time using the RTDS is reported in China, which uses 34 parallel computers (RTDS racks)[16]. This was reported in the year 2014.

There are different equivalencing methods available to reduce the computational burden of EMT simulations. One equivalencing approach is to model the power system in two parts: (1) study area simulated in detail, and (2) the rest of the simulation represented by an equivalent impedance. The simplest method to model the equivalent network is to use a Thevenin voltage source behind an impedance. The impedance is calculated by matching the short circuit impedance of the equivalent system. The use of such simplified models reduces the accuracy of the EMT model since it does not capture the frequency response of the system accurately. For many EMT studies, the frequency response of the equivalent system is important and a constant Thevenin impedance would not successfully reproduce transients. This problem is addressed in literature by using frequency-dependent admittance as the equivalent which is called Frequency Dependent Network Equivalent (FDNE) [17], [18]. The problem with FDNE as an equivalent is that it only matches the high-frequency response of a system. However, for many studies, it is important to model the electromechanical oscillations and controller interactions of the system to study their interactions with the EMT study zone.

There has been a significant amount of work done on interfacing electromechanical and electromagnetic simulations as a hybrid simulator [19], [20], [21], [22], [23]. A small part of the network that requires detailed modelling is simulated using a detailed EMT type model and the rest of the system is modelled using a TS model. The part modelled in EMT is called the internal system which contains the components like power electronics devices which need detailed modelling. The rest of the system is called the external system and it is modelled using a computationally inexpensive stability model like the TS model. Using this approach, fast transients in the internal system can be studied with the EMT model with the low-frequency influence on the internal system represented by the TS based external system model.

The bandwidth of frequency that an EMT model covers is much wider than the bandwidth that a TS model can cover. Hence, interfacing these two simulation models can be challenging. The problems associated with this type of connection is summarized in [19]. At the interface, the external system should represent the high-frequency behaviour of the external system [24]. This problem has been overcome by using a Frequency Dependent Network Equivalent (FDNE) at the interface. FDNE is used to represent the high frequency (e.g electromagnetic transients) dynamics of the external system whereas the TS models the electromechanical oscillations. FDNE is a fitted admittance derived from the frequency response of the system. A rational transfer function is obtained using the frequency response of the system by applying curve-fitting techniques. A lumped parameter model of the network is obtained by applying the recursive convolution method to the rational transfer function. The lumped parameter model contains many RL and RC branches to represents the frequency response of the external systems. However, FDNE could cause the following problems:

1. Deriving the FDNE is an extra-step that the user has to perform. Automating the procedure to obtain a system equivalent is difficult. The user must have a specialized knowledge on the system to design the FDNE and it could be time-consuming. [25].

2. FDNE reduces the computational efficiency. The accuracy of the co-simulation model depends on the tuning of the FDNE. Frequency band and the number of iterations are some parameters that should be considered when tuning the FDNE. The number of computational steps depends on the level of accuracy.

3. The numerical stability of the model depends on the passivity of the FDNE model [26], [27]. The methods used to derive FDNE tend to give non-passive

models (i.e. the resultant model generates energy) [28]. Passivity guaranteeing techniques introduce errors to the simulation [29] and add extra computations.

1.2 Thesis Statement

The objective of the thesis is to develop a convenient, user friendly alternative to FDNE for real-time EMT-TS co-simulation of large power systems. This thesis will approach the design problem in two steps.

1.2.1 Step 1: Electromagnetic Transient and Dynamic Phasor Co-simulation

The first part of the thesis will focus on replacing the FDNE and the transient stability part of the EMT-TS co-simulation model by a dynamic phasor model. The interface between the two models does not require the additional step of designing an FDNE since the dynamic phasors can represent high-frequency electromagnetic transients. This is achieved by modelling the network dynamics using differential equations. One objective of this thesis is to show that an accurate, numerically stable real-time simulation can be achieved by replacing the TS part using dynamic phasors. A discussion on dynamic phasor models for power system simulation is presented in this thesis. The network components are solved using nodal analysis based method.

Achieving numerical stability is one of the main challenges in a co-simulation. Since the dynamic phasor part of the simulation is modelled separately there is a time-step delay when exchanging the simulation variables between EMT

and DP. If this is not properly addressed it can make the simulation unstable. This numerical instability can happen anywhere when there are two models interfaced, i.e. interfacing a synchronous machine to the network. A stability criterion is developed to demonstrate the requirements for stability. Techniques to make a co-simulation numerically stable are also investigated. One of these techniques is applied in the proposed EMT-DP co-simulation model to ensure numerical stability caused by time-step delay.

The pursuit of modelling network components has led to an investigation of a proper synchronous machine model suitable for dynamic phasor simulation. The existing synchronous machine models used in EMT simulations either does not satisfy the derived stability criterion or they are not efficient for nodal analysis based simulations. Guaranteeing numerical stability in existing synchronous machine models requires extra computations which can make a real-time simulation challenging. A numerically robust and efficient voltage source type synchronous machine model was developed in this thesis.

1.2.2 Step 2: Electromagnetic Transient and Transient Stability Co-simulation

In order to analyse a large power system, a large time-step must be used in solving dynamic phasor model of the external system to reduce the computational burden. However, there are many factors affecting the limit of the dynamic phasor simulation time-step in a real-time co-simulation (e.g. time-step delay is correspondingly long when the time-step is large). Also, the transient stability models are more convenient to use with larger time-steps due to the simplified models used. Therefore, the second objective of this thesis is to replace the FDNE of an EMT-TS co-simulation by a DP model. A multi-port buffer zone containing the

boundary buses between EMT and TS is modelled using DP (Fig. 1.2). The idea of using a buffer zone is first reported in [30] and [31] as a method to compute an efficient equivalent for EMT simulation of large scale power systems. This approach of obtaining an equivalent with the buffer zone is called the Two Layer Network Equivalent (TLNE). It is introduced to address the bottleneck of simulating large power systems in real-time by computing an efficient equivalent for the external system. The external system was further divided into two regions named surface layer and a deep region (Fig. 1.2). The deep region was modelled as a low-frequency model whereas the surface layer (in this case the "buffer zone") was modelled to capture high-frequency dynamics. In the research presented in this thesis, the buffer zone connecting the internal and external system is modelled using DP. The high-frequency signals in the EMT system will travel only a short electrical distance due to high attenuation. Therefore, the interactions of the high-frequency signals with the external system can be accurately modelled by modelling the buffer zone using DP. At the low frequencies, both the buffer zone and the deep region will contribute to the dynamic response.

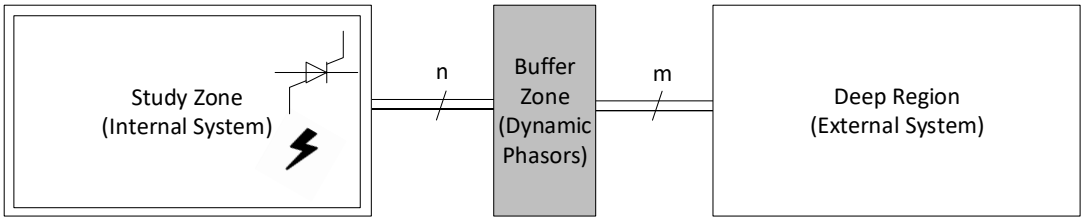

FIGURE 1.2: Using a buffer zone for the interface between EMT and TS

The goals and the characteristics of the proposed EMT-TS co-simulation can be summarized as below:

(a) The purpose of the proposed method is to study the dynamics in a portion of a large power system. The interested portion of the network is referred to as the

internal system of the large power system. The internal system is simulated using EMT. Any low-frequency interactions between the internal and external systems is necessary for planning and design studies. Therefore, in this thesis, the external system is modelled using a Thevenin type TS model that is capable of capturing those frequencies. The common industry practice of using a system equivalent can be replaced with the proposed method to produce reliable information on controller interactions and electromechanical oscillations.

(b) The available co-simulation models use FDNEs at their boundary between EMT and TS. As discussed before, FDNE has to be tuned in order to get accurate results. Tuning an FDNE for a multi-port boundary is a time-consuming task that the user has to perform. Therefore, this thesis uses a DP modelled buffer zone to avoid the use of FDNEs. The goal is to propose a method that is convenient for the user. The proposed method is validated against a complete EMT simulation.

(c) This thesis considers simulating a multi-port buffer-zone using DP. The size of the buffer zone and the number of interface nodes are not limited by the DP model.

(d) Another goal is to perform real-time simulations.

The transmission lines in the surface layer of the external system are modelled using DP. By modelling the transmission lines in the boundary of the external system using dynamic phasors, the accuracy of the simulation can be significantly improved in an EMT-TS co-simulation [31]. Another advantage of using DP is that interfacing EMT to DP is easier than interfacing EMT to TS since the frequency bandwidth that DP covers is wider than TS bandwidth. The challenge in the simulation only comes due to the time-step delay. EMT-DP-TS co-simulation model is presented in [32] for a small network containing only transmission lines. In [32], it was shown that the accuracy of the co-simulation

can be improved by modelling the transmission line connecting the internal and the external system using DP. However, to be convenient and also to be more accurate it is appropriate to allow a multi-port buffer-zone between the internal and external systems. According to the TLNE concept, a larger buffer-zone will also improve the accuracy compared to a single line buffer-zone. In many large power systems, it is convenient to select a multi-port buffer zone that connects the EMT model to the external model than to find a single transmission line. As an example, in New England & New York 68 bus system [33] if one models the New England Power System (NEPS) using EMT and New York Power System (NYPS) as the external system, there are more than one transmission line connecting the two models.

As mentioned in the previous section, the challenge in co-simulation comes from the numerical instability of interfacing different simulation models. The proposed EMT-TS co-simulation model has two interfaces: i) Interfacing DP to EMT model, ii) Interfacing DP to TS model. The former interface would be more challenging since simulation variables in both sides change rapidly within a small time-step. The challenge of using two different time-steps in DP-TS part of the co-simulation is successfully addressed in this work.

The effectiveness of the proposed co-simulation model was demonstrated using the New England & New York 68 bus system with an HVDC in-feed in the internal system. The RTDS simulator is used as the real-time simulation platform and the results of the co-simulation model were validated by a real-time EMT simulation.

1.3 Outline of the Thesis

Introduction to the thesis topic was presented in this chapter. Limitations of current simulation models and the need for co-simulation models were highlighted. The problems in the existing EMT-TS co-simulation models and the uniqueness of the research topic were also presented.

An introduction to simulation models is given in Chapter 2. The concept of dynamic phasors is discussed and representation of basic power system elements in dynamic phasors is also presented in the same chapter.

Chapter 3 presents a stability criterion for interfacing an external system into a dynamic phasor simulation. A dynamic phasor based synchronous machine model suitable for a Nodal analysis type DP simulation is also developed in this chapter. The numerical stability of the interface between the synchronous machine model and the network is analysed using the stability criterion developed.

Interfacing a dynamic phasor model to a real-time EMT model is presented in Chapter 4. The challenges of interfacing EMT and DP is discussed with a particular focus on numerical instability. The implementation of the EMT-DP co-simulation model, using a proposed numerically stable interface method, on a real-time platform is presented. The proposed model is implemented for New England & New York 68 bus system and the results are validated using a complete EMT simulation. The limitations of EMT-DP co-simulation are presented and the need for combining a TS model to the EMT-DP model for analysing a large power system is discussed.

Chapter 5 presents the proposed real-time EMT-TS co-simulation model using dynamic phasors as a buffer zone. Interfacing DP to a TS model is discussed with an appropriate communication algorithm. The numerical stability of the

co-simulation model is analysed. The basic blocks of the proposed EMT-TS co-simulation model are presented in the chapter.

Testing and the validation of the proposed EMT-TS co-simulation model on a real-time platform is presented in Chapter 6.

Chapter 7 gives conclusions and the contributions of this thesis. Some recommendations for future work are also presented in Chapter 7.

Chapter 2

Review of Simulation Models to Analyse a Power System

2.1 Modelling of a Power System using Dynamic Phasors

2.1.1 Introduction

The concept of dynamic phasors is presented in this section along with some examples of dynamic phasor models. Dynamic Phasor concept was first introduced for power system modelling in 90s and it was then referred to as "time-varying phasors" [7]. Time-varying phasor concept has been used in communication theory over a long time and the modulation of signals is used for analysing narrowband signals with signal bandwidth much less compared to the carrier frequency. This phasor representation is very useful since the dynamics of a sinusoidal signal can be represented using the magnitude and the angle of the modulated signal and the

carrier signal can be filtered out. The same narrowband assumption can be made on the phasor signals of power systems since power system transients usually lie around the fundamental frequency. However, the bandwidth of the signal has to be much less than the carrier signal frequency which is equal to 60 Hz. However, after making this assumption this model will be similar to a quasi-stationary analysis and therefore, there won't be much of new information that can be gained from the study. The tools such as Hilbert transformation used in establishing the time-varying phasors are not only for narrowband signals. Hence, this method can be extended to a range where the signal frequency can go up to 60 Hz frequency. This will allow capturing most of the dynamics in power system transients. The signals where the frequency is below 60 Hz are referred to as "low-pass" phasor signals. It has been shown in [34] that band-limited signal assumption is a fundamental requirement for modulating signals. It can be shown that the band-limited assumption along with the low-pass phasor signals preserve the non-linear power balance equations.

Let us consider the modulated signal $u(t)$, where the carrier frequency equals to ω_c. The magnitude of $u(t)$ is denoted as $A(t)$ and the angle is denoted by $\delta(t)$.

$$u(t) = A(t)cos\left(\omega_c t + \delta(t)\right) \tag{2.1}$$

The phasor representation of the signal $u(t)$ is,

$$\hat{u}(t) = A(t)e^{j\delta(t)} = A(t)\angle\delta(t) \tag{2.2}$$

The modulated signal $u(t)$ can be written using the phasor signal $\hat{u}(t)$ by

$$u(t) = Re(\hat{u}(t)e^{j\omega_c t}) = Re(A(t)e^{j(\omega_c t+\delta(t))}) \tag{2.3}$$

which results in (2.1).

Therefore, for a given phasor signal $\hat{u}(t)$ there is a unique modulated signal $u(t)$ which satisfies (2.3). However, finding a unique phasor signal $\hat{u}(t)$ from the modulated signal $u(t)$ is not possible since different values of $\hat{u}(t)$ result in same $u(t)$. In order to represent network variables such as instantaneous voltages and currents in the phasor domain, the phasor operation in (2.3) has to be valid for both directions. The phasor representation of power system variables is important since it filters out the carrier frequency allowing us to use larger integration time-step to capture any dynamics associated with the signal. This can be further explained as follows.

Due to the baseband characteristics of the power system transients, the frequency spectrum of the power system dynamics lies around the fundamental (i.e. system base) frequency. If the frequency spectrum of the system is shifted by its fundamental frequency the system becomes a narrowband signal which has a lower bandwidth around the fundamental frequency (signals that have such a frequency spectrum are called bandpass signals). This will allow the dynamic phasors to use a larger integration time step than the EMT simulations resulting in faster simulations [35], [36]. The frequency spectrum of a bandpass signal is shown in Fig. 2.1. After shifting the frequency from the carrier frequency (f_c), the frequency spectrum becomes narrow banded as shown in Fig. 2.2.

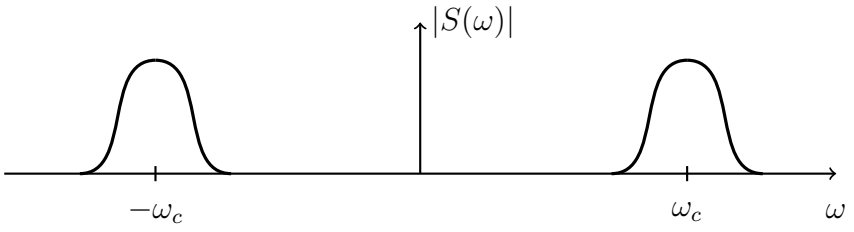

FIGURE 2.1: Frequency spectrum of a band-pass signal

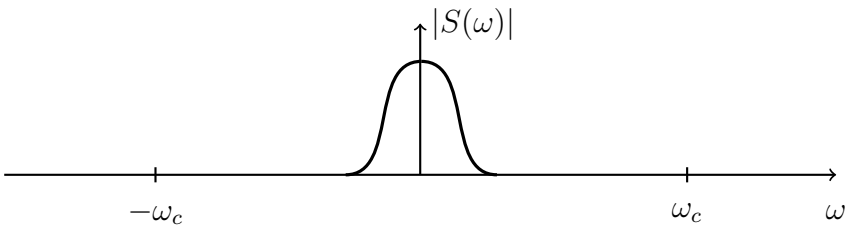

FIGURE 2.2: Frequency spectrum of dynamic phasors

If the baseband assumption can be made to the power system, the phasor representation improves the simulation efficiency significantly. However, in the presence of higher-order harmonics, the spectrum of transients also lies around the harmonic frequencies in the system other than the fundamental frequency. In such a situation, there is not much advantage gained [9].

In [7], it was shown using Hilbert transformation that in order for the operation in (2.3) to be valid in both directions the phasors has to be low pass phasor signals on their bandwidths (i.e. bandwidth of the phasor signal has to be smaller than the carrier frequency). This is a general requirement to solve non-linear power equations. In a nodal analysis-type approach for network solving, the objective of the simulation is to observe the voltages and currents in the system for a sinusoidal excitation of a source. Hence, the problem becomes simple, where a set of linear differential equations are solved for a time-varying sinusoidal input. There is no restriction on the bandwidth on the validity of the phasor representation for such a purpose. However, the equations are written in the complex phasor domain and the dimension of the system becomes twice the size of the original system.

Derivative Operation

The main difference of dynamic phasors with the phasors used in traditional transient stability studies is the way that it handles differential equations. In TS type

studies, the derivatives are substituted by the constant term $j\omega_c$ as a phase shift. Let the dynamic phasor of the signal $u(t)$ is equal to $U(t)$:

$$u(t) = Re(U(t)e^{j\omega_c t}) \tag{2.4}$$

By differentiating the signal $u(t)$:

$$\frac{d}{dt}u(t) = Re\left(\frac{d}{dt}U(t)e^{j\omega_c t}\right) \tag{2.5}$$

The derivative of the signal $u(t)$ using $U(t)$ is then expressed as (2.6):

$$\frac{d}{dt}u(t) = Re\left(\left(\frac{d}{dt}U(t) + j\omega_c U(t)\right)e^{j\omega_c t}\right) \tag{2.6}$$

Hence, in dynamic phasors, the derivative is equal to the addition of the derivative of the phasor signal and the $j\omega_c$ multiplied by the phasor signal [7]. Using this property, differential equations for the voltage of a capacitor (capacitance=C) and the current in an inductor (inductance=L) can be written as (2.8) and (2.10).

$$i_c(t) = C\frac{d}{dt}v_c(t) \tag{2.7}$$

Taking the dynamic phasor of both sides of (2.7):

$$I_c(t) = C\frac{d}{dt}V_c(t) + j\omega_c C V_c(t) \tag{2.8}$$

$$v_L(t) = L\frac{d}{dt}i_L(t) \tag{2.9}$$

Taking the dynamic phasor of both sides of (2.9):

$$V_L(t) = L\frac{d}{dt}I_L(t) + j\omega_c L I_L(t) \tag{2.10}$$

where signals $I_c(t)$, $V_c(t)$, $V_L(t)$ and $I_L(t)$ are dynamic phasor voltages and currents. It should be noted that the above equations are derived for the fundamental frequency component. As we can see, in DP we have voltages and currents in the network as state variables which allows capturing network dynamics. In TS studies, currents and voltages are allowed to change in discrete steps and for the above reason in DP they, change continuously through time. Therefore, DP can be used to analyse phenomena such as sub-synchronous resonance, HVDC interactions etc.

2.1.2 Dynamic Phasor Representation of Network Components

2.1.2.1 Representation of a Series RL Branch

Let us consider a series connected RL branch shown in Fig. 2.3, where the voltages of the opposite sides equal to $V_1 = V_{1R} + jV_{1I}$ and $V_2 = V_{2R} + jV_{2I}$ and current in the branch equal to $I = I_R + jI_I$.

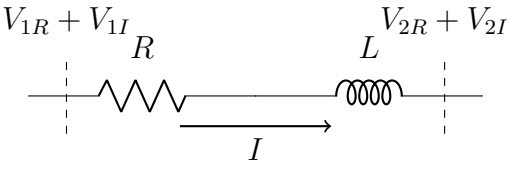

FIGURE 2.3: Series RL branch

$$V_{12}(t) = L\frac{d}{dt}I(t) + (R + j\omega_0 L)I(t) \tag{2.11}$$

$$\frac{d}{dt}I(t) = -(\frac{R}{L} + j\omega_0)I(t) + \frac{1}{L}V_{12}(t) \tag{2.12}$$

Separating the real and the imaginary parts of (2.12) results (2.13),

$$\frac{d}{dt}\begin{pmatrix} I_R(t) \\ I_I(t) \end{pmatrix} = \begin{pmatrix} \frac{-R}{L} & \omega_0 \\ -\omega_0 & \frac{-R}{L} \end{pmatrix} \begin{pmatrix} I_R(t) \\ I_I(t) \end{pmatrix} + \begin{pmatrix} \frac{1}{L} & 0 & -\frac{1}{L} & 0 \\ 0 & \frac{1}{L} & 0 & -\frac{1}{L} \end{pmatrix} \begin{pmatrix} V_{1R}(t) \\ V_{1I}(t) \\ V_{2R}(t) \\ V_{2I}(t) \end{pmatrix} \tag{2.13}$$

where,

$$\dot{\underline{x}} = A\underline{x} + B\underline{u} \tag{2.14}$$

The eigenvalues of the system are complex conjugates located at at $-\tau \pm j\omega_0$ in the complex plane, where τ is the time constant of the system which equals to $\tau = \frac{R}{L}$. The system oscillates at the frequency ω_0 which is the carrier frequency. Hence, the eigenvalue depicts the interactions between the original system and the carrier.

The Norton equivalent of the series RL branch can be derived for nodal analysis approach. Let us apply Trapezoidal rule of integration to (2.12).

$$\begin{aligned} I(t) = I(t-1) + \Bigg[&- \left(\frac{R}{L} + j\omega_0\right) I(t-1) + \frac{1}{L} V_{12}(t-1) \\ &- \left(\frac{R}{L} + j\omega_0\right) I(t) + \frac{1}{L} V_{12}(t) \Bigg] \frac{\Delta t}{2} \end{aligned} \tag{2.15}$$

Rearranging (2.15),

$$\begin{aligned} \left(1 + \frac{R\Delta t}{2L} + j\frac{\omega_0 \Delta t}{2}\right) I(t) = &\left(1 - \frac{R\Delta t}{2L} + j\frac{\omega_0 \Delta t}{2}\right) I(t-1) + \\ &\frac{\Delta t}{2L} V_{12}(t-1) + \frac{\Delta t}{2L} V_{12}(t) \end{aligned} \tag{2.16}$$

$$I(t) = h_1 V_{12}(t-1) + h_2 I(t-1) + Y V_{12}(t) \tag{2.17}$$

Where,

$$h_2 = \frac{1 - \frac{R\Delta t}{2L} - j\frac{\omega_0 \Delta t}{2}}{1 + \frac{R\Delta t}{2L} + j\frac{\omega_0 \Delta t}{2}} \tag{2.18}$$

$$h_1 = Y = \frac{\frac{\Delta t}{2L}}{1 + \frac{R\Delta t}{2L} + j\frac{\omega_0 \Delta t}{2}} \tag{2.19}$$

The Norton equivalent circuit model for the series RL branch is shown in Fig. 2.4, where I_H denotes the history term which is expressed in (2.20) and $V = V1 - V2$.

$$I_H = h_1 V_{12}(t-1) + h_2 I(t-1) \tag{2.20}$$

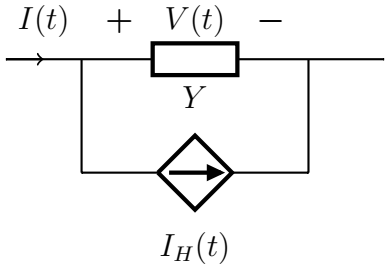

FIGURE 2.4: Norton equivalent of RL/RC branch in discrete domain

2.1.2.2 Representation of a Shunt RC Branch

Let us analyse the shunt RC branch shown in Fig. 2.5. The voltage and the current across the branch are denoted by V and I respectively.

$$I(t) = C\frac{d}{dt}V(t) + (G + j\omega_0 C)\,V(t) \tag{2.21}$$

$$\frac{d}{dt}V(t) = -\left(\frac{G}{C} + j\omega_0\right)V(t) + \frac{1}{C}I(t) \tag{2.22}$$

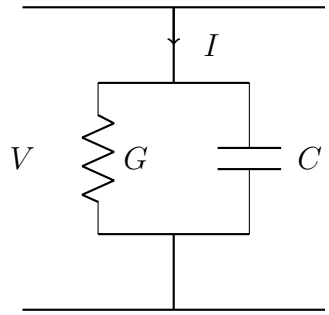

FIGURE 2.5: Shunt RC branch

$$\frac{d}{dt}\begin{pmatrix} V_R(t) \\ V_I(t) \end{pmatrix} = \begin{pmatrix} -G/C & \omega_0 \\ -\omega_0 & -G/C \end{pmatrix}\begin{pmatrix} V_R(t) \\ V_I(t) \end{pmatrix} + \begin{pmatrix} 1/C & 0 \\ 0 & 1/C \end{pmatrix}\begin{pmatrix} I_R(t) \\ I_I(t) \end{pmatrix} \tag{2.23}$$

The eigenvalues of the state space model lie at $-\tau \pm j\omega_0$, where τ is the time constant of the system which equals to $\tau = \frac{G}{C}$. The system oscillates at the frequency of carrier frequency (ω_0).

The Norton equivalent of the shunt RC branch can be derived for nodal analysis approach. Let us apply Trapezoidal rule of integration to (2.22).

$$V(t) = V(t-1) + \Bigg[-\left(\frac{G}{C} + j\omega_0\right)V(t-1) + \frac{1}{C}I(t-1) + \left(\frac{G}{C} + j\omega_0\right)V(t) + \frac{1}{C}I(t)\Bigg]\frac{\Delta t}{2} \tag{2.24}$$

$$\frac{\Delta t}{2C}I(t) = -\frac{\Delta t}{2C}I(t-1) - \left(1 - \frac{G\Delta t}{2C} - j\frac{\omega_0 \Delta t}{2}\right)V(t-1) + \left(1 + \frac{G\Delta t}{2C} + j\frac{\omega_0 \Delta t}{2}\right)V(t) \tag{2.25}$$

$$I(t) = h_1 V(t-1) + h_2 I(t-1) + YV(t) \tag{2.26}$$

Where,

$$h_2 = -1 \tag{2.27}$$

$$h_1 = -\frac{1 - \frac{G\Delta t}{2C} - j\frac{\omega_0 \Delta t}{2}}{\frac{\Delta t}{2C}} \tag{2.28}$$

$$Y = \frac{1 + \frac{G\Delta t}{2C} + j\frac{\omega_0 \Delta t}{2}}{\frac{\Delta t}{2C}} \tag{2.29}$$

The Norton equivalent circuit of the shunt RC branch can also be represented using Fig. 2.4, where I_H denotes the history term which is expressed in (2.30) and the admittance Y is given by (2.29).

$$I_H = h_1 V(t-1) + h_2 I(t-1) \tag{2.30}$$

The modelling of transformers in dynamic phasors is also similar to the derivation presented above and it is presented in Appendix B.

2.2 Dynamic Phasors for Interfacing Electromagnetic Transient Model to a Transient Stability Model

2.2.1 Electromagnetic Transient Simulation

EMT simulation is the most accurate tool for studying the behaviour of a power system in detail. It requires detailed modelling of power system components and the simulation is done using a small time-step. Typical EMT studies use $50\mu s$ as the time-step. It models the three-phase power system allowing to capture effects on unbalances in the system. EMT simulation can be solved using nodal

analysis or state-space system. Many commercialized EMT models use nodal analysis approach where each component in power system is modelled as a Norton equivalent by discretising its governing equation. This approach is called Dommel's algorithm. As an example, let us consider the equation governing the voltage and current characteristics of an inductor given in,

$$\frac{d}{dt}i = \frac{1}{L}v \tag{2.31}$$

By applying the Trapezoidal rule to (2.31) we can obtain the Norton equivalent model (2.33), where I_H is the history term, which can be regarded as the current source of the Norton equivalent. The term Y can be regarded as the conductance parallel with the current source. The equivalent circuit of the inductor can be represented as Fig. 2.4.

$$i(t) = i(t - \Delta t) + \frac{\Delta t}{2L}\Big[v(t - \Delta t) + v(t)\Big] \tag{2.32}$$

$$i(t) = Yv(t) + I_H(t - \Delta t) \tag{2.33}$$

$$Y = (\frac{\Delta t}{2L}) \tag{2.34}$$

$$I_H = i(t - \Delta t) + Yv(t - \Delta t) \tag{2.35}$$

Compared to DP, the current source value is a real quantity in parallel with a resistor.

In EMT simulations, detailed models of power system components are used (e.g. frequency-dependent transmission lines, machine models with stator dynamics, non-linear loads).

2.2.2 Transient Stability Model

The efficiency of the TS models is gained by using simplified models of the power system components. One main assumption it does is that it ignores the dynamics in the networks caused by inductors and capacitors. It is assumed that the network dynamics die out faster than a time-step of a TS simulation. Therefore, the network differential equations are modelled using simple algebraic equations ($V = Y^{-1}I$). The dynamics of the mechanical devices connected to the network are considered. Synchronous machines are modelled by ignoring the dynamics in the stator winding and the speed deviation term in the stator voltage equations [37]. The differential equations corresponding to rotor, field and damper windings are solved at every time-step and the node voltages of the machines are updated. The differential equations are commonly solved using Runge Kutta integration. Switching transients in power electronic devices are ignored. The power system is modelled as a balanced system and the negative and zero sequence currents generated during an unbalanced fault are represented using negative and zero sequence impedances.

2.2.3 EMT-TS Interfacing using Dynamic Phasor Model as a Buffer Zone

A comparison of the three simulation programs described in this chapter is summarized in Table 2.1.

The objective of this thesis is to use the three simulation programs as a co-simulation model to capture the high-frequency dynamics in the study zone, which is modelled using EMT. Dynamic phasors are used to model a buffer-zone between an EMT and TS model. The buffer zone mainly contains transmission lines and

TABLE 2.1: Comparison of the three simulation programs: EMT, DP and TS

	EMT	**DP**	**TS**
Computational burden	High	Higher than TS. Lower than EMT.	Low
Frequency boundary assumptions	None	None for solving linear set of equations	Phasors vary slowly compared to ω_0: Narrowband
Variation of voltages and currents	Continuously change during a disturbance.	Constant in steady-state. Continuously change in a disturbance.	Constant in steady-state. Change in discrete steps.
Signals	Three-phase real instantaneous quantities	Complex numbers	Complex numbers
Differential equations	$\frac{d}{dt}x(t)$	$\frac{d}{dt}X(t) + j\omega_0 X(t)$	$j\omega_0 X(t)$
Inductor voltage equation	$L\frac{d}{dt}i(t)$	$L\frac{d}{dt}I(t) + j\omega_0 LI(t)$	$j\omega_0 LI(t)$
Capacitor current equation	$C\frac{d}{dt}v(t)$	$C\frac{d}{dt}V(t)+j\omega_0 CV(t)$	$j\omega_0 CV(t)$
Handling unbalances	Yes	System is modelled assuming balanced conditions	System is modelled assuming balanced conditions

loads. The purpose of the buffer zone is a) gap the frequency bandwidth difference between the EMT and TS b) Capture some of the high frequency dynamics close to the EMT-TS boundary. This chapter has briefly explained the characteristics of the three simulation model and modelling techniques used in the three models.

2.3 Summary

An overview of simulation models available to study a power system was presented in this chapter. The concept of dynamic phasors and the representation of basic power system components using dynamic phasors were presented.

Chapter 3

Interfacing a Synchronous Machine Model to a Dynamic Phasor Simulation

3.1 Introduction

Synchronous machine is a fundamental part of the power system network and there are several models available to represent it in simulations. The derivation of a synchronous machine model that is suitable for a DP simulation is presented in this chapter. Guaranteeing numerical stability in existing synchronous machine models requires extra computations which can make a real-time simulation challenging. The stability and efficiency of the existing synchronous machine models are investigated and a relevant stability criterion for interfacing a synchronous machine to a DP simulation is presented in this chapter.

The approach of nodal based analysis in dynamic phasors results in a

linear set of equations. The state equations of the synchronous machine have to be solved separately since it is a non-linear device. At the end of every time-step the machine model will update (or read) currents/voltages in the interface node of the network that it is connected to. In this way, the network equations are still linear and the Trapezoidal rule can be applied. However, this method results in a time-step delay when exchanging data. In this chapter, the stability of the interface when an external device is connected to a DP simulation is analysed and a necessary condition for numerical stability is derived. This analysis is published in [38].

In Section 3.3, the derivation of a novel voltage source type synchronous machine model is presented for nodal analysis based DP simulation. The derivation of the proposed synchronous machine model is a simple extension to the well-known transient stability model. However, the proposed model takes the dynamics in the stator winding into the account. The proposed model is efficient and numerically robust. The robustness of the machine model is evaluated by interfacing the machine into different networks. The novel synchronous machine model is published in [39].

3.2 Stability Criterion

Interfacing two different network models under one simulation platform (co-simulation) is a challenging task. The interface can introduce numerical instabilities to the simulation due to the time-step delay in communicating of simulation variables at the interface. In this section, the numerical stability of an externally connected device as a current injection device and a voltage source is analysed. Necessary

condition for stability is proposed when interfacing a device into a simulation that involves a time-step delay.

Fig. 3.1 shows the basic steps for interfacing a device into a network model using an iterative algorithm. Simple network shown in Fig. 3.2 is used to illustrate the numerical stability when interfacing two different networks models. The synchronous machine can be interfaced to a network as a voltage source or as a current injection device. The stability of the two approaches are analysed as Method 1 and Method 2 as below.

Method 1

Suppose that an iterative method is used to solve the network in Fig. 3.2. At each iteration, the voltage at the interface bus is read from the right-hand side network and the current is calculated in the left-hand side. At end of the iteration the left-hand side will inject the calculated current to the right-hand side network. And then again at the next iteration, the right-hand side will update the voltage from the current output of the left-hand side and this process will go on until the end of simulation. Let us assume that the voltage at the interface bus is "V" and at r^{th} iteration, $V = V(r-1)$ Then,

$$I_1 = \frac{E_s - V(r-1)}{R_1} \tag{3.1}$$

At $(r+1)^{th}$ iteration, $V = V(r)$ and $I_2 = I_1$

$$V = V(r) = \frac{E_s - V(r-1)}{R_1} R_2 + E_n \tag{3.2}$$

$$V(r) = E_n + E_s \frac{R_2}{R_1} - V(r-1)\frac{R_2}{R_1} \tag{3.3}$$

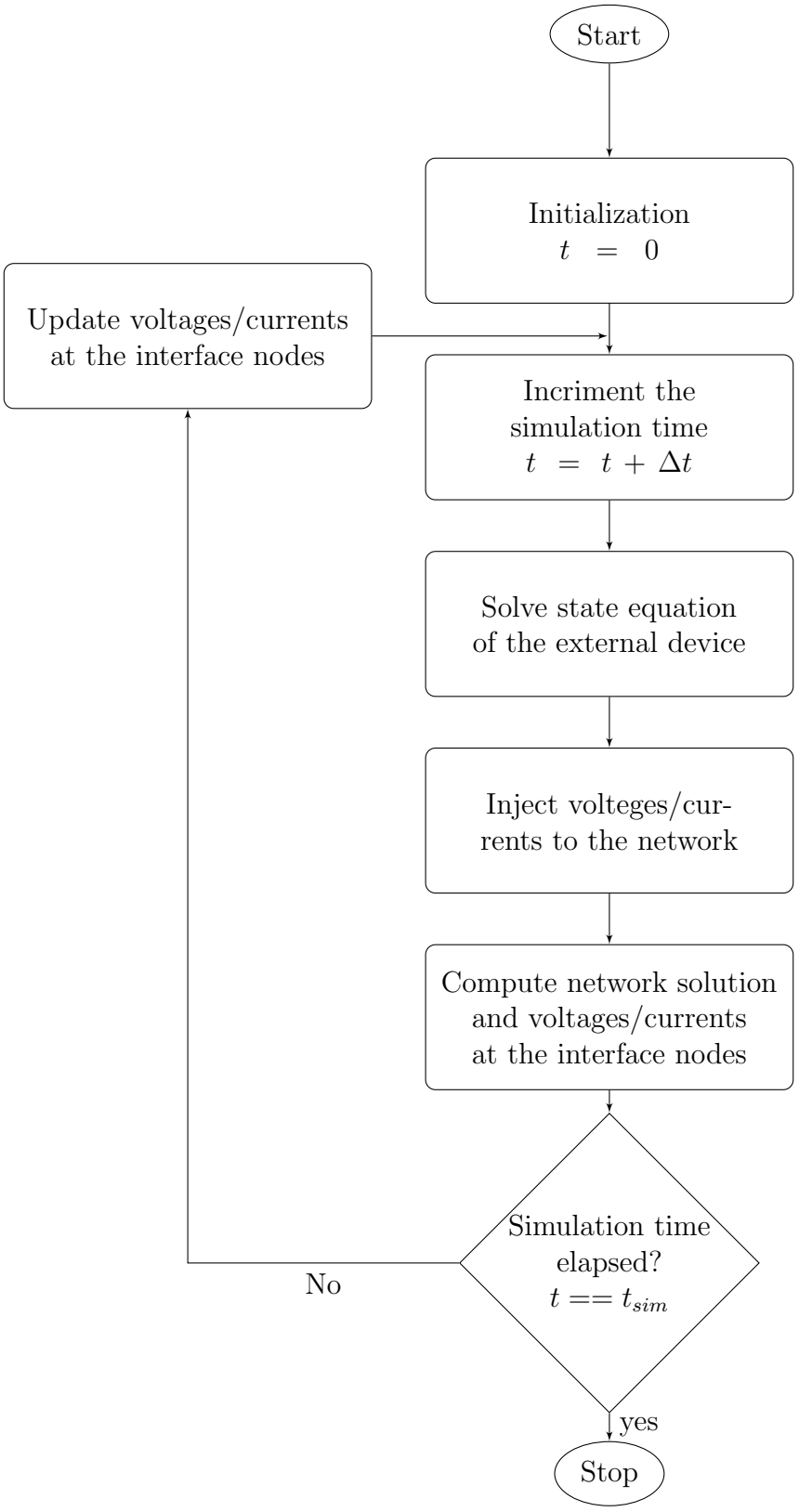

FIGURE 3.1: Flow chart for interfacing an external device into a network

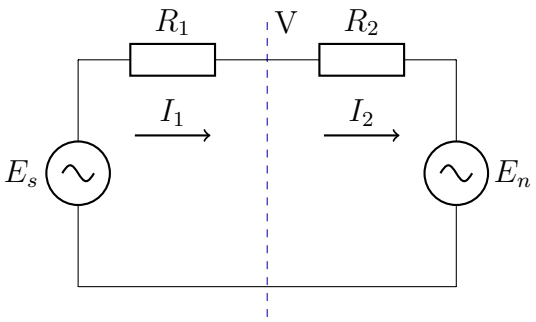

FIGURE 3.2: Simple network to analyse numerical stability

Equation (3.3) can be written in discrete domain as,

$$V = E_n + E_s\frac{R_2}{R_1} - z^{-1}V\frac{R_2}{R_1} \tag{3.4}$$

$$V\left(1 + z^{-1}\frac{R_2}{R_1}\right) = E_n + E_s\frac{R_2}{R_1} \tag{3.5}$$

The discrete domain pole associated with (3.5) is given by $z = -\frac{R_2}{R_1}$ and for stability $|z| \leq 1$. Hence, it is clear that to ensure numerical stability of this procedure the following relationship (3.6) should stand.

$$|R_2| \leq |R_1| \tag{3.6}$$

Method 2

Instead of reading voltages from the right-hand side one can read current (I_2), and the left-hand side voltage can be updated by using I_2 as,

$$V = E_s - I_2R_1 \tag{3.7}$$

The calculated voltage (V) can be passed on to the right-hand side to calculate the injected current for the next iteration. The z-domain analysis of this method

will show that the numerical stability is preserved only if the condition in (3.8) is satisfied.

$$|R_1| \leq |R_2| \tag{3.8}$$

Note that the conditions in (3.6) and (3.8) are opposite to each other. Therefore, the numerical stability of the simulation depends on the way the external device is modelled in the network.

To demonstrate the above result, the circuit in Fig. 3.2 is simulated with $R_1 = 2\,\Omega$, $R_2 = 1\,\Omega$, $E_s = 5\,\text{kV}$ and $E_n = 4\,\text{kV}$. The initial voltage of the interface bus was assumed as "$V = 4.5\,\text{kV}$". In each iteration the interface bus voltage was updated as in method 1. The results for this scenario is shown in Fig. 3.3 and it can be seen that after few iterations the interface bus voltage is converged to the actual value. This is expected as the condition (3.6) is satisfied.

Results for the same network with $R_1 = 1\,\Omega$ and $R_2 = 2\,\Omega$ where $R_1 < R_2$ is shown in Fig. 3.4 and for these network parameters the simulation is numerically unstable. It can be shown that the same network is numerically stable if method 2 is used for interfacing (Fig. 3.5).

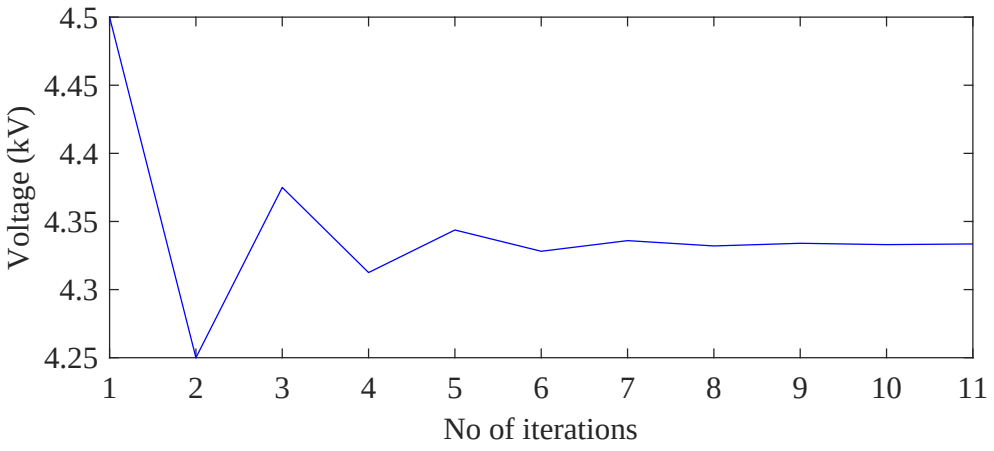

FIGURE 3.3: Simulation results for Fig. 3.2 with $R_1 = 2\,\Omega$ and $R_2 = 1\,\Omega$ using Method 1

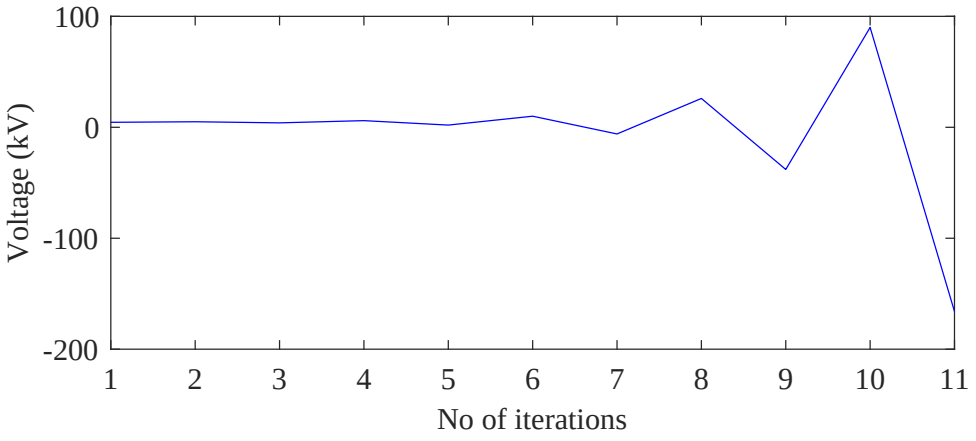

FIGURE 3.4: Simulation results for Fig. 3.2 with $R_1 = 1\,\Omega$ and $R_2 = 2\,\Omega$ using Method 1

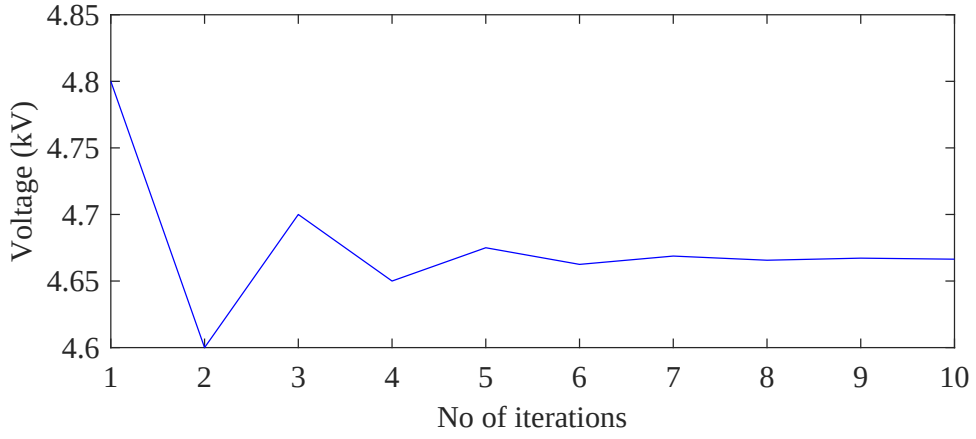

FIGURE 3.5: Simulation results for Fig. 3.2 with $R_1 = 1\,\Omega$ and $R_2 = 2\,\Omega$ using Method 2

The scenario discussed previously is very much similar to a case where simulation models in two different platforms are interfaced to solve a large network (co-simulation). Since there is a time-step delay between the two models the data read from each side is not completely accurate at that instant of time. It must be noted that the above stability analysis was carried out for a steady state condition and the actual simulations are usually dynamic simulations. However, if the steady state solution is numerically unstable the dynamic solution is not going to be stable. It can be concluded from this study that when there is an interface

between two models involving a time-step delay, if the simulation is unstable when one part of the network is modelled as a voltage source, then it is going to be stable when it is modelled as a current source or vice versa. If the steady state stability criterion discussed above is not satisfied, the dynamic simulation will be numerically unstable. However, the steady state numerical stability does not guarantee the stability of the dynamic simulation. Therefore, this criterion is only a necessary condition.

The applicability of derived stability criterion for a dynamic simulation is demonstrated using Single-Machine-Infinite-Bus (SMIB) system [37] shown in Fig. A.1 in Appendix A.1. The data of the SMIB system is given in Table A.1. The synchronous machine constants are given in Table A.3. The synchronous machine in the system is modelled as a TS model and the transmission network is modelled using DP. It is shown that depending on the network parameters the equivalent synchronous machine model can only be numerically stable either as a current source or as a voltage source.

3.2.1 Validation of the Derived Stability Criterion for SMIB System

A general 6^{th} order synchronous machine model with one field winding, one damper winding on the d-axis, and two damper windings on the q-axis is used to validate the derived stability criterion. The dynamics involved in the stator windings are neglected. Equations (3.9) and (3.10) are the state equations that define the dynamics of the mechanical systems [37].

$$\Delta\dot{\omega}_r = \frac{1}{2H}\left(T_m - T_e - K_D\Delta\omega_r\right) \tag{3.9}$$

$$\dot{\delta} = \Delta\omega_r\omega_0 \tag{3.10}$$

Here, δ and $\Delta\omega_r$ are the rotor position and the angular speed deviation and T_m and T_e are the mechanical torque and the electrical torque respectively. Synchronous machine inertia constant is denoted by H and the damping coefficient is denoted by K_D. The differential equations for the flux in the field winding and damper windings are given by (3.11) to (3.14) [37]. The terms φ_{fd} is the flux in the field winding, φ_{1d} is the flux in the damper winding in the d-axis, φ_{1q} and φ_{1q} are the flux in the damper windings in the q-axis.

$$\dot{\varphi_{fd}} = \omega_0 \left(e_{fd} + \frac{\varphi_{ad} - \varphi_{fd}}{X_{fd}} R_{fd} \right) \tag{3.11}$$

$$\dot{\varphi_{1d}} = \omega_0 \left(\frac{\varphi_{ad} - \varphi_{1d}}{X_{1d}} R_{1d} \right) \tag{3.12}$$

$$\dot{\varphi_{1q}} = \omega_0 \left(\frac{\varphi_{aq} - \varphi_{1q}}{X_{1q}} R_{1q} \right) \tag{3.13}$$

$$\dot{\varphi_{2q}} = \omega_0 \left(\frac{\varphi_{aq} - \varphi_{2q}}{X_{2q}} R_{2q} \right) \tag{3.14}$$

Where φ_{ad} and φ_{aq} defined by,

$$\varphi_{ad} = X_{ad}^{''} \left(-i_d + \frac{\varphi_{fd}}{X_{fd}} + \frac{\varphi_{1d}}{X_{1d}} \right) \tag{3.15}$$

$$\varphi_{aq} = X_{aq}^{''} \left(-i_q + \frac{\varphi_{1q}}{X_{1q}} + \frac{\varphi_{2q}}{X_{2q}} \right) \tag{3.16}$$

The terms R_{fd}, R_{1d}, R_{1q} and R_{2q} are the rotor circuit resistances. The terms X_{fd}, X_{1d}, X_{1q} and X_{2q} are the rotor circuit reactances. The subscripts fd, id, $1q$ and $2q$ denote the field winding, damper winding in the d-axis, first damper winding in the q-axis and second damper winding in the q-axis respectively. The superscripts ' relates to transient constants and " relates to sub-transient constants. The terms $X_{ad}^{''}$ and $X_{aq}^{''}$ in (3.15) and (3.16) are sub-transient mutual reactances in d-axis

and q-axis respectively. The notations used in (3.9) to (3.16) are same as the notations in [37]. In this study, the state equations of the synchronous machine are solved separately and interfaced to the network as a voltage/current source. In this way, the state equations of the network will be solved separately and the network sees the machine as a voltage/current source at each time-step. The synchronous machine can be represented by it's internal voltage behind the sub-transient reactance as in Fig. 3.6 [37]. The dq components of the internal voltage are given by (3.17) and (3.18).

$$E_d^{''} = -X_{aq}^{''}\left(\frac{\varphi_{1q}}{X_{1q}} + \frac{\varphi_{2q}}{X_{2q}}\right) \tag{3.17}$$

$$E_q^{''} = -X_{ad}^{''}\left(\frac{\varphi_{fd}}{X_{fd}} + \frac{\varphi_{1d}}{X_{1d}}\right) \tag{3.18}$$

The dq components of the voltage can be then converted into phasor quantities (RI frame) using dq to RI transformation matrix [37].

$$\begin{bmatrix} E_R^{''} \\ E_I^{''} \end{bmatrix} = \begin{bmatrix} \sin(\delta) & \cos(\delta) \\ -\cos(\delta) & \sin(\delta) \end{bmatrix} \begin{bmatrix} E_d^{''} \\ E_q^{''} \end{bmatrix}$$

The internal (i.e.sub-transient) voltage behind the impedance is given by (3.19) where $E_R^{''}$ and $E_I^{''}$ are the real and imaginary parts of the internal voltage. The impedance equals to $X^{''} = X_d^{''} = X_q^{''}$ by ignoring the sub-transient saliency of the machine. The resistor R_a is the stator resistance.

$$E^{''} = E_R^{''} + jE_I^{''} \tag{3.19}$$

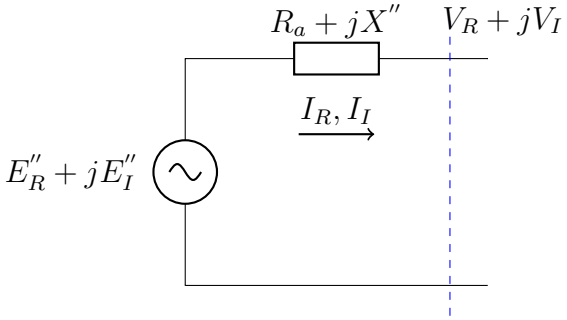

FIGURE 3.6: Synchronous machine represented by it's internal voltage behind the sub-transient reactance

Finally, by using the bus voltage $(V_R + jV_I)$ in Fig. 3.6, the current in the machine can be calculated as in (3.20).

$$I_R + jI_I = \frac{(E''_R + jE''_I) - (V_R + jV_I)}{R_a + jX''} \tag{3.20}$$

The transmission network of the SMIB system considered in this chapter contains an RL branch. The dynamic phasor equation for the series RL branch used in Chapter 2 is re-arranged as a differential equation as (3.21).

$$\frac{d}{dt}I_L = \frac{1}{L}\left(V_L - (R + j\omega L)\, I_L\right) \tag{3.21}$$

Validation of the Stability Criterion

According to the stability criterion presented in Section 3.2 and 3.2 either method 1 or method 2 can be numerically stable. The synchronous machine is modelled as both voltage (method 2) and current (method 1) source to study the numerical stability. If the synchronous machine is represented using a voltage source behind an impedance, its equivalent circuit connected to the network can be represented as Fig. 3.7. Here, V_{net} represents the network Thevenin's voltage and Z_{net} represents network Thevenin's impedance. The parameters i_{mc} and i_{net} are used to define the

current in the machine and the current in the network. The network in Fig. 3.7 is very much similar to the network in Fig. 3.2, which was used previously to develop the stability criterion. However, network quantities in the SMIB are in time domain phasor quantities. It can be shown using simulations that a similar stability criterion exist for the SMIB equivalent circuit.

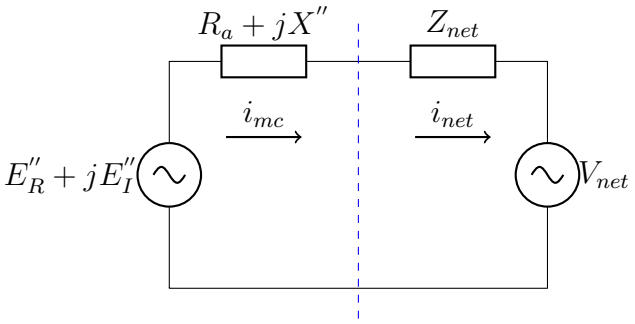

FIGURE 3.7: Equivalent circuit model for SMIB system

Fig. 3.8 and Fig. 3.9 show the generator voltage when the synchronous machine is connected to the network as a current source (method 1) and a voltage source (method 2). It can be seen that only the method 2 where the machine is interfaced as a voltage source provides a stable solution.

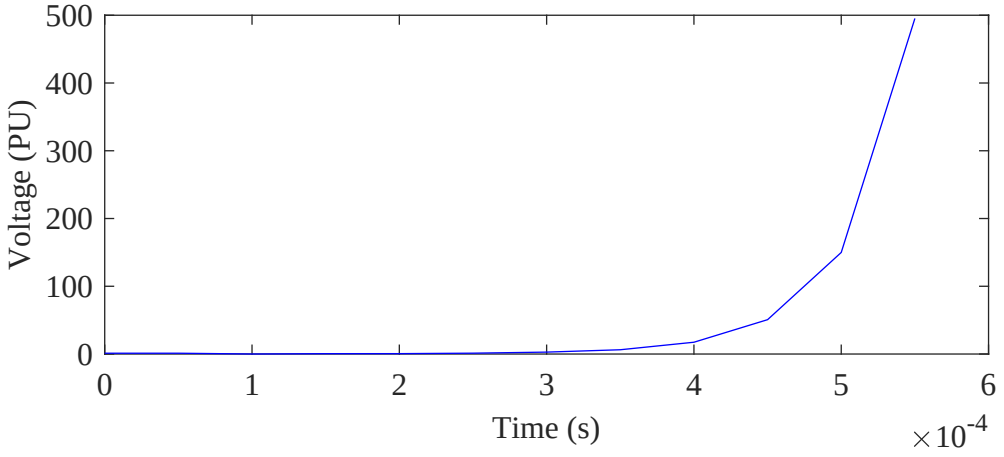

FIGURE 3.8: Synchronous machine modelled as a current source

If we reduce the value of the network impedance in the same SMIB system, it can be shown that the synchronous machine modelled as a voltage source

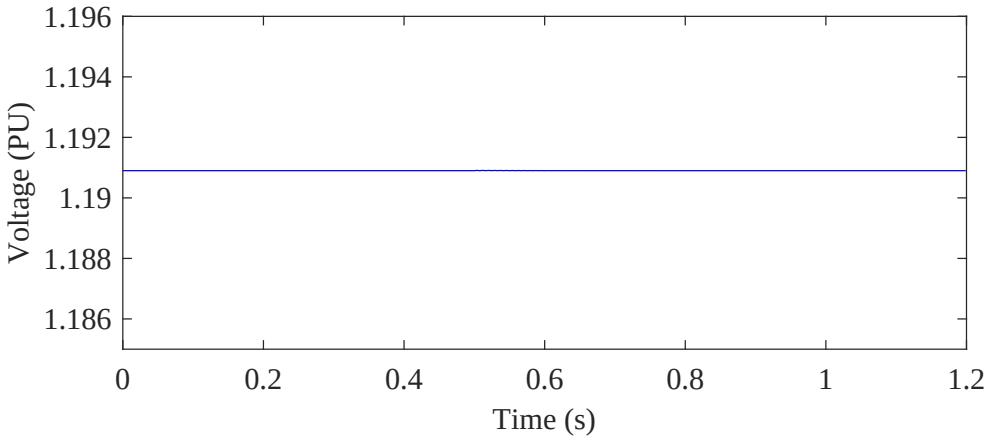

FIGURE 3.9: Synchronous machine modelled as a voltage source

(method 2) provides an unstable solution. It is difficult to state an exact network condition for a stable dynamic simulation in general. However, it can be stated that one of the methods will lead to an unstable simulation.

The conclusion of this study is that depending on the network impedance the equivalent synchronous machine model can only be numerically stable either as a current source or as a voltage source. In DP simulations, it is required to include the stator dynamics of a synchronous machine. However in the model used in this section TS modelling of the synchronous generator was used in order to show the necessary requirements for the interconnection. A synchronous machine model that is suitable for DP simulation will be presented in Section 3.3 below.

3.3 Novel Synchronous Machine Model for Dynamic Phasor Simulations

This section presents a novel synchronous machine model suitable for nodal analysis type dynamic phasor simulation. Depending on the study objective, the extent of modelling of the synchronous machine is different in simulation programs. The

oscillations in the rotor of the machine are slow electromechanical oscillations. The dynamics in the stator winding of the machine has higher oscillatory frequencies and they fall under electromagnetic transients. In TS studies that focus only on electromechanical oscillations, the high frequency oscillations from the network are ignored [37]. Therefore, it is not necessary to model dynamics in the stator windings in stability studies. However, it is important to model the dynamics in the stator winding fluxes in EMT simulations [1]. To be consistent with the dynamic network model, the synchronous machine model with stator winding dynamics used in EMT studies is used in the DP model.

Different full order synchronous machine models are used in EMT simulation platforms. A synchronous machine can be interfaced to the network as a voltage or current source. In Section 3.2, it has been shown that one of these methods would be numerically stable depending on the network parameters.

The dq transformation is commonly used to analyse the machine equations and it results in a simplified set of equations. This transformation can be considered as a transformation of the stator parameters to the rotor side [37]. In the EMT studies, this model is known as the qd method. The qd machine model can be interfaced to the network as a Thevenin equivalent or as a current source in phasor domain [40], [41]. Another way of interfacing the qd model is to represent the network as a Thevenin equivalent in dq domain. All of these three methods except the current source method require prediction of data (electrical and mechanical variables) for numerical stability and accuracy of the model. In PSCAD-EMTDC program the synchronous machine is modelled using the current source method and the value of the current source is calculated using previous time-step values [40]. The numerical issues due to time-step delay between the machine and the network are addressed by using a resistor with a compensated current source at the interface bus. The stability criterion presented in Section

3.2 has pointed out that the device modelled as either current source or voltage source (not both) will be stable at steady state depending on the input impedance of the network that it is connected to. In nodal approach, the state equations of the synchronous machine are solved separately from the network and therefore, an inherent time-step delay exists in the simulation. Since the network impedance is usually much higher than the sub-synchronous reactance of the machine the current source-type synchronous machine will be numerically unstable without a compensating current source described above.

The synchronous machine can be also represented using the original coupled circuit model in abc phasor domain. This method is called the Phase-Domain (PD) method [42]. Time-variant inductance terms in the equations increase the computational burden of the simulation [37].

Voltage Behind Reactance (VBR) models of synchronous machines for EMT simulations are discussed in [43], [44], [45] and [42], where the rotor of the machine is modelled using qd coordinates and the stator equations are modelled using the phasor coordinates. The machine is represented using a Thevenin equivalent with an equivalent impedance and the equivalent impedance can be included in the network equations. This is more numerically stable since the stator is part of the network's admittance matrix. However, this method is computationally demanding for the nodal analysis approach since the equivalent impedance is time-varying.

The VBR method is extended for the EMT nodal analysis method in [41] where the machine model is interfaced to the network by discretizing the stator voltage using the implicit trapezoidal rule. Then the discretized equations are used to come up with a general form given in (3.22) that can be included into

EMT solution as a Thevenin equivalent circuit.

$$v_{abc}(t) = R_{eq}(t)i_{abc}(t) + E_h(t) \tag{3.22}$$

Here, the terms $R_{eq}(t)$ and $E_h(t)$ are the equivalent resistance and history term respectively. The term R_{eq} is time-dependant and is modelled externally to the network as a Thevenin impedance. A constant parameter VBR model is presented in [46] with an aproximation of the time dependant rotor speed (ω_r) to ω_0.

This thesis proposes an alternative approach where the stator reactance is split into two components: (a) a fixed reactance corresponding to base frequency ($L\omega_0$) and (b) a component representing change of reactance due to change in frequency ($L\Delta\omega_r$). The fixed component is included in the network and the variable component is included in the sub-transient voltage.

The proposed Voltage Source (VS) type synchronous machine model is derived in Section 3.3.3 using the same set of steps that are used to derive the synchronous machine model in typical transient stability studies [37]. The synchronous machine model presented in this thesis is numerically robust and it has a constant impedance that can be included in the admittance matrix of the DP part of the network. Hence, at each time-step the voltage source value is given as an input to the DP model as a boundary voltage.

3.3.1 Synchronous Machine Model

The synchronous machine model considered in this chapter is the same machine model used in Section 3.2 but with stator flux dynamics included. Hence, there are eight differential equations governing the dynamics of a synchronous machine. Equations (3.9) and (3.10) are used to represent the dynamics of the rotor [37].

The dynamics of the field winding and damper winding flux are expressed as in (3.11) to (3.14), where the terms φ_{ad} and φ_{aq} are given by:

$$\varphi_{ad} = L''_{ad}\left(-i_d + \frac{\varphi_{fd}}{L_{fd}} + \frac{\varphi_{1d}}{L_{1d}}\right) \tag{3.23}$$

$$\varphi_{aq} = L''_{aq}\left(-i_q + \frac{\varphi_{1q}}{L_{1q}} + \frac{\varphi_{2q}}{L_{2q}}\right) \tag{3.24}$$

The notations and the current direction conventions that are used in this thesis are same with [37]. Using the terms φ_{ad} and φ_{aq} the electric torque of the machine can be expressed as (3.25) .

$$T_e = \varphi_{ad} i_q - \varphi_{aq} i_d \tag{3.25}$$

The dynamics of the stator winding flux in the d and q axes are expressed by (3.26) and (3.27).

$$\dot{\varphi}_d = \omega_r \varphi_q + R_a i_d + e_d \tag{3.26}$$

$$\dot{\varphi}_q = -\omega_r \varphi_d + R_a i_q + e_q \tag{3.27}$$

The main difference with the TS model and the DP model is that TS model neglects the dynamics described in (3.26) and (3.27) by removing the terms $\dot{\varphi}_d$ and $\dot{\varphi}_q$. However, adding these two differential equations for the dynamics of the stator flux components in d-q axes are necessary when the AC network is represented using dynamic phasors. Along with these two stator winding flux equations, there are 8 state variables for round rotor type synchronous generators.

3.3.2 Voltage-Behind-Reactance Model of Synchronous Machine

The derivation of the VBR model for 8^{th} order synchronous machine is explained in this section. Let us consider (3.26), which can be re-written as (3.28).

$$e_d = \dot{\varphi}_d - \omega_r \varphi_q - R_a i_d \tag{3.28}$$

Equation 3.28 can be then written as (3.29) using (3.23), (3.24) and the relationships of $\varphi_d = \varphi_{ad} - L_l i_d$ and $L_d^{''} = L_{ad}^{''} + L_l$,

$$e_d = -L_d^{''} \frac{d}{dt} i_d + \omega_r L_q^{''} i_q - R_a i_d + E_d^{''} \tag{3.29}$$

where the term $E_d^{''}$ is equals to:

$$E_d^{''} = \frac{L_{ad}^{''}}{L_{fd}} \dot{\varphi_{fd}} + \frac{L_{ad}^{''}}{L_{1d}} \dot{\varphi_{1d}} - \omega_r \frac{L_{aq}^{''}}{L_{1q}} \varphi_{1q} - \omega_r \frac{L_{aq}^{''}}{L_{2q}} \varphi_{2q} \tag{3.30}$$

The difference between the above model and the commonly used TS model of a synchronous machine is that (3.29) has the extra term, $L_d^{''} \frac{d}{dt} i_d$, representing the dynamics of the d-axis component of the stator current. The first three terms in (3.29) are identical to the dynamic equation of an RL branch in DP and thus it can be modelled as part of the network solution. The term ω_r in (3.29) depends on the rotor position and it is time-varying. Therefore, it does not allow this equation to be directly included into the nodal analysis method. If one tries to solve this equation using the nodal approach, the admittance matrix of the network has to be updated at each time-step. Computing the inverse of the network's admittance matrix at each time-step is computationally demanding.

3.3.3 Proposed Voltage Source Type Synchronous Machine Model

The synchronous machine model suitable for nodal analysis method is derived in this section. Let us go back to (3.29) and replace the term ω_r using $\omega_r = \Delta\omega_r + 1$. It should be noted that the speed terms considered here are in per unit values.

$$\begin{aligned} e_d = -L_d^{''}\frac{d}{dt}i_d + (\Delta\omega_r + 1)L_q^{''}i_q - R_a i_d + \frac{L_{ad}^{''}}{L_{fd}}\dot{\varphi_{fd}} + \\ \frac{L_{ad}^{''}}{L_{1d}}\dot{\varphi_{1d}} - \omega_r\frac{L_{aq}^{''}}{L_{1q}}\varphi_{1q} - \omega_r\frac{L_{aq}^{''}}{L_{2q}}\varphi_{2q} \end{aligned} \tag{3.31}$$

Now (3.31) can be re-arranged as (3.32) and (3.33).

$$e_d = -L_d^{''}\frac{d}{dt}i_d + L_q^{''}i_q - R_a i_d + E_{\omega d}^{''} \tag{3.32}$$

$$E_{\omega d}^{''} = \frac{L_{ad}^{''}}{L_{fd}}\dot{\varphi_{fd}} + \frac{L_{ad}^{''}}{L_{1d}}\dot{\varphi_{1d}} - \omega_r\frac{L_{aq}^{''}}{L_{1q}}\varphi_{1q} - \omega_r\frac{L_{aq}^{''}}{L_{2q}}\varphi_{2q} + \Delta\omega_r L_q^{''}i_q \tag{3.33}$$

In (3.33), suffix ω is used with the sub-transient voltage $E_{\omega d}^{''}$ to differentiate it from the commonly used term $E_d^{''}$. With this re-arrangement, $(\Delta\omega_r + 1)L_q^{''}i_q$ is separated into $L_q^{''}i_q$ and $\Delta\omega_r L_q^{''}i_q$. The former is included in (3.32) and the latter is included in (3.33). The terms $\dot{\varphi_{fd}}$ and $\dot{\varphi_{1d}}$ in (3.33) can be found from (3.11), (3.12) and (3.23).

Similarly, we can write the q-axis voltage equation using (3.27) as shown in (3.34)

$$e_q = -L_q^{''}\frac{d}{dt}i_q - L_d^{''}i_d - R_a i_q + E_{\omega q}^{''} \tag{3.34}$$

where $E_{\omega q}^{''}$ is equals to,

$$E_{\omega q}^{''} = \frac{L_{aq}^{''}}{L_{1q}}\dot{\varphi_{1q}} + \frac{L_{aq}^{''}}{L_{2q}}\dot{\varphi_{2q}} + \omega_r\frac{L_{ad}^{''}}{L_{fd}}\varphi_{fd} + \omega_r\frac{L_{ad}^{''}}{L_{1d}}\varphi_{1d} - \Delta\omega_r L_d^{''}i_d \tag{3.35}$$

and the terms $\dot{\varphi_{1q}}$ and $\dot{\varphi_{2q}}$ can be found from (3.13), (3.14) and (3.16).

Equation (3.36) can be derived by adding (3.32) and (3.34) as follows:

$$\begin{aligned} e_d + je_q = -L_d^{''}\frac{d}{dt}i_d + L_q^{''}i_q - R_a i_d + E_{\omega d}^{''} + \\ j\left(-L_q^{''}\frac{d}{dt}i_q - L_d^{''}i_d - R_a i_q + E_{\omega q}^{''}\right) \end{aligned} \tag{3.36}$$

With sub-transient saliency neglected $L_d^{''} = L_q^{''} = L^{''}$, (3.36) can be re-written as,

$$E_t = -L^{''}\frac{d}{dt}I_t - jL^{''}I_t - R_a I_t + E_t^{''} \tag{3.37}$$

where $E_t = e_d + je_q$, $E_t^{''} = E_{\omega d}^{''} + jE_{\omega q}^{''}$ and $I_t = i_d + ji_q$. All the parameters in these equations are in per-unit. However, to integrate these equations to the network, the per-unit time needs to be converted into seconds. Per-unit time is equal to the time in seconds multiplied by the angular speed (ω_0) corresponds to fundamental frequency. The resulting equation can be written as (3.38).

$$E_t = -\frac{L^{''}}{\omega_0}\frac{d}{dt}I_t - jL^{''}I_t - R_a I_t + E_t^{''} \tag{3.38}$$

The derived model of the synchronous machine can then be interfaced to the network as a Thevenin voltage source (Fig.3.10).

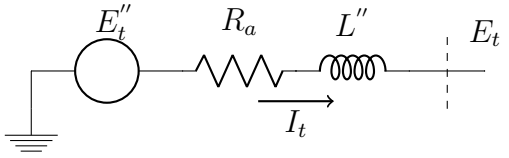

FIGURE 3.10: Synchronous machine represented by its internal voltage behind the sub-transient reactance

It is straightforward to interface the equivalent model of the synchronous machine shown in Fig. 3.6 to nodal analysis method. The term $R_a + jL^{''}$ can be

added to the network's admittance matrix and the voltage E_t'' can be considered as a time-varying boundary voltage updated at each integration time-step.

3.3.4 Test System and Simulation Results

The SMIB system shown in Appendix A.1 is used as the simulation case to test the proposed synchronous machine model. The data of the SMIB system is given in Table A.2 and synchronous machine constants are given in Table A.3. The equivalent circuit of the SMIB system is shown in Fig. 3.11, where E_t is the infinite bus voltage. The synchronous machine is modelled using the novel voltage source model. The transmission line connected to the machine is modelled using a DP model. The transmission line of the SMIB system is represented using an RL branch. Equation (3.39) is used to model the transmission line. The terms R and L are the resistance and the inductance of the transmission line respectively.

$$\frac{d}{dt}I = \frac{1}{L}\left(V - (R + j\omega L)\, I\right) \tag{3.39}$$

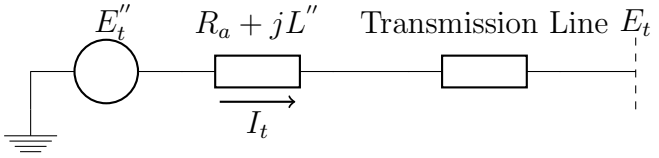

FIGURE 3.11: Synchronous machine connected to the infinite bus through a transmission line

The results of the proposed synchronous machine model is validated using the synchronous machine model available in RTDS. Figures 3.12-3.15 show the comparison of machine variables (speed, electric torque, generator terminal voltage and d-axis current respectively) with the EMT simulation when the infinite bus voltage is dropped to 2% for a period of 100 ms. It can be seen from the figures that the novel voltage source type synchronous machine model closely follow the

EMT simulation results. It accurately captures the high frequency component in electric torque and d-axis current.

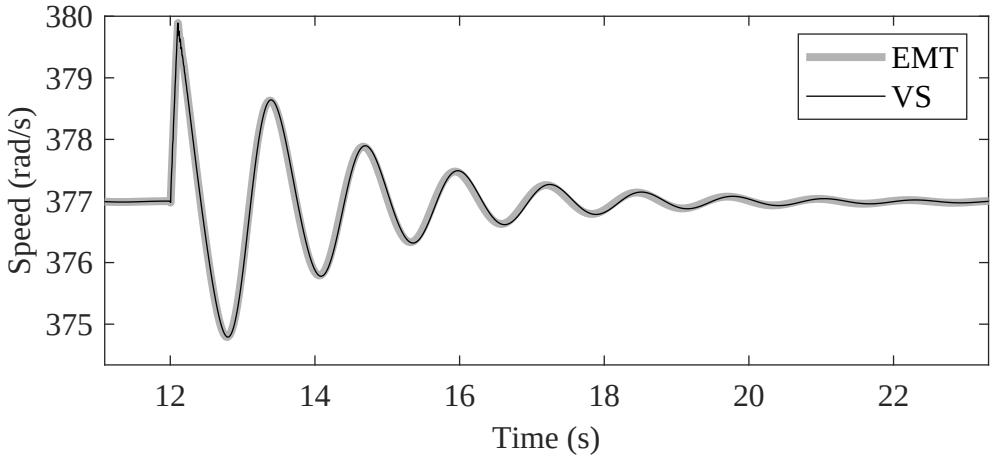

FIGURE 3.12: Comparison of generator speed

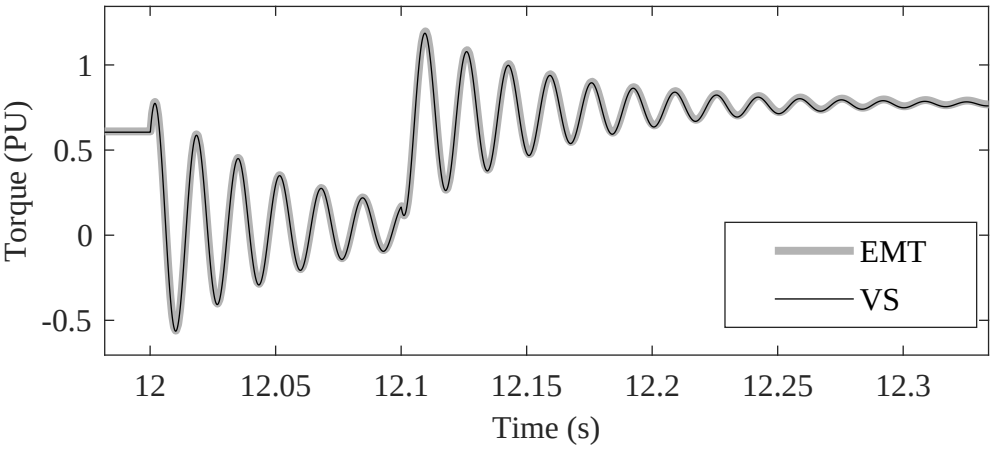

FIGURE 3.13: Comparison of generator electrical torque

3.3.5 Discussion

In the previous section, it was shown that the proposed synchronous machine model produces same results as the existing synchronous machine models. One advantage of the proposed method compared to existing synchronous machine models is that the proposed formation leads to a network bus admittance matrix that is independent of time. This leads to a significant reduction in computation

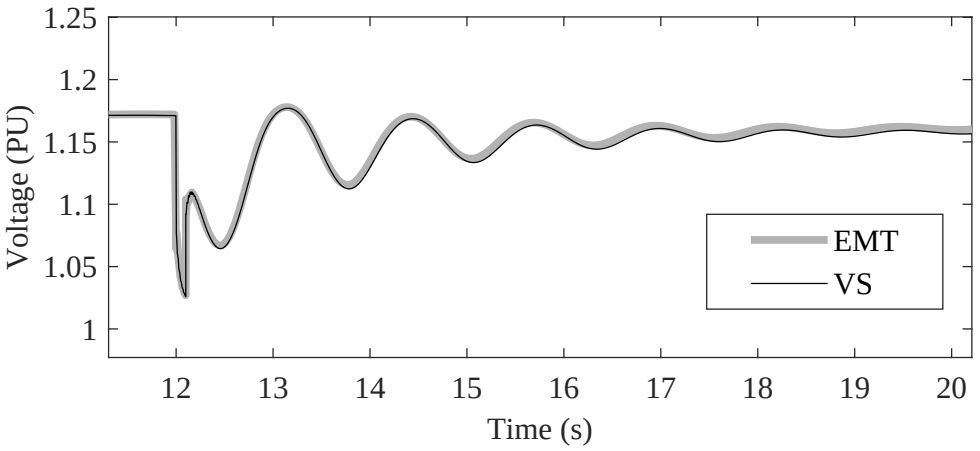

FIGURE 3.14: Comparison of generator terminal voltage

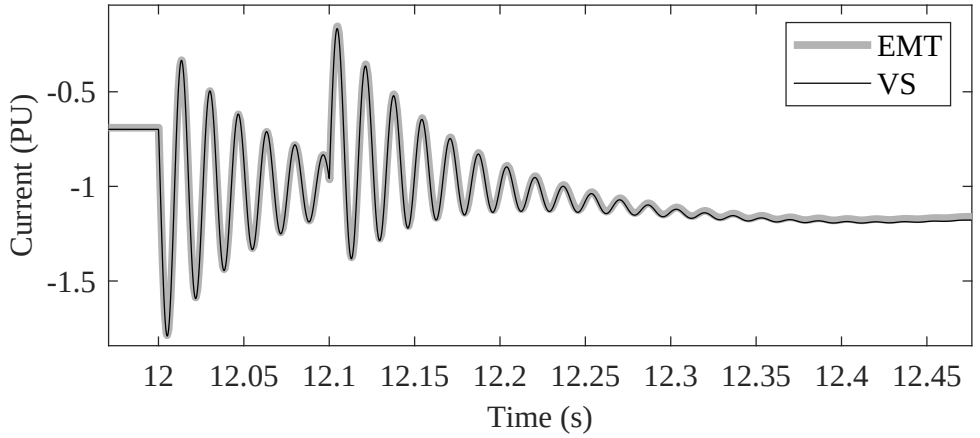

FIGURE 3.15: Comparison of generator d-axis current

time, a requirement for real-time simulation. The other advantage is that the proposed model is numerically stable regardless of the network that it connected to. The proposed interface does not require any filters at the interface for numerical stability. These points will be further explained in Section 3.3.5.1 and 3.3.5.2 below.

3.3.5.1 Stability Considerations for Interfacing Voltage Injection Type Synchronous Machine Model

Let us consider the circuit given in Fig. 3.2. According to the stability criterion given in Section 3.2 if the left hand-side reads current from the right hand side and updates the voltage V at the boundary bus, for numerical stability, the following relationship between the impedances should stand.

$$R_1 \leq R_2 \tag{3.40}$$

If we model the machine by including the impedance of the machine's Thevenin equivalent as part of the network impedance, R_1 is almost zero. Hence, the stability criterion given is satisfied with any value of R_2. This results in the simulation to be stable with any network impedance. The theory is validated by using different network impedances in the SMIB system as shown in figures 3.16, 3.17 and 3.18. The network side impedance is further reduced in each case. As expected, the results validate that the simulation is always stable regardless of the network impedance.

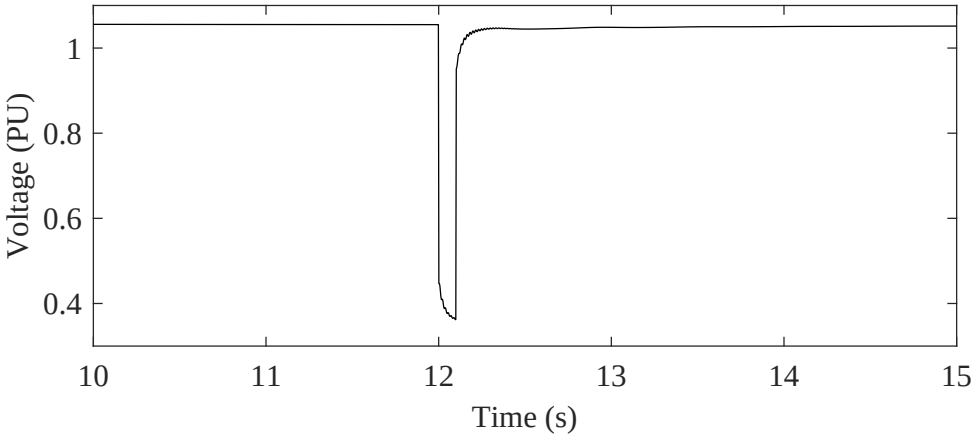

FIGURE 3.16: Generator terminal voltage when the network impedance is reduced to 10%

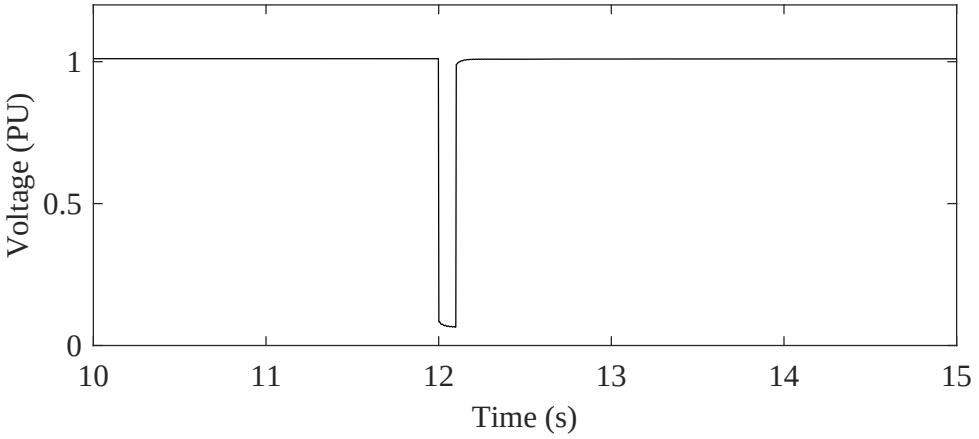

FIGURE 3.17: Generator terminal voltage when the network impedance is reduced to 1%

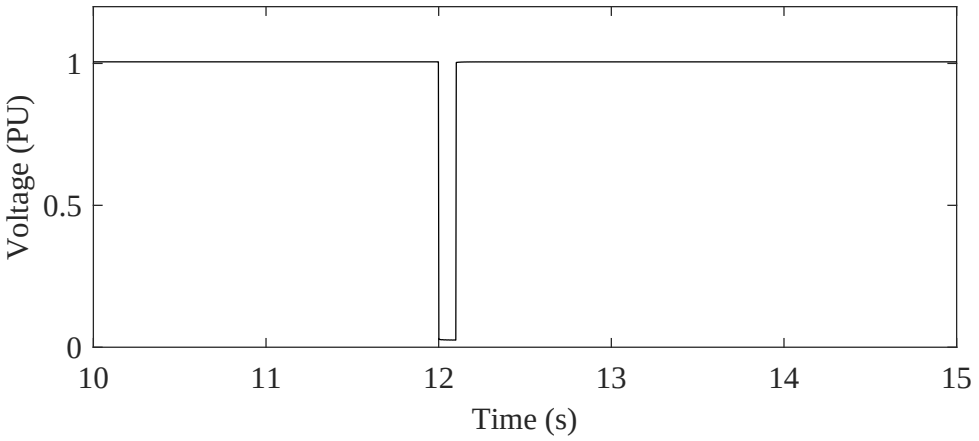

FIGURE 3.18: Generator terminal voltage when the network impedance is reduced to 0.1%

3.3.5.2 Computational Efficiency

In the proposed method, the impedance of the Thevenin impedance of the synchronous machine is not time-dependent and therefore the network admittance matrix stays as a constant. Hence, matrix inversion is not required in every time-step and it could be done only at the beginning of the simulation. A significant computational advantage can be gained by the novel voltage source type synchronous machine model due to this reason.

3.3.5.3 Applicability of the Synchronous Machine Model for an EMT Type Simulation

In this thesis, the novel synchronous machine model is interfaced directly to DP type network model. However, it can also be interfaced to any EMT type network model. It can be modelled using modified nodal analysis approach [47].

3.3.5.4 Modelling Saturation Effects of the Synchronous Machine

The non-linearities in the machine such as saturation effect are important for many studies. In the machine model considered in this chapter, the effects in stator and rotor iron saturation are neglected. A common method of representing saturation is to write sub-transient reactance ($L_d^{''}$ and $L_q^{''}$) as a function of the magnetizing current (e.g. $-i_d + i_{fd} + i_{1d}$ in d-axis). According to this, the sub-transient reactance ($L^{''}$) becomes time dependent.

This can be illustrated using Fig. 3.19 as shown below.

$$v = \frac{d}{dt}\lambda = \frac{d}{di}\lambda * \frac{d}{dt}i \tag{3.41}$$

If we now represent the non-linear inductance using $L(i)$,

$$v = L(i) * \frac{d}{dt}i \tag{3.42}$$

the linear part of the impedance in (3.42) can be modelled as the constant inductance and the non-linear region can be modelled as a voltage or a current source. Therefore, in the voltage source type synchronous machine model, the time-dependent part of $L^{''}$ can be included into the sub-transient voltage $E^{''}$ and

the unsaturated value of the sub-transient reactance can be represented as a linear inductance. The modelling of saturation in the proposed model is illustrated in Fig. 3.20. In this way, the difference in the saturated value of sub transient reactance ($L_{sat}^{''}$) is subtracted from the unsaturated value of sub transient reactance ($L^{''}$) and the voltage drop due to this difference in reactance is subtracted from the sub-transient voltage.

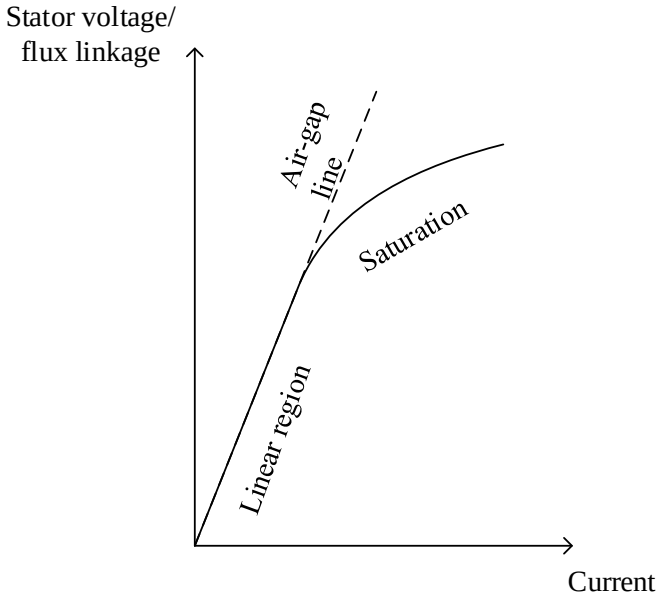

FIGURE 3.19: Saturation curve

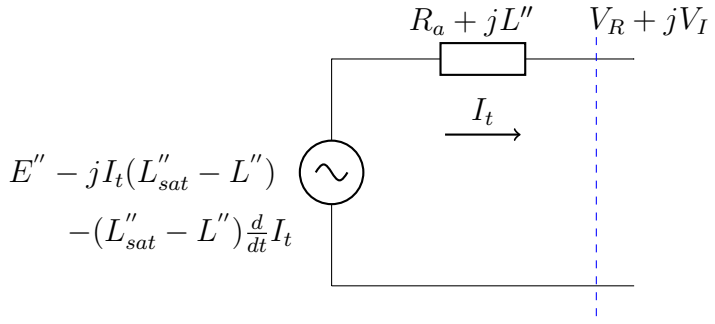

FIGURE 3.20: Modelling saturation in synchronous machine

3.3.5.5 Modelling Sub-Transient Saliency of the Synchronous Machine

In the proposed synchronous machine model, the sub-transient saliency was ignored. Sub-transient saliency is defined as the difference between d and q-axis sub-transient reactances (i.e. $X_d'' - X_q''$). If the saliency is negligible the sub-transient reactance can be modelled as part of the transmission network as presented in Section 3.3.3. If it is not equal to zero, any difference results from the saliency can be included in the sub-transient voltage so that the sub-transient reactance can still be included as part of the network. Fig. shows the comparison of the generator terminal voltage with and without the machine saliency (i.e. X_q'' is changed to 0.375 in Fig. 3.11 to include saliency).

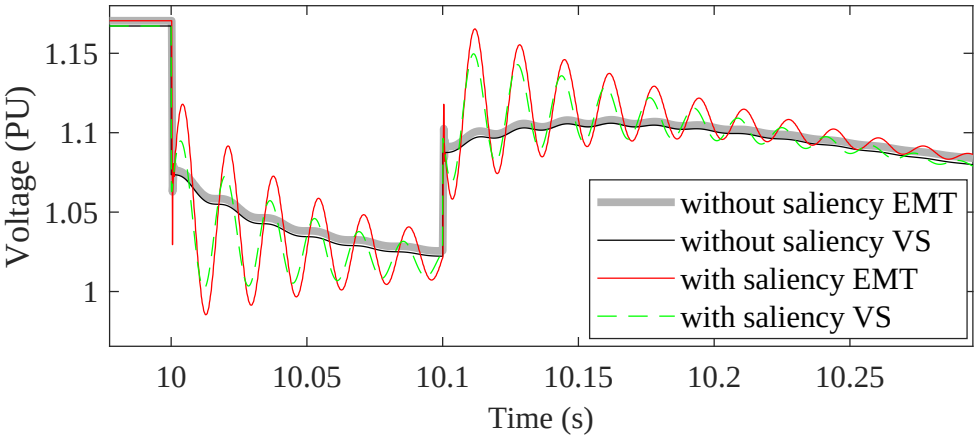

FIGURE 3.21: Generator terminal voltage with saliency included

3.4 Summary

A stability criterion for interfacing a synchronous machine model to a DP simulation was presented in this chapter. The proposed stability criterion is equally valid for interfacing two types of simulation models. A novel voltage source type

synchronous machine model was presented in this chapter to interface into a DP simulation.

Chapter 4

Interfacing Dynamic Phasor Model to Real-Time Electromagnetic Transient Simulation

In this chapter, a dynamic phasor model is interfaced to an EMT simulation to reduce the computational burden of simulating large power systems. This chapter presents the concept and validation of the proposed real-time EMT-DP co-simulation model. The first part of the chapter investigates the challenges of interfacing DP to an EMT model. Achieving a numerically stable EMT-DP interface is difficult due to the time-step delay in communicating simulation variables between the two models. The numerical instability due to time-step delay is investigated and a set of solutions is proposed in this chapter. Among these methods, the data prediction method is adopted in this work for a numerically stable EMT-DP co-simulation. A comparison of some commonly used data prediction methods

is presented in this chapter. Linear extrapolation method is chosen in this work considering its favourable performance during a disturbance. The implementation and the testing of the of the proposed EMT-DP co-simulation in real-time for the New England & New York 68 bus benchmarked power system is explained at the end of this chapter. The co-simulation results are validated using a complete EMT simulation. The content of this chapter has been published as a journal article in Cigre Science and Engineering Journal [48].

4.1 Numerical Stability in Electromagnetic Transient and Dynamic Phasor Interface

The co-simulation model proposed in this chapter contains EMT and DP models. The solutions of the two models are calculated separately and at the end of every time-step, the simulation variables are exchanged. The data that is communicated arrives into the other model with a time-step delay. Therefore, the data received from the connected model is not the correct value but correspond to the previous time-step. Co-simulation is a challenging task due to the time-step delay. If the time-step delay is not properly addressed, the simulation could lead to numerical instability. A necessary stability criterion for interfacing two simulation models was discussed in the previous chapter. According to the stability criterion, the numerical stability of a co-simulation depends on the input impedance of the two interfacing models. In a co-simulation, changing the impedance values of the given network model is unacceptable since the internal and external systems are defined by the user. Also, it does not guarantee numerical stability for a dynamic simulation. Therefore, alternatives have to be investigated to design a numerically stable co-simulation model.

The instability due to time-step delay in a co-simulation can arise when there is an inductor at one side of the interface and the other side injects a current to the model through this inductor. This is a typical scenario in a power system since the transmission network is inductive and the interface points usually consist of one or more branches with inductors. As the current in an inductor is a state variable, injecting a slightly different current (e.g. current in the previous time-step) from the connected model to the inductor, can lead to a numerically unstable simulation. The numerical instability can be avoided by connecting a snubber resistor to the inductor connected to the interface. Hence, one solution for instability is to connect a large resistor (eg. $500\,\Omega$) in parallel to all the inductors at the interface nodes. The resistor provides a path for the difference in the current entering the interface point to flow. The drawback of this method is that the value of the resistor depends on the inductor value. Therefore, the fictitiously added resistor can alter the network impedance. This could result in inaccurate results. Also, it is a tedious work for the user to do this for every inductor that is connected to the interface.

The numerical instability due to time-step delay is discussed in [49], [50], [51] and [52]. Following are some methods that can be used to avoid numerical instability due to time-step delay.

- Use of the natural time delay in the travelling waves of a transmission line separating the internal and external systems to overcome the time-step delay.
- Prediction of current time-step values from previous data.
- Utilizing iterative methods for the solution.
- Adding a smoothing filter to the interface.
- Adding a resistor to the interface buses with a compensation current source.

Among these methods the natural time delay in the travelling waves of a transmission line is used in real-time EMT simulators for partitioning networks to simulate in different processors. The minimum length of a transmission line required to decouple the networks is proportional to the simulation time-step by the following relationship: $s = d/\Delta t$, where the propagation across the line is at the speed of light ($s = 3 * 10^8$ m/s), Δt is the simulation time-step, and d is the transmission line length. As an example, if the time-step of the simulation is 1ms, there should be a transmission line of length 300km.

In [52], the delay of the transmission line is used to interface the EMT solution to the DP solution in an EMT-DP co-simulation. The dynamic phasor model used in this paper is a three-phase dynamic phasor model. Therefore, all together there are six phasors considering the real and imaginary parts. The computational burden is higher compared to an EMT simulation in such an EMT-DP co-simulation and user must be able to use a larger time-step in the DP model to achieve any computational gain. When the time step of the DP simulation is high the length of the transmission line separating the internal and external systems has to be appropriately large. The user will end up having a restriction on the point where the two subsystems are divided. Finding such a long transmission line at the interface is not always possible. Therefore, in many cases, a fictitiously long transmission line has to be added and it can add inaccuracies to the simulation.

In [51], extrapolation of data is used in an EMT co-simulation to overcome the time-step delay. In this thesis, the feasibility of using a data prediction technique to interface a DP model to an EMT model is analysed. Hence, the interface variables at the current time step are predicted using the values at the previous time-step. There are no constraints for choosing the interface points when data prediction methods are used and therefore it is more convenient for the users. However, the use of natural time delay in the propagation of waves in a

transmission line is more accurate compared to a data prediction method if there exists a long transmission line at the interface points. It will be shown that the accuracy sacrificed by not using the natural time delay in the proposed approach is not noticeable.

4.1.1 Data Prediction Techniques to Overcome Time-Step Delay

The time-step delay in a co-simulation model can be avoided by a forward time-step shifting of data. Time-shift can be achieved by predicting future data which is called the extrapolation of data.

4.1.1.1 Extrapolation Techniques

Let us take the set points on x-axis $x_1, x_2, x_3, ...x_n$ for a function $f(x)$. Let us say that the function $f(x)$ is unknown and coordinates are known for a given set points. The problem of finding the function value for an unknown x-value between x_1 and x_n is known as an interpolation problem. Finding a value for an x beyond the range of x_1 and x_n is known as an extrapolation problem. Many techniques are available for interpolation of data and the same techniques can be applied for extrapolation to predict the values outside the range of known values. It should be noted that the data interval has to be kept as small as possible for the accuracy of this procedure.

The most common method used for interpolation is the linear method where one finds a point in somewhere in between given two data points using the linear approximation. This is illustrated in (4.1) and Fig. 4.1. Here, the function values corresponding to time "t" and "$t - \Delta t$" are known and the function value

for "$t + \Delta t$" is unknown.

$$\frac{x(t+\Delta t) - x(t)}{t + \Delta t - t} = \frac{x(t) - x(t-\Delta t)}{t - (t - \Delta t)} \tag{4.1}$$

$$x(t+\Delta t) = 2x(t) - x(t-\Delta t) \tag{4.2}$$

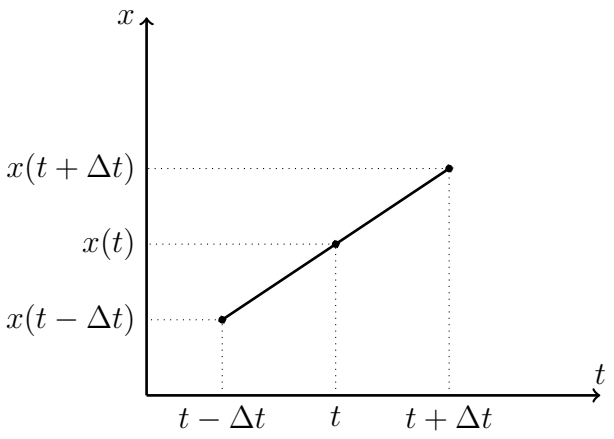

FIGURE 4.1: Linear extrapolation

A polynomial approximation of the unknown function provides a more accurate prediction compared to the linear approximation. Polynomial methods require more than two history values of the function for extrapolation and therefore the transition from one point to another is smoother. In this chapter, two polynomial methods are considered and compared against the linear method. The two methods considered are Lagrange's polynomial method and cubic splines method.

In Lagrange's method [53], an n number of points are approximated for an $(n-1)^{th}$ order polynomial (4.3) and the coefficients of the polynomial are calculated using (4.4), where $y_j = f(x_j)$.

$$L(x) = \sum_{j=1}^{n} l_j(x) \tag{4.3}$$

$$l_j(x) = y_j \prod_{k=1, k\neq j}^{n} \frac{x - x_k}{x_j - x_k} \tag{4.4}$$

With certain types of data, it is hard to fit the data points with one polynomial due to the Runge's phenomenon. In cubic spline method, a cubic function for each data interval is generated [54]. A cubic spline consists of 3^{rd} order piecewise polynomials passing through a number of predefined points (knots). A comparison of the three methods is shown in Fig. 4.2. A sinusoidal signal with magnitude of 230 is generated and the next time-step value is predicted using the three methods mentioned above. A disturbance to the waveform is added at $t = 0.1s$ time-step by adjusting the magnitude to 5 for a period of $0.02s$. A data interval of 50 μs is used (which is the typical time-step of an EMT simulation). From the figure, it can be seen that for this time interval the predictions from all three methods are accurate. The error in the polynomial methods are relatively lower compared to the linear method. However, for the time-step chosen, the error is negligible for all three methods. Since all these methods depend on the history data points, during a disturbance all the methods generate a spike. This spike could lead to erroneous results in a simulation under a disturbance. In the linear method, the height of the spike is relatively lower compared to cubic spline and Lagrange's methods. Therefore, the level of inaccuracy added is relatively larger for higher-order functions under a disturbance.

In this research, linear extrapolation method is used for extrapolation to overcome the time-step delay. The boundary bus simulation variables transferring to DP side from the EMT side are extrapolated to get the current time-step data at the DP side.

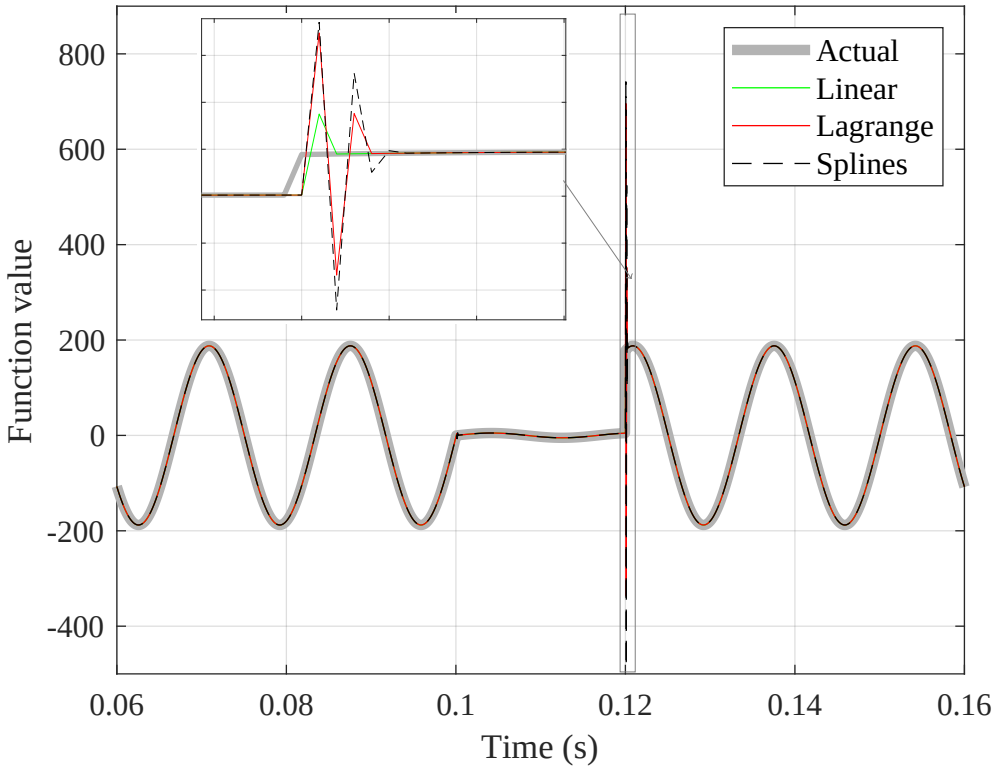

FIGURE 4.2: Comparison of extrapolation methods

4.2 Implementation of the EMT-DP Co-Simulation on a Real-Time Platform

The implementation of the proposed DP-EMT co-simulation model in a real-time platform is presented here.

4.2.1 Dynamic Phasor model

The DP network is solved using the nodal analysis model described in Chapter 2. The inputs to the DP model are the voltages of the interface buses from the EMT side. After every time-step, the DP side will update the currents in the interface buses feeding to the EMT model. The synchronous machines are modelled using the voltage source type synchronous machine model proposed in

Chapter 3 (Fig. 3.10). The time-independent part of the stator impedance is modelled as part of the network and is included in the network impedance bus matrix. The sub-transient voltage in (3.38) is given to the DP model as a boundary voltage at every time-step. The equations to derive the network solution of DP are listed below from (4.5) to (4.11).

Let us consider a DP model with n number of interface buses (including EMT-DP interface buses and generator buses) and m number of internal buses. The network solution can be written as (4.5).

$$\underline{I} = Y\underline{V} + \underline{I_h} \tag{4.5}$$

where, voltage and current vectors are given by (4.6) and (4.7). The vector $\underline{I_h}$ contains the current source values of Norton equivalents (e.g. Fig. 2.4).

$$\underline{V} = [V_{a1} \quad V_{a2} \quad \cdots \quad V_{an} \quad V_{b1} \quad V_{b2} \quad \cdots \quad V_{bm}] \tag{4.6}$$

$$\underline{I} = [I_{a1} \quad I_{a2} \quad \cdots \quad I_{an} \quad I_{b1} \quad I_{b2} \quad \cdots \quad I_{bm}] \tag{4.7}$$

The admittance bus matrix can be written as (4.8) where suffix "a" corresponds to interface buses and "b" corresponds to internal nodes.

$$Y = \begin{bmatrix} [Y_{aa}]_{n\times n} & [Y_{ab}]_{n\times m} \\ [Y_{ba}]_{m\times n} & [Y_{bb}]_{m\times m} \end{bmatrix} \tag{4.8}$$

Let us partition the current vector as $\underline{I_a}$ and $\underline{I_b}$. The current injection vector $\underline{I_a} = [I_{a1}I_{a2}...I_{an}]^T$ is the vector containing current injections to the interface buses. $\underline{I_b} = [I_{b1}I_{b2}...I_{bm}]^T$ is the vector containing current injections to the internal nodes which is equal to zero. The voltage vectors also follow the same definitions and can be defined as $\underline{V_a} = [V_{a1}V_{a2}...V_{an}]^T$ and $\underline{V_b} = [V_{b1}V_{b2}...V_{bm}]^T$. The vector containing

the history current injections is also partitioned as $\underline{I}_{ha} = [I_{ha1} I_{ha2} ... I_{han}]^T$ and $\underline{I}_{hb} = [I_{hb1} I_{hb2} ... I_{hbm}]^T$.

$$\underline{I}_a = \begin{bmatrix} [Y_{aa}] & [Y_{ab}] \end{bmatrix} \underline{V} + \underline{I}_{ha} \tag{4.9}$$

$$\underline{I}_b = 0 = \begin{bmatrix} [Y_{ba}] & [Y_{bb}] \end{bmatrix} \underline{V} + \underline{I}_{hb} \tag{4.10}$$

$$\underline{V}_b = -[Y_{bb}]^{-1}[Y_{ba}]\underline{V}_a - [Y_{bb}]^{-1}\underline{I}_{hb} \tag{4.11}$$

Computational steps of deriving the DP network solution using the above equations are as follows:

1. Obtain the interface bus voltages from the EMT side and also the sub-transient voltages from the generator buses inside the DP model.
2. Compute the history current vector I_h.
3. Compute the internal bus voltages from (4.11).
4. Compute injected currents to the interface buses using (4.9).
5. Compute instantaneous values of the injected currents to EMT-DP interface.

4.2.2 Data Transfer Between EMT and DP Models

4.2.2.1 Extraction of Phasors from the EMT Side

The solution of an EMT model is derived using time domain instantaneous values of three-phase voltages and currents. The DP model uses phasor quantities in the complex domain throughout its simulation process. At the interface buses between EMT and DP, there is a need to convert abc instantaneous quantities to phasor (RI) quantities and vice versa. The conversion of three-phase instantaneous values to phasors is done in EMT-TS co-simulation by using a Fast Fourier Transform

(FFT) [55], consecutive curve fitting technique [56] or by balancing the energy in two sides [23]. A real-time simulation requires a computationally efficient conversion method. FFT method requires data in previous cycles and therefore phasor update could give errors when there is a disturbance in the system. In this thesis, the phasor information is extracted by using the alpha-beta transformation. This is a very simple and straightforward approach compared to available methods and it does not add any delays to the simulation.

Let us consider the time-varying three-phase signals v_a, v_b and v_c, where $v_a = V_m sin(\theta)$ and the angle of v_b and v_c are -120^0 and 120^0 shifted in phase from v_a. The $\alpha\beta$ components (v_α, v_β) of a three-phase signal is calculated using the transformation in (4.12).

$$v_{\alpha\beta} = T_{\alpha\beta} V_{abc} \tag{4.12}$$

where,

$$T_{\alpha\beta} = \begin{bmatrix} 1 & -\frac{1}{2} & -\frac{1}{2} \\ 0 & -\frac{\sqrt{3}}{2} & \frac{\sqrt{3}}{2} \end{bmatrix} \tag{4.13}$$

The magnitude and the angle of the phasors can then be calculated as in (4.14) and (4.15) using $v_{\alpha\beta}$. The parameters V_m, θ, ω_0 and t are magnitude, phase angle, base frequency and time respectively. The alpha beta components resulting from (4.12) are also sinusoidal signals. Therefore, the $60Hz$ rotational component of the voltages is removed by subtracting the term $\omega_0 t$ as shown in (4.15).

$$V_m = \sqrt{v_\alpha^2 + v_\beta^2} \tag{4.14}$$

$$\theta = \tan^{-1}\left(\frac{v_\alpha}{v_\beta}\right) - \omega_0 t \tag{4.15}$$

In order to use the alpha-beta transformation for the phasor conversion,

the system voltages and currents have to be balanced three-phase signals rotating at the speed corresponding to the fundamental frequency (e.g. $f_0 = 60Hz$). In (4.15), to remove the rotational component the fundamental frequency is used. However, in a power system, the system frequency can settle on a different frequency than the fundamental frequency in the absence of proper governor controls. If the frequency deviation is significant the above transformation can result in inaccurate results. The alpha-beta transformation matrix transforms a positive sequence three-phase signal into the phasor quantities. If there is a negative sequence signal mixed with the positive sequence signal (i.e. unbalanced signal) the transformation will result in inaccurate phasors.

4.2.2.2 Converting Phasors from DP Model to EMT Model

The solution generated at the DP side is a complex signal. The conversion to three-phase signal from the complex phasor signal is straightforward. The phasor solution of the DP model is converted back to three-phase signal as shown in (4.16)-(4.18).

$$V_a = V_m sin(\omega_0 t + \theta) \tag{4.16}$$

$$V_b = V_m sin(\omega_0 t + \theta - \frac{2\pi}{3}) \tag{4.17}$$

$$V_c = V_m sin(\omega_0 t + \theta + \frac{2\pi}{3}) \tag{4.18}$$

4.2.3 Representing the DP Solution in the EMT Model

The DP solution of the network is interfaced to the EMT model as a current source in parallel with an impedance. This is the typical way of representing component models in a nodal analysis based EMT simulation. The DP side of the network

takes voltages of the interface buses as the input and the external network is solved to find the injected currents. If the interfacing point to the EMT program has a transmission line there will be a three-phase capacitor (i.e. the capacitors resulting from a π-section model of a transmission line) connected to the interface bus. This is also an EMT type component modelled using the Dommel's algorithm. Dynamic phasor block contains the capacitors in the interface along with the dynamic phasor model of the rest of the external system. Then the total current to an interface node would be the addition of the current injection from the capacitor and the dynamic phasor model. And the impedance parallel to the total current will be equal to "$\Delta t/2C$". This concept is illustrated in Fig. 4.3 for a three port interface. Current injections from the DP model are represented as I_{dy1}, I_{dy2} and I_{dy3} and the current source values result from the capacitors are denoted as I_{cap1}, I_{cap2} and I_{cap3}.

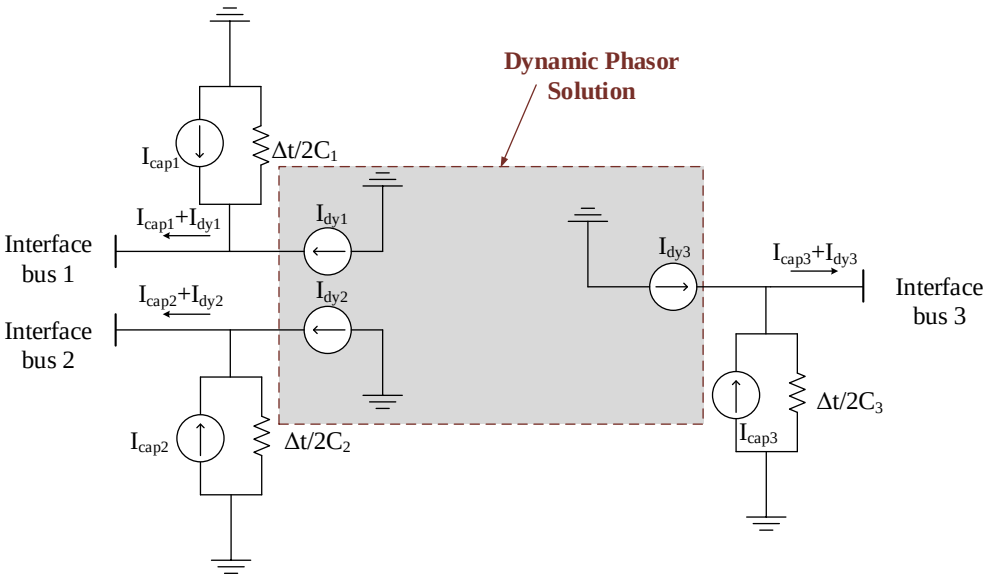

FIGURE 4.3: Implementing the DP solution as a Norton equivalent in the EMT model

The impedance of the Norton equivalent can be represented using a very large value when there is no transmission line at the interface points.

4.3 Implementation of the Proposed System in a Real-Time Platform

The steps of implementing the DP model in a real-time EMT simulation are summarized in this section. The RTDS is used as the real-time EMT simulation platform. The internal system is constructed using existing library components in RTDS. The DP model of the external system is a user-written model incorporated into RTDS as a single power system component. Hence, the EMT model and DP model run in parallel as separate network solvers in real-time. The DP part of the network is interfaced to the EMT model as a Norton equivalent. The current source value of the Norton equivalent is updated at every DP time-step. The EMT solution is represented in the DP model as a known boundary voltage at each time-step. The time-step delay of reading the boundary voltages from EMT model at the DP side is overcome by linear extrapolation of EMT interface bus voltages. Fig. 4.4 shows the block diagram of the complete EMT-DP co-simulation. In the figure, double line arrows indicate phasor quantities and single line arrows indicate three-phase quantities. The both EMT and DP simulations use the same time-step which is equal to $h_s = 50\,\mu$s. This is the typical time-step used in EMT simulations. The sequence of operation corresponding to Fig. 4.4 can be expressed as follows.

1. Let us say that both simulations start at $t = t_0$. EMT and DP run from t_0 to $t_0 + h_s$ at the first time-step. Any non-linear devices connected to the DP side (e.g. synchronous generators) will solve their state equations and calculate the interface bus voltages. Both models will solve the nodal equations for the internal and external systems respectively. DP model will convert its injected currents to the three-phase quantities.

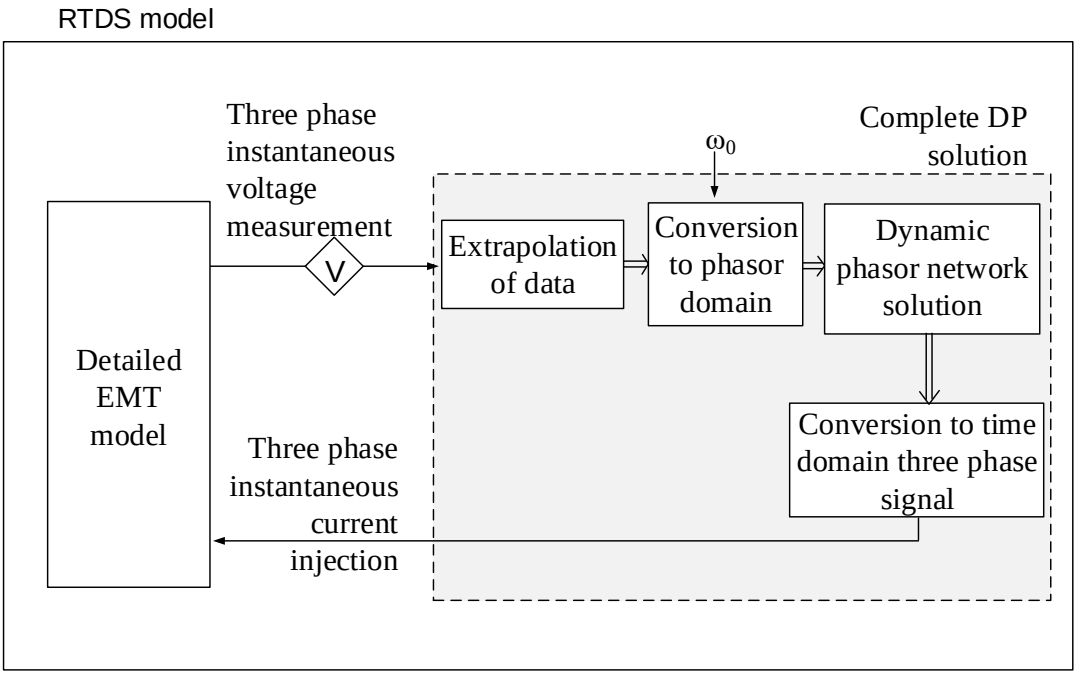

FIGURE 4.4: Block diagram of a single port of the proposed EMT-DP co-simulation model

2. At the end of every h_s time-step, EMT and DP exchange their solutions. Current injections to any non-linear devices are also updated at the DP model.

3. DP model will extrapolate the voltage input from the EMT side and it will convert the three-phase quantities to the phasor domain.

4. These steps are continued until the end of the simulation.

4.3.1 Test System and Simulation Hardware

The proposed interfacing approach is validated using the New England & New York 68 bus system (Appendix A.2). It contains two subsystems. Subsystem 1 is the simplified New York Power System (NYPS) and subsystem 2 is the New England 39 bus Test System (NETS). The system has 16 generators. NYPS and

NETS are connected through three transmission lines: from bus 53 to 54, from bus 53 to 27 and bus 61 to 60. A portion of New England & New York 68 bus case (shown in blue colour in Fig. 4.5 (A)) containing the buses 11, 30, 32, 33, 34, 38 are modelled using DP and the rest of the system is modelled as an EMT model. Buses 30, 34 and 38 are the interface buses connected to the EMT simulation. Therefore, this is a three port interface. The proposed method is, however, valid for any number of ports. Generator 11 in the DP side of the network is modelled using the voltage source type synchronous machine proposed in Chapter 3 Section 3.3.3. It was modelled without an exciter and a turbine model. Generator 10 in the EMT side of the network is replaced by a voltage source to fix the base frequency of the system to $60Hz$.

RTDS is a real-time EMT simulator with a custom-built parallel processing computer. It is developed specifically to carry out real-time EMT simulation. A unit of RTDS hardware is called a rack and it contains rack-mounted processor cards (i.e. GTWIF, PB5, GPC). The interface to the RTDS hardware is done through the software RSCAD. RSCAD software can be run in a general-purpose computer and it allows the user to build and run a simulation. The circuit construction is done in RSCAD/DRAFT and it contains a library of component models. A compiled draft is sent to RTDS hardware where it is processed. The monitoring of outputs and real-time control of simulation variables are done in RSCAD/RUNTIME. RSCAD/CBUILDER allows the user to develop their own component models to use in RSCAD/DRAFT. It can be used to create both power system and control system components. Power system components are directly connected to the power system. The output of a control type components is processed from the inputs from other components. The code for the component is developed using the c-language.

The components in the EMT side of the New England & New York 68

bus system are modelled using existing library components in the RSCAD library. The generator 1 in the EMT side is replaced by the CIGRE HVDC benchmark model . The CIGRE HVDC benchmark system is a mono-polar 500kV dc system with a rating of 1000MW. The single line diagram of the HVDC system and the network data are given in Appendix A.3. This model will allow us to use the EMT-DP co-simulation model to analyse HVDC system interactions with the power system. Fig. 4.5 (B) shows the relevant part of the RSCAD simulation case with the connection of the user-written DP component to the rest of the 68 bus system. The parameter "TIME" in the figure is used to send the simulation time into the DP model.

The New England & New York 68 bus system is simulated in RTDS using two RTDS racks. In this way, one RTDS rack is used to simulate one subsystem. Each of these racks contains five PB5 cards. The travelling wave delay in transmission lines connecting the two sub-systems (connecting bus 54 to 27, 54 to 53 and 60 to 61) are used to simulate the system in two different racks. The DP model is written using the CBUILDER software in RTDS. The DP component is implemented as a power system component. Therefore, it is connected to the network. In this case, there are three interface buses between EMT and DP. Therefore there are three physical connections (buses 30, 34 and 38) to the DP model from the EMT side. At each of these connection point, DP solution is modelled as Norton equivalents. Hence, inside the DP block shown in Fig. 4.5 (B), there are three Norton equivalents.

4.3.2 Simulation Results

The objective of the proposed co-simulation model is to study the dynamics in the network modeled using EMT. The entire New England & New York 68 bus

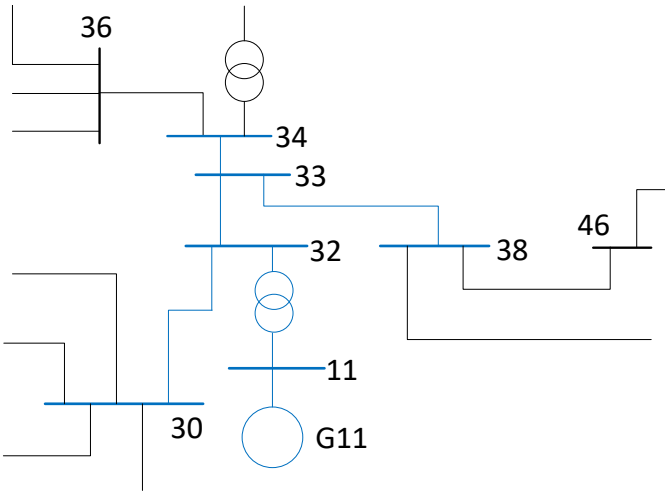

(A) The DP part of the New England & New York 68 bus system

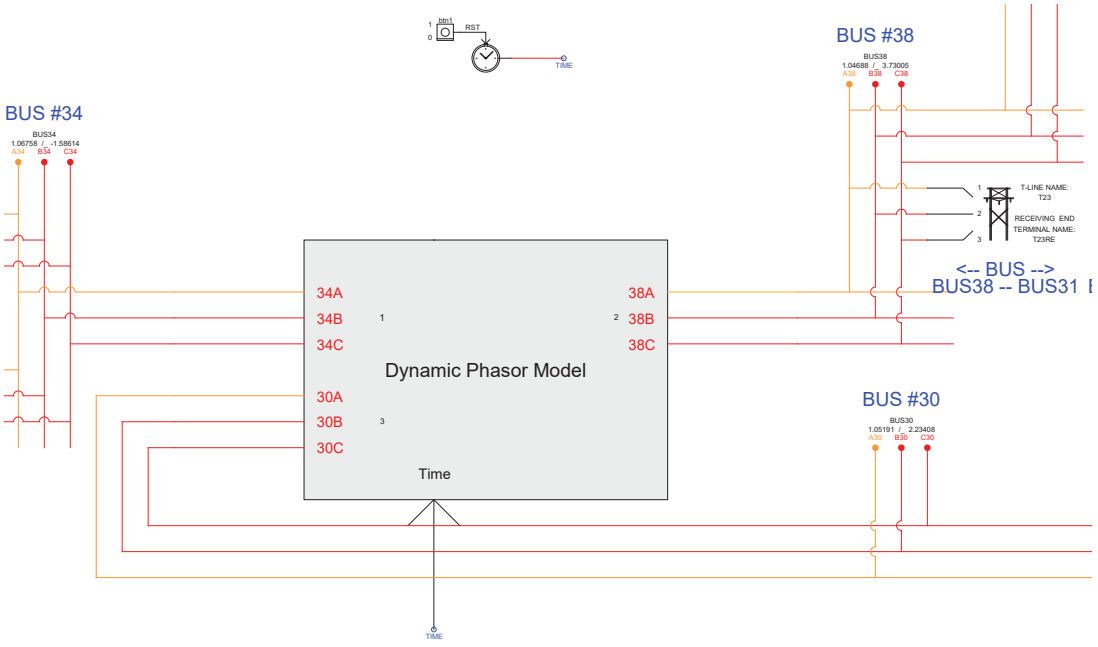

(B) Snapshot of RSCAD draft containing the DP model

FIGURE 4.5: DP part of the New England & New York 68 bus system

system is also modeled using EMT simulation in RTDS for comparison against the co-simulation model. Faults are applied at different locations of the 68 bus system to analyze the accuracy of the co-simulation model. The simulation is carried out using a time-step of 50 μs in both EMT and DP simulations. A three-phase fault (fault resistance is 0.1 Ω) is applied at $t = 5$ s for a period of five cycles at HVDC converter bus (bus 54). The voltage at bus 54 and the current through the DC line are shown in Fig. 4.6. The voltage of bus 30 which is one of the interface buses of EMT-DP shown in Fig. 4.7. The speed of the generator 8 which is the nearest generator to the HVDC in-feed is shown in Fig. 4.8. As can be seen from the figures, the co-simulation results closely match with the EMT simulation results.

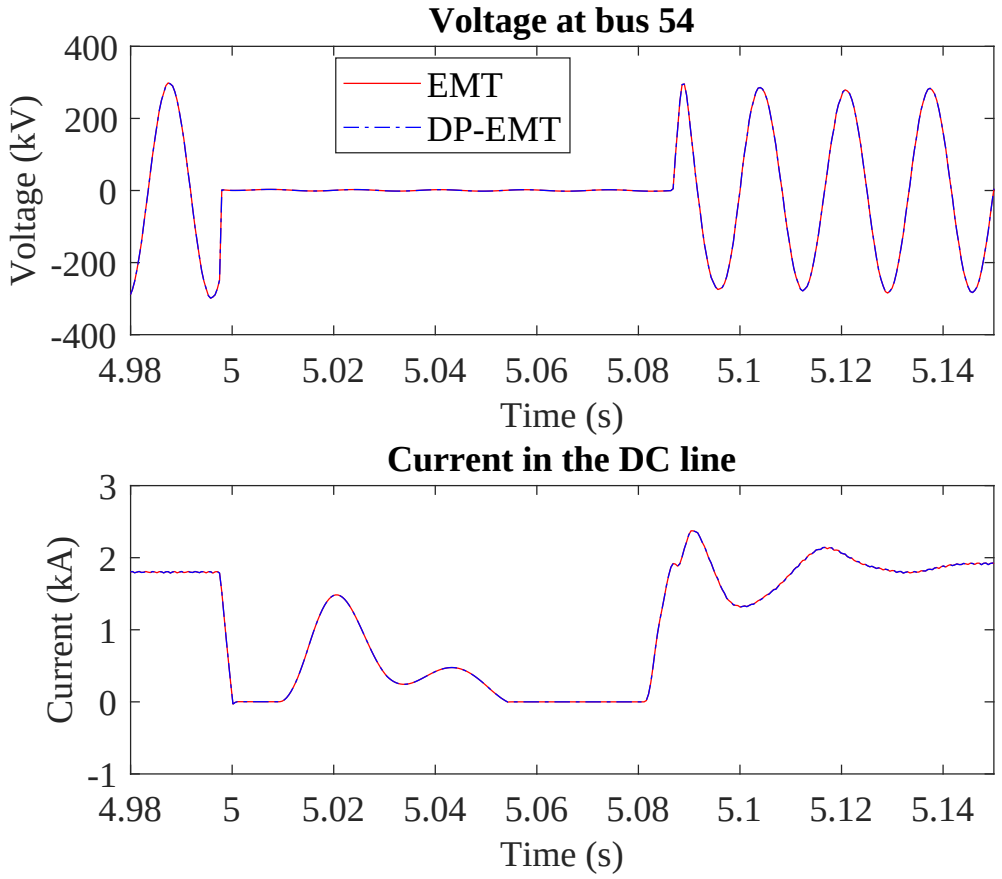

FIGURE 4.6: Comparison of inverter side voltage and DC current for a three-phase to ground fault at the converter bus

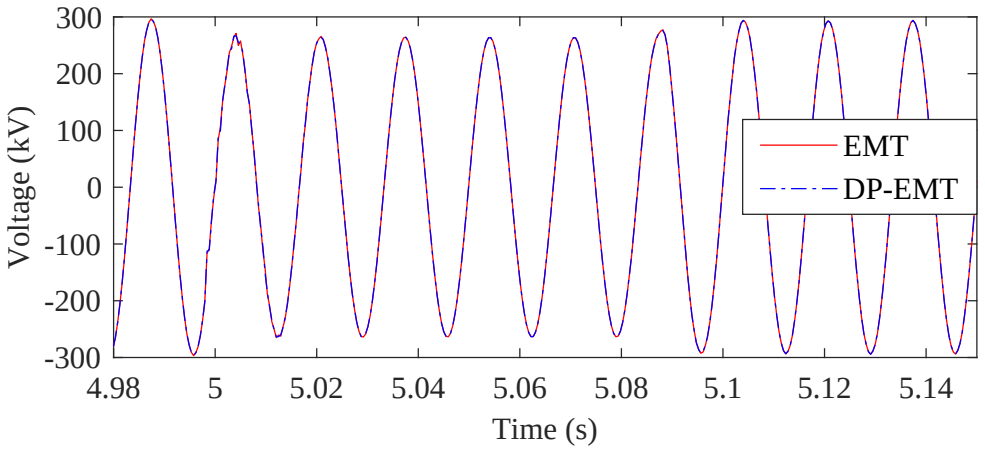

FIGURE 4.7: Comparison of bus 30 voltage for a three-phase to ground fault at the converter bus

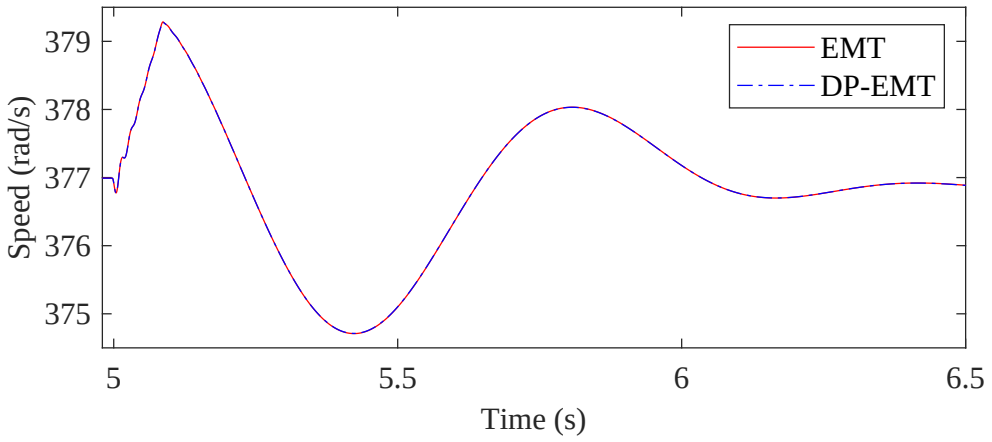

FIGURE 4.8: Comparison of generator 8 speed for a three-phase to ground fault at the converter bus

The three-phase fault is then applied at bus 38 which is one of the EMT-DP interface buses. Fig. 4.9 shows a comparison of the voltages of phase 'a' at the EMT-DP interface buses. The co-simulation voltages closely follow the shape of the EMT simulation results except for minor differences in voltage spikes during the transient. The phase 'a' line current from bus 36 to 34 and its magnitude are shown in Fig. 4.10 and 4.11. Fig. 4.10 shows the current during the transient and the results match with the EMT simulation results. Fig. 4.11 shows the current magnitude a few seconds after the fault, and it can be seen that the co-simulation

and EMT simulation results settle down at the same value. The electric torque and speed of generator 11 obtained with co-simulation are compared against EMT solution in Fig. 4.12. The generator 11 is in the DP part of the co-simulation model. This confirms that the results of co-simulation faithfully reproduce the results of the EMT simulation.

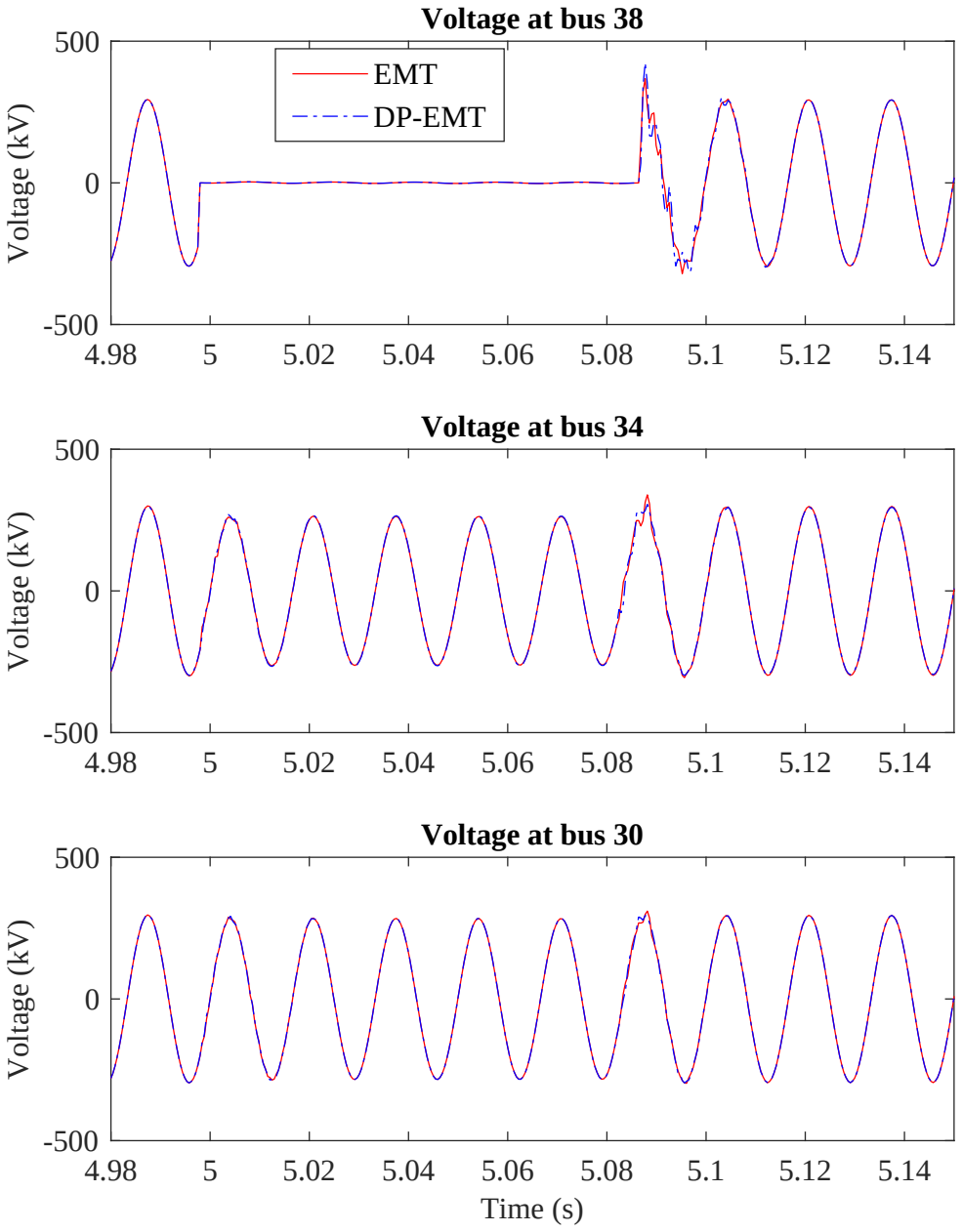

FIGURE 4.9: Interface bus voltages for a three-phase to ground fault at the interface bus 38

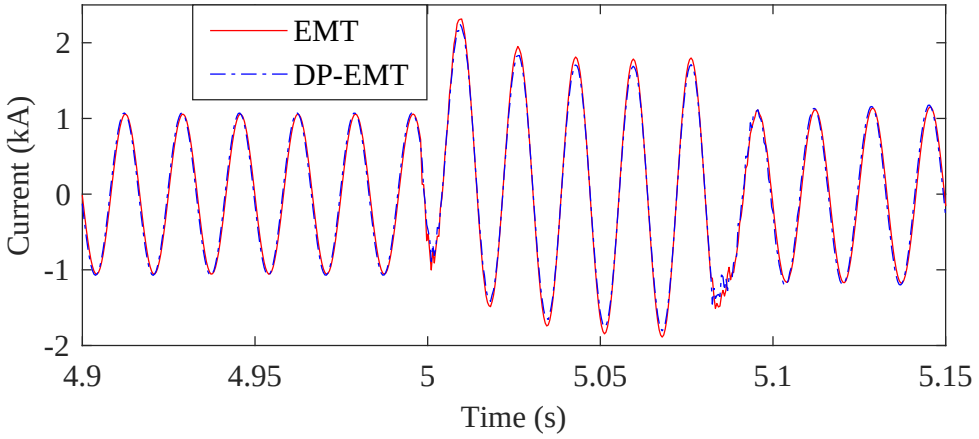

FIGURE 4.10: Current from bus 36 to 34 for a three-phase to ground fault at the interface

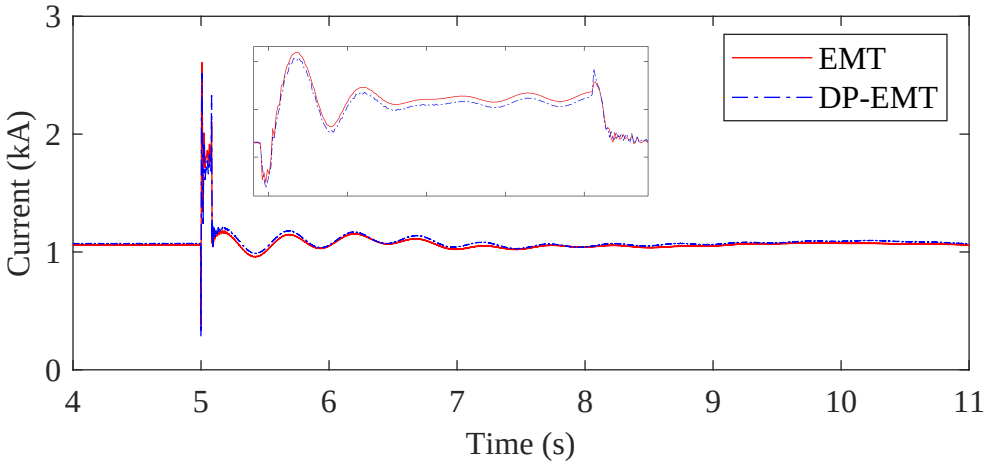

FIGURE 4.11: Current magnitude from bus 36 to 34 for a three-phase to ground fault at the interface

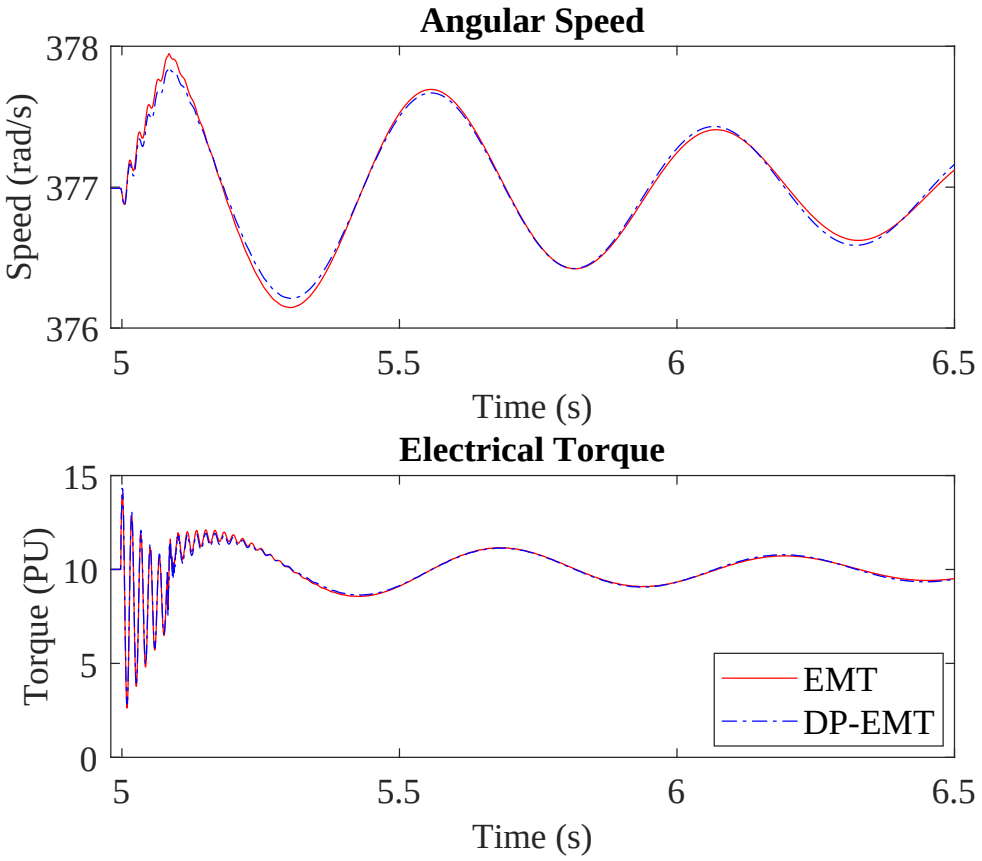

FIGURE 4.12: Comparison of speed and torque of generator 11 for a three-phase to ground fault at the interface bus 38

The co-simulation model was also validated by applying faults at different locations of the New England & New York 68 bus system. The results for a three-phase fault at bus 46 is shown in Fig. 4.13 to Fig. 4.15. As seen from the figures, co-simulation results agree with the complete EMT simulation results.

The robustness of the proposed interface was validated by moving the dynamic phasor part of the network to different locations in the 68 bus case.

It can be shown that when the system is unstable the co-simulation also simulates it as unstable. This scenario was created by removing a Power System Stabilizer (PSS). The magnitude of the current in the line between buses 36 and 34 is shown in Fig. 4.16. The results between EMT and DP-EMT agree up until

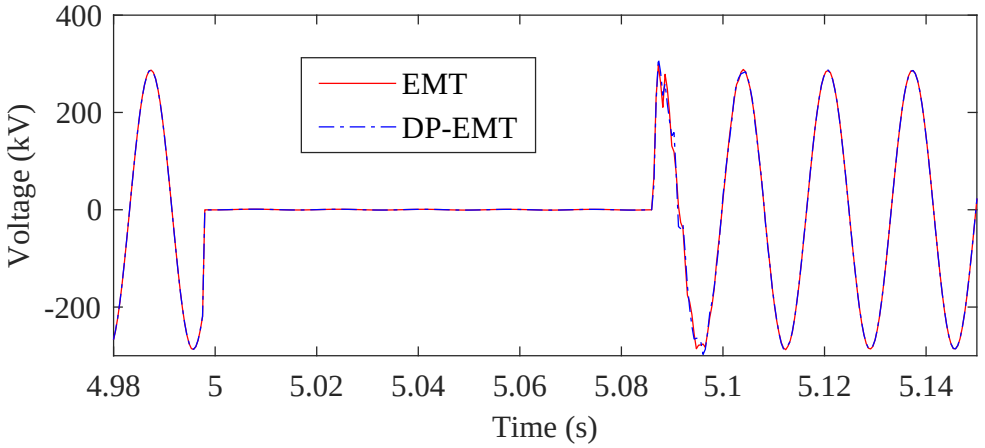

FIGURE 4.13: Phase A voltage at bus 46 for a three-phase to ground fault at bus 46

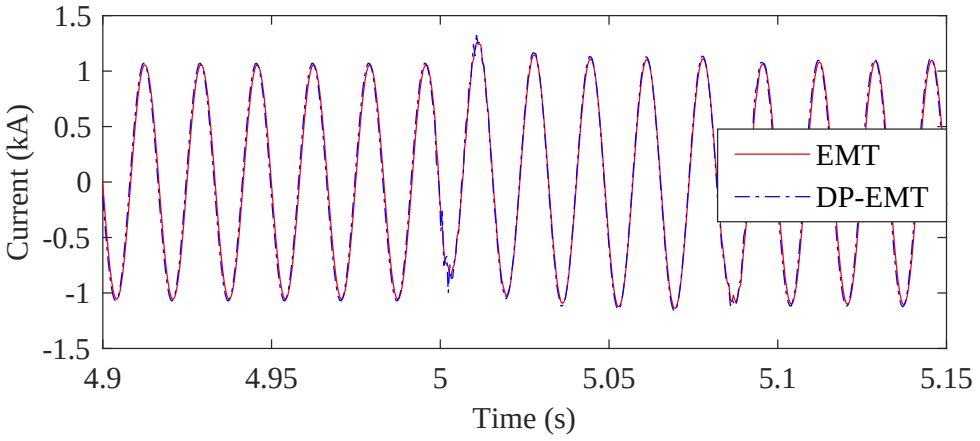

FIGURE 4.14: Phase A current from bus 36 to 34 for a three-phase to ground fault at bus 46

the first 13 seconds at which point the results begin to diverge. The difference between the EMT and DP-EMT for unstable scenarios is not a concern as their initial transients are accurately captured.

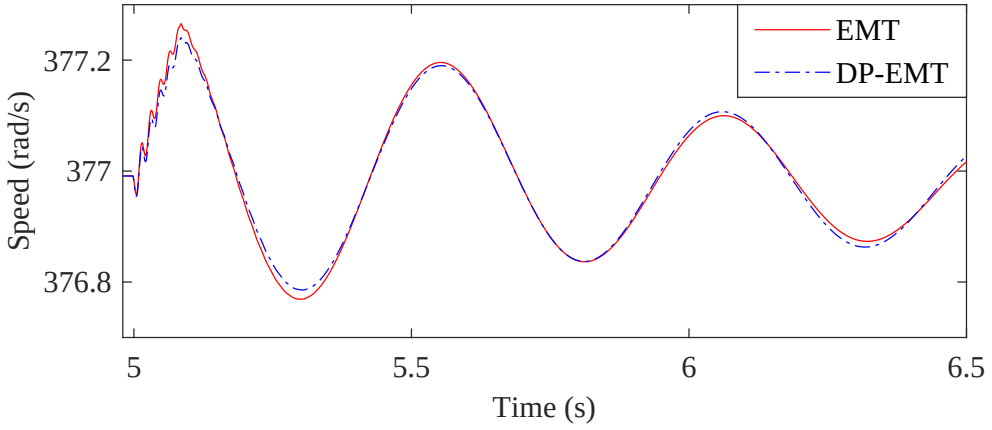

FIGURE 4.15: Comparison of speed of generator 11 for a three-phase to ground fault at bus 46

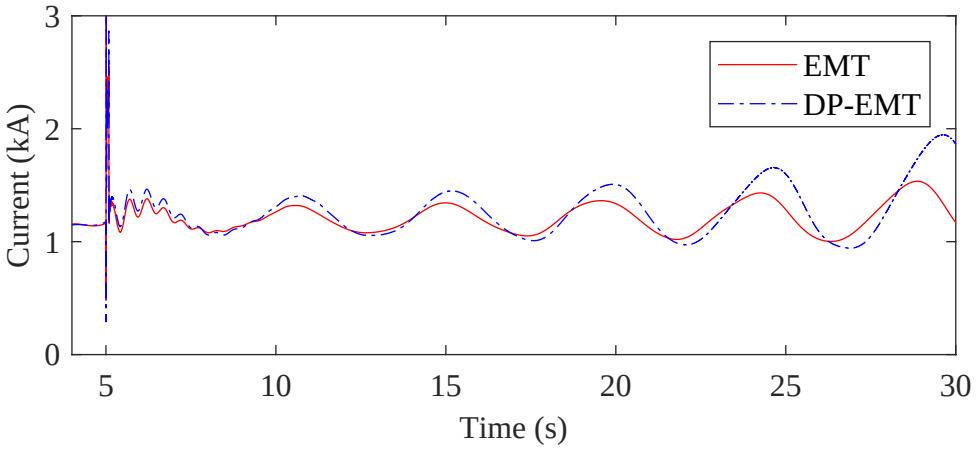

FIGURE 4.16: Line current of an unstable case for a three-phase to ground fault at the interface

4.3.3 Discussion

4.3.3.1 Computational Efficiency and Recommendations

A comparison of numerical efficiency of a DP simulation with an EMT simulation is carried out in this section. In the EMT simulation, currents and voltages are computed as three-phase quantities, whereas the proposed DP model uses single-phase quantities which therefore reduces the computational burden. However, the phasors in the DP model are complex signals unlike in the EMT simulation which

only considers real values. Assume that in EMT simulation, the inverse of the admittance matrix is computed only once at the beginning (in some implementations it is computed in every time-step). Then the computing burden in real-time simulation is predominantly for the multiplication of a square matrix by a column vector. The Floating Point Operations (flops) required to calculate the network solution ($\underline{V} = Y^{-1}\underline{I}$) for EMT and DP simulations for a system with n number of buses can be calculated as follows:

For the EMT system, the size of the admittance matrix is $3n \times 3n$ and the size of the current vector is $3n \times 1$. Matrix multiplication requires $9n^2$ multiplications and $(3n-1) * 3n$ additions giving $18n^2 - 3n$ total flops. For the DP network solution, the admittance matrix size is $n \times n$ and the size of the current vector is $n \times 1$. Each n sized row and vector multiplication results in n number of complex number multiplications and $n-1$ number of complex number additions. Multiplication of two complex numbers requires four multiplications of real numbers and two additions of real numbers. The addition of two complex numbers requires two real number additions. Therefore, for one row there will be $4n + 2n + 2(n-1)$ flops giving total flops of $8n^2 - 2n$ for n number of rows. For an example, consider a network of 50 buses. The EMT requires 44,850 flops whereas DP requires only 19,900 flops. The computations at the interface nodes do not depend on the size of the network and it depends only on number of interface nodes.

4.3.3.2 Limitations of the Proposed Model

The DP part of the co-simulation model is modelled using only positive sequence voltages and currents. Phase "A" to ground fault (fault resistance is 0.1 Ω) is applied at $t = 5\,\mathrm{s}$ for a period of five cycles at the interface bus 38. Fig. 4.17 shows the phase "A" and "B" voltages at bus 38. The phase "A" line current from bus

36 to 34 is shown in Fig. 4.18. As it can be seen from the figures that the co-simulation results closely follow EMT results. However, the accuracy of the model under an unbalance fault is case dependent. Therefore, to achieve robustness, the negative and zero sequence components of the voltages at the EMT interface buses have to taken in to account in the DP model.

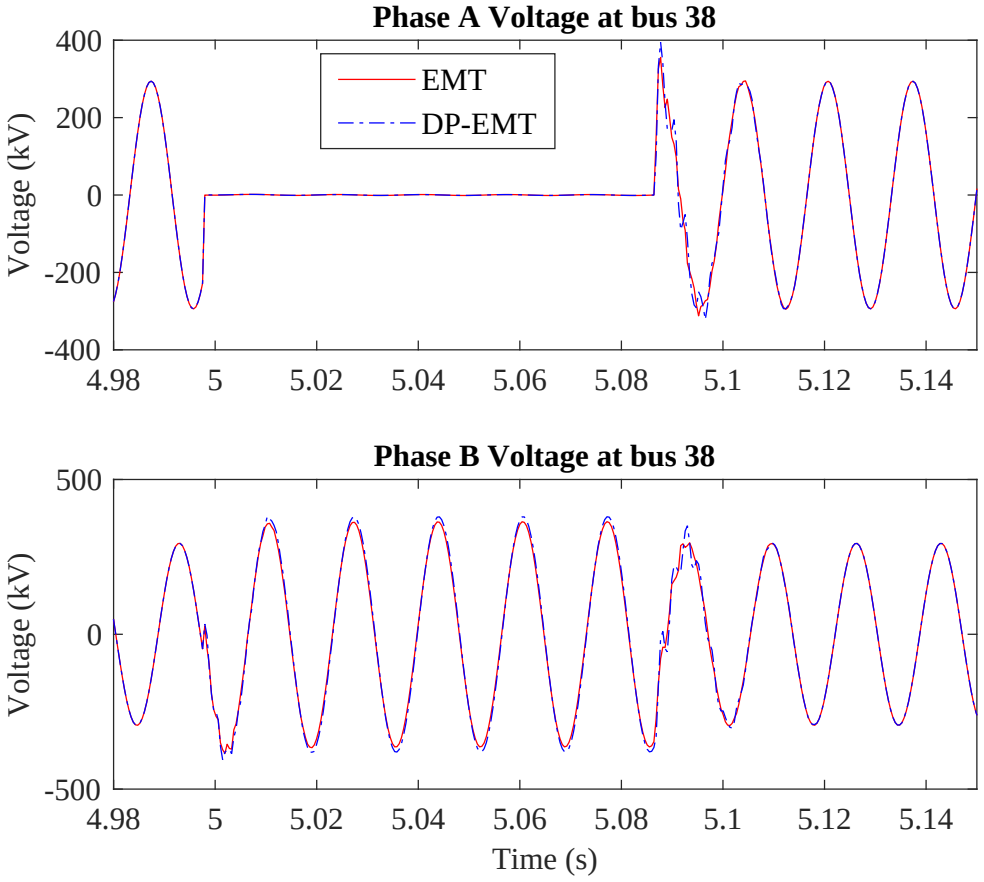

FIGURE 4.17: Voltages for a phase "A" to ground fault at bus 38

In order to gain more computational gain, the DP part can be implemented using a larger time-step. The proposed interface does not guarantee numerical stability when the DP side is simulated using a larger time-step. The simulation is numerically stable for DP time-step of 100 μs however a further increase of time-step made the simulation unstable. One of the reasons for instability

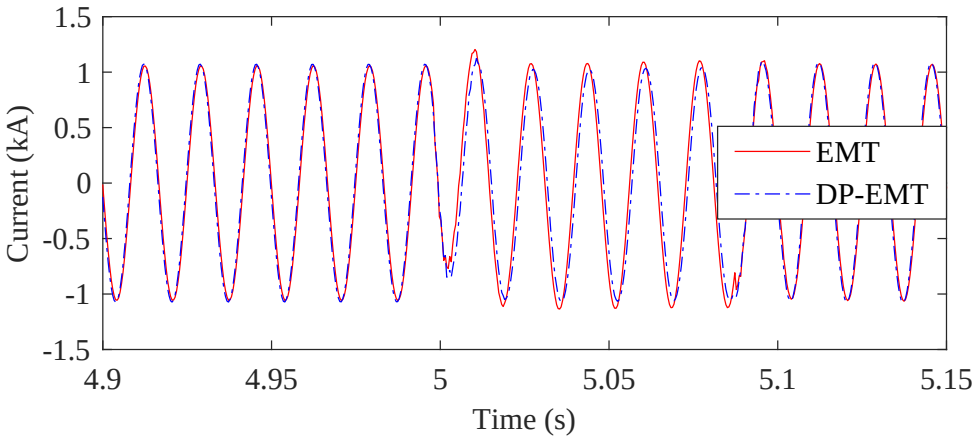

FIGURE 4.18: Phase A current from bus 36 to 34 for a phase "A" to ground fault at bus 38

could be the error in extrapolation of interface variables. In this thesis, the challenges of implementing DP using a larger time-step are not addressed since TS models are more appropriate to run using a larger time-step. For large networks, we recommend the use of DP as a surface layer that connects the TS simulation to the EMT model. This EMT-DP-TS co-simulation model will have a computational burden similar to an EMT-TS co-simulation model while avoiding the need for an FDNE. This will be presented in Chapter 5 and Chapter 6.

4.4 Summary

A real-time implementation of the EMT-DP co-simulation model in RTDS was presented in this Chapter. It was shown that the results of the co-simulation model closely follow the EMT simulation results. The efficiency of the model was compared to a typical EMT model. It was concluded that to increase the efficiency further it is appropriate to use a TS model to model the external system of the power system. A boundary between the external and the internal models can

be modelled using DP. The proposed EMT-DP-TS co-simulation model will be explained in the next two chapters.

Chapter 5

Real-Time Electromagnetic Transient and Transient Stability Co-Simulation Using a Dynamic Phasor Buffer Zone

5.1 Introduction

This Chapter presents the real-time EMT-TS co-simulation model suitable for analysing electromagnetic transients in a large power system. The co-simulation model contains an EMT model of the internal system and a TS model of the external system. A buffer-zone in the external system at the EMT-TS interface is modelled using dynamic phasors. The DP buffer zone replaces the need for an FDNE in a typical EMT-TS co-simulation. In this thesis, a multi-port buffer zone connecting EMT and TS simulations is modelled using DP. The buffer zone

contains transmission lines and loads but it is not limited to these components. The challenges of interfacing DP model to a real-time EMT model was discussed in Chapter 4. The same interface used in Chapter 4 is used to interface DP to EMT in EMT-TS co-simulation model. In this chapter, the challenges of interfacing DP to TS are discussed in Section 5.2.2. In the proposed method, EMT and DP are simulated using identical time-steps. However, the TS part of the simulation is carried out using a relatively larger time-step. The problems caused due to the use of different time-steps are discussed in Section 5.2.2. The basic components of the proposed co-simulation model are discussed in Section 5.3.

5.2 Interfacing Challenges of the Proposed Co-Simulation Model

Interfacing EMT and TS models as one simulation model is difficult due to their contrasting characteristics. Transient stability programs consist of simplified component models and focus only on low-frequency oscillations and therefore use a larger integration time-step compared to EMT programs. Interfacing different simulations can be challenging due to reasons such as (a) different frequency bandwidth, (b) time-step delay between the models, and (c) different integration time-steps. Any numerical inaccuracies due to the difference in the frequency bandwidth of EMT and TS models are mitigated by the DP buffer zone. However, this results in two interfaces instead of one (i.e. EMT-DP and DP-TS). The numerical stability of both of these interfaces has to be ensured for a robust EMT-TS co simulation model.

5.2.1 Achieving a Numerically Stable EMT-DP Interface

The challenges of interfacing DP to EMT was discussed in Chapter 4. The numerical instability due to time-step delay was addressed using the linear extrapolation method. The same interface technique is used to interface DP to EMT in the EMT-TS co-simulation model.

5.2.2 Achieving a Numerically Stable DP-TS Interface

The TS part of the network is simulated using a much larger integration time-step than the DP model. Similar to the EMT model, voltages and currents in the DP model change much faster compared to that of the TS model. If these two models run at two different time-steps, the response of the TS model corresponding to a change that occurs in the DP model will arrive at the DP model after many DP time-steps. For example, if the ratio of time-steps of TS and DP is 100 the DP model has to wait for 99 DP time-steps to see a change in the TS model corresponding to a change in the DP model. This could result in numerical instability in a real-time simulation.

Let us define the time-step of DP as h_s and the time-step of TS as h_t. It should be noted that h_t is much larger compared to h_s. A large time-step in the TS side results in instability problems when interfacing the two models [23]. In Chapter 3 of this thesis, it was shown that depending on the input impedance of TS and DP models, the interface can only be stable either as a voltage source or as a current source. However, this theory does not hold when one of the DP or TS components is modelled using a larger time-step. Section 5.2.2.1 below is added to clarify this further.

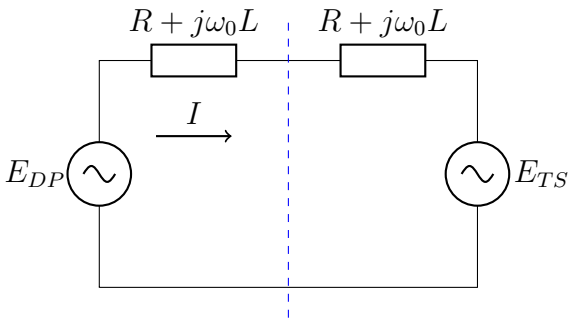

FIGURE 5.1: Simple network to analyse numerical stability for two different integration time-steps

5.2.2.1 Analysis of Requirements for Numerical Stability When Interfacing Different Time-Step Models

Let us use the simple circuit shown in Fig. 5.1 to represent the TS and DP models with each having a voltage source and an RL branch. The circuit parameters are given in Table 5.1.

TABLE 5.1: Circuit parameters for Fig. 5.1

	DP	**TS**
Voltage source magnitude	230 kV	221.8 kV
Voltage source angle	0	30^0
R	1 Ω	1 Ω
L	0.01 H	0.01 H

The simulation is carried out few times by changing the ratio of h_t/h_s. A fixed time-step of 50 μs is used at the DP side. Time-step of the TS side is changed at each simulation and the current (I) in the circuit is plotted. Fig. 5.2 shows results with different time-step ratios of DP-TS simulation. Fig. 5.2-(a) shows the results for h_t/h_s ratio of 1, Fig. 5.2-(b) shows the results for h_t/h_s ratio of 5, Fig. 5.2-(c) shows the results for h_t/h_s ratio of 10 and Fig. 5.2-(d) shows

the results for h_t/h_s ratio of 20. As it can be seen from the figure, higher the time-step ratio more closer the system will be to the numerical instability. This proves that communication of interface data only in the TS time-step could lead the simulation to go unstable.

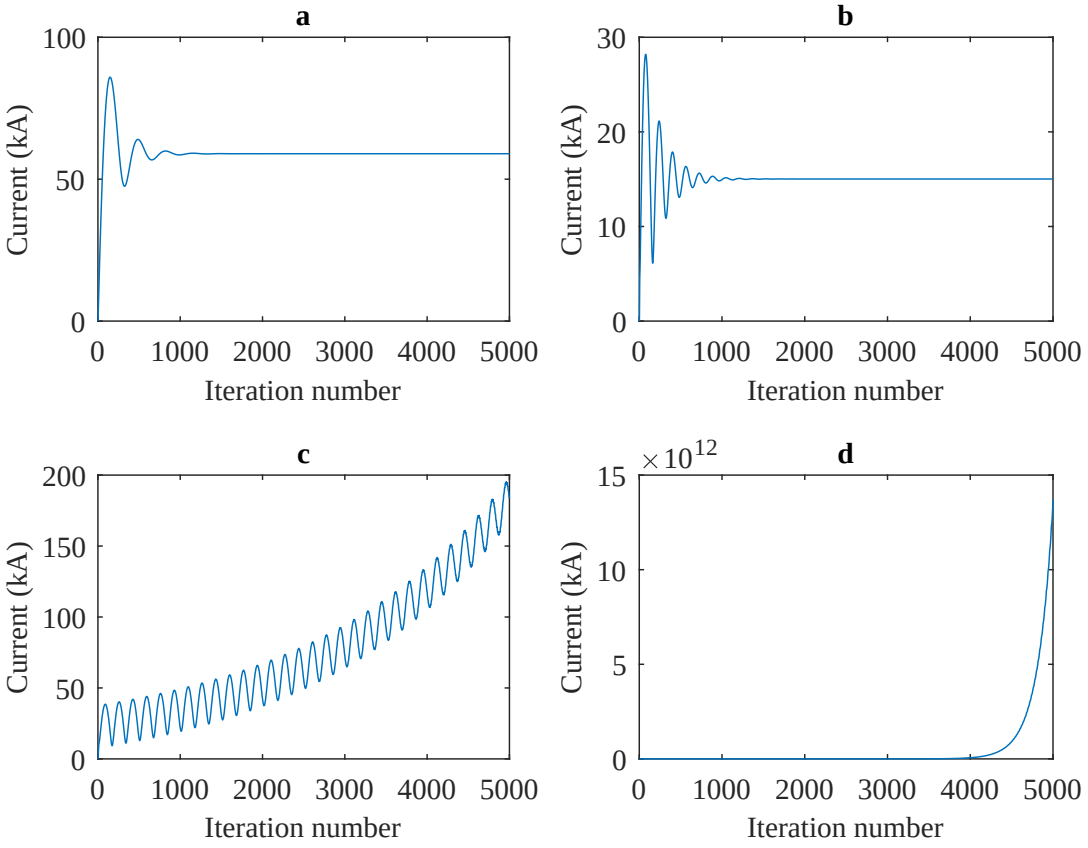

FIGURE 5.2: Results for different time-step ratios: (a) $h_t/h_s = 1$, (b) $h_t/h_s = 5$, (c) $h_t/h_s = 10$, (d) $h_t/h_s = 20$

Further studies revealed that the ratio of the impedances between the TS and DP models impacts the numerical stability for a particular time-step ratio. Let us define the impedance at the DP side as Z_{DP} and impedance at the TS side as Z_{TS}. Fig. 5.3 shows the results with different impedance ratios between DP and TS. Fig. 5.3-(a) shows the results for Z_{DP}/Z_{TS} ratio of 3 and Fig. 5.3-(b) shows the results for Z_{DP}/Z_{TS} ratio of 6 for the same unstable case with h_t/h_s ratio of 20. The simulation becomes more stable with higher impedance at the

DP side. However, changing the impedance of the two sides of the interface will restrict the user on their freedom to partition the network. Therefore, the most reliable solution would be to update boundary voltages at every h_s time-step for numerical stability since we cannot control the values of Z_{DP} and Z_{TS}. However, doing so will increase the computation burden of the TS model.

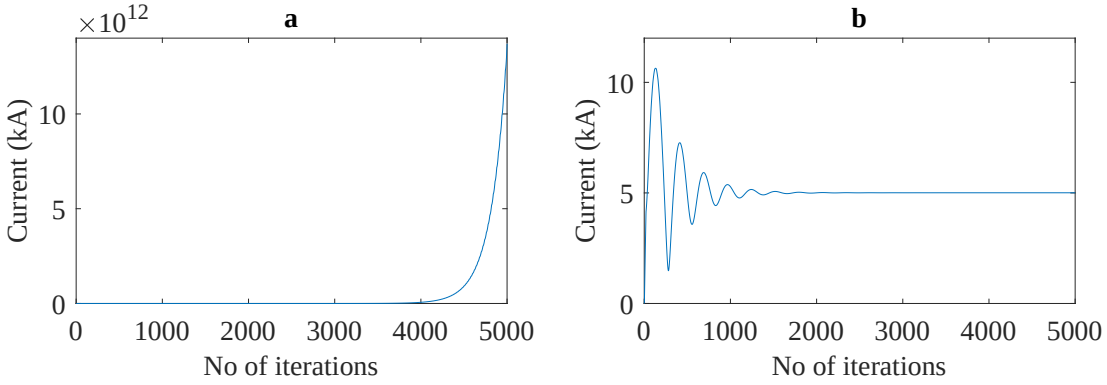

FIGURE 5.3: Results for different impedance ratios with time-step ratio of $h_t/h_s = 20$: (a) $Z_{DP}/Z_{TS} = 3$, (b) $Z_{DP}/Z_{TS} = 6$

The numerical stability of many EMT-TS co-simulations that run in parallel is achieved by using iterations with data predictions in the TS model [23]. In a real-time simulation, the calculations for one time-step should be completed in actual clock time. Even though, the entire TS simulation does not take much time it does not guarantee that the iterative algorithm will converge during the period of a time-step. The reason for this is that the calculations in some time-steps can take a longer time and the iterative algorithm would require appropriately long time to converge. Therefore, iterative approaches are not recommended in a real-time simulation environment.

Hence, in this work, an additional step is incorporated into the DP solution to calculate the boundary bus voltages using the relevant elements of the TS admittance bus matrix and currents in the DP-TS boundary. The calculations for this step is given in Section 5.2.4. This step will enforce the DP model to receive

an update from the TS side at every DP time-step. However, the majority of the TS model calculations are done using the TS time-step.

5.2.3 Solution Algorithm

All simulations run in parallel and after each time-step, the solution of each simulation model is sent to the connected model. In EMT model, the DP side is represented as a current source at each boundary bus. At every time-step, current source values are updated using the DP solution. In the DP model, the EMT side is modelled as a voltage source. Voltages at the boundary buses are calculated at each time-step in EMT and sent to the DP model.

The conversion of three phase instantaneous values to phasor domain is done using the alpha-beta conversion explained in Chapter 4. The phasor solution of the DP model is transformed back to the three-phase instantaneous signal as $V_a = V_m sin(\omega_0 t + \theta)$, $V_b = V_m sin(\omega_0 t + \theta - \frac{2\pi}{3})$ and $V_c = V_m sin(\omega_0 t + \theta + \frac{2\pi}{3})$, where V_m is the magnitude and θ is the angle of the phasor signal.

Interfacing a DP model to a TS model is straightforward since they both are phasor models. In the TS model, the DP side is represented as a current source. In the DP model, the TS side is modelled as a voltage source.

5.2.4 Calculation of Transient Stability Boundary Bus Voltages Inside the Dynamic Phasor Model

As mentioned before in Section 5.2.2.1, an additional calculation step is added to the DP model to mitigate any negative effects coming due to the different time-step used in the TS side. Let us consider that the number of boundary buses

connected to DP is "n", number of machines connected nodes in TS model is "m" and number of internal nodes in the TS model is "k". The network solution of a system with $n + m + k$ order is shown in (5.1). The voltage and current vectors are as given in (5.2) and (5.3).

$$\underline{V} = Y^{-1}\underline{I} \tag{5.1}$$

$$\begin{aligned}\underline{V} = [V_{p1} \quad V_{p2} \quad \cdots \quad V_{pn} \quad V_{q1} \quad V_{q2} \quad \cdots \quad V_{qm} \\ V_{r1} \quad V_{r2} \quad \cdots \quad V_{rk}]^T\end{aligned} \tag{5.2}$$

$$\begin{aligned}\underline{I} = [I_{p1} \quad I_{p2} \quad \cdots \quad I_{pn} \quad I_{q1} \quad I_{q2} \quad \cdots \quad I_{qm} \\ I_{r1} \quad I_{r2} \quad \cdots \quad I_{rk}]^T\end{aligned} \tag{5.3}$$

The inverse of the admittance bus matrix can be represented as (5.4) where $[Z_{pp}]$ contains the impedances corresponding to DP interface buses, $[Z_{qq}]$ contains the impedances corresponding to generator buses and $[Z_{rr}]$ contains the impedances corresponding to TS internal nodes.

$$Y^{-1} = \begin{bmatrix} [Z_{pp}]_{n\times n} & [Z_{pq}]_{n\times m} & [Z_{pr}]_{n\times k} \\ [Z_{qp}]_{m\times n} & [Z_{qq}]_{m\times m} & [Z_{qr}]_{m\times k} \\ [Z_{rp}]_{k\times n} & [Z_{rq}]_{k\times m} & [Z_{rr}]_{k\times k} \end{bmatrix} \tag{5.4}$$

Let us partition the current vector as $\underline{I}_p$, $\underline{I}_q$ and $\underline{I}_r$, where $\underline{I}_p = [I_{p1}I_{p2}...I_{pn}]^T$ is the vector containing current injections from the DP side and $\underline{I}_q = [I_{q1}I_{q2}...I_{qm}]^T$ is the vector containing the machine currents in the TS model. The vector $\underline{I}_r = [I_{r1}I_{r2}...I_{rk}]^T$ contains the current injections in the internal nodes at the TS side. The voltage vectors also follow the same naming order and $\underline{V}_p = [V_{p1}V_{p2}...V_{pn}]^T$, $\underline{V}_q = [V_{q1}V_{q2}...V_{qm}]^T$ and $\underline{V}_r = [V_{r1}V_{r2}...V_{rk}]^T$. The voltages at the boundary bus at time t can be written as:

$$\underline{V}_p(t) = Z_{pp}\underline{I}_p(t) + Z_{pq}\underline{I}_q(t) + Z_{pr}\underline{I}_r(t) \tag{5.5}$$

During one TS time-step, The values of $\underline{I}_q(t)$ and $\underline{I}_r(t)$ do not change. The value of $\underline{I}_q(t)$ is updated only when the state equations of the machines in the TS side are solved and it happens only at every TS time-step. The internal currents in the TS side ($\underline{I}_r(t)$) are equal to zero. The value of $\underline{I}_p$ changes in every DP time-step. Therefore, the voltage vector at $t = t + h_s$ can be written as:

$$\underline{V}_p(t + h_s) = Z_{pp}\underline{I}_p(t + h_s) + Z_{pq}\underline{I}_q(t) + Z_{pr}\underline{I}_r(t) \tag{5.6}$$

As $\underline{I}_q(t + h_s) = \underline{I}_q(t)$ and $\underline{I}_r(t + h_s) = \underline{I}_r(t)$. By subtracting (5.6) from (5.5),

$$\Delta\underline{V}_p = \underline{V}_p(t + h_s) - \underline{V}_p(t) = Z_{pp}\left(\underline{I}_p(t + h_s) - \underline{I}_p(t)\right) \tag{5.7}$$

$$\Delta\underline{V}_p = Z_{pp}\Delta\underline{I}_p \tag{5.8}$$

Where $\Delta\underline{I}_p = \underline{I}_p(t+h_s) - \underline{I}_p(t)$ is the change in DP-TS boundary currents in a DP time-step. $\Delta\underline{I}_p$ can be calculated by comparing the injected currents from the DP side to TS in consecutive DP time-steps. Therefore, (5.8) is solved in every DP time-step (h_s) and $t \neq jh_t$; where j is a positive integer and h_t is the time-step of the TS model. In every DP time-step, the DP-TS boundary bus voltages are updated by adding the term ΔV calculated in (5.8). In this way, the DP side DP-TS boundary voltages are updated at every DP time-step. The number of calculations needed to solve (5.8) is independent on the number of nodes in TS but depends on the number of TS-DP boundary buses. For example, if there are four boundary buses between TS and DP with shunt impedances and transfer impedances on the buses, the calculation involves only a 4^{th} order complex matrix to vector multiplication. Therefore, the extra calculation step would not add much computational burden to the proposed co-simulation model.

5.2.5 Implementing Transient Stability Model in a Real-Time Platform

The TS model proposed for the co-simulation is similar to commercially available transient stability programs. Therefore, it can be replaced by using an existing TS program. However, for this research, a transient stability model is developed from the scratch and it is implemented in the RSCAD software as a user-written model. The developed model does not use any iterations and it is modelled using an integration time-step of 5 ms. The modelling steps are summarized below:

- The TS network is modelled using a constant admittance matrix and the network voltages and currents are calculated by solving the algebraic equation $\underline{V} = Y^{-1}\underline{I}$.

- The transmission lines in the TS side are implemented as π-section models with inductors and capacitors having constant impedances.

- The synchronous machines in the TS part of the system are modelled as 6^{th} order models by neglecting the dynamics of the stator winding flux. Generic machine model with two stator windings, one field winding in d-axis, one damper winding in d-axis and two damper windings in the q-axis (GENROU type synchronous machine model) is considered. The equations defining the machine model are given by (3.9) to (3.16). The synchronous machine is modelled as a voltage behind the sub-transient impedance model shown in (Fig. 3.6) [37]. The impedance $R_a + jX''$ is included in the network admittance bus matrix and sub-transient voltage E'' is considered as a boundary voltage. In this way, an additional node per machine is added to the network. After calculating the network solution, the currents of the machines can be calculated. As an example, considering (5.1) to (5.4) for

the system of $n + m + k$ order, the current injections to the machine nodes can be calculated as (5.9):

$$\underline{I}_q = Z_{qq}^{-1}\underline{V}_q - Z_{qq}^{-1}Z_{qp}\underline{I}_p \tag{5.9}$$

- The current injections from the DP model to the DP-TS boundary are represented as current sources in the TS solution. And for the same system, the voltage injections for the DP-TS boundary from the TS model can be calculated using (5.10).

$$\underline{V}_p = Z_{pp}\underline{I}_p + Z_{pq}\underline{I}_q \tag{5.10}$$

- Any non-linear devices that are in the TS side can be represented either as a voltage source or a current source in the model. In this way, the network impedance matrix stays constant and the inversion of the matrix has to be calculated only at the beginning of the simulation. As an example, a constant power (PQ) load connected to a node can be represented as a current source using the node voltage of the previous time-step (e.g. $I_{pq}(t) = (\frac{S}{V(t-\Delta t)})^*$), where I_{pq} is the currents source value, S is the apparent power $(P + jQ)$ of the PQ load and $V(t - \Delta t)$ is the node voltage calculated in the previous time-step.

The block diagram of the TS solution is shown in Fig. 5.4. The non-linear devices in the TS network can either be modelled as a current source or a voltage source, therefore, the arrows corresponding to that are represented with arrowheads in both sides in the diagram.

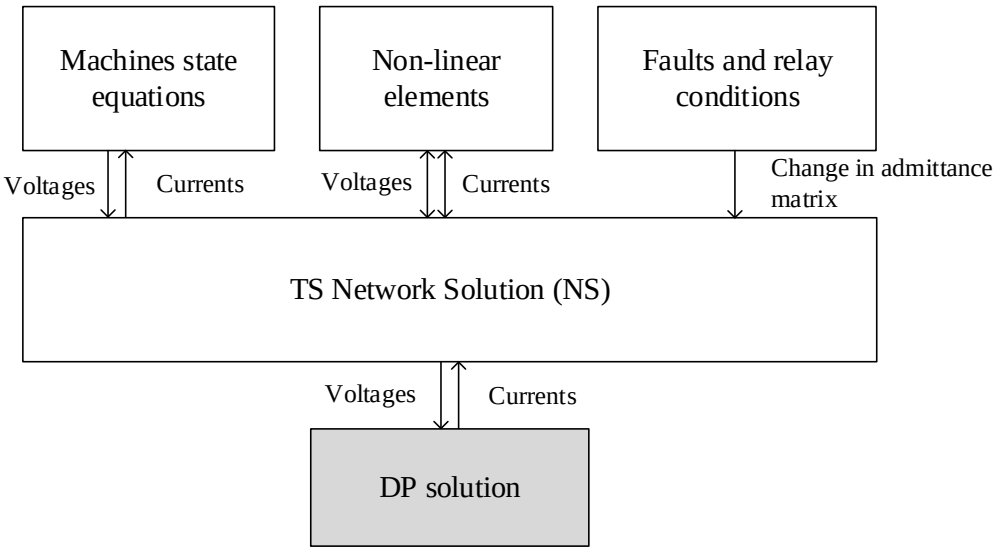

FIGURE 5.4: Block diagram of the TS solution

5.3 Proposed Co-simulation Model

The complete Block diagram of the proposed co-simulation platform is shown in Fig. 5.5. EMT solution and DP solution use a typical EMT time-step and the TS model uses a larger time-step. The parameters ΔI_{BDR} and ΔV_{BDR} are the DP-TS boundary currents and voltages in (5.8). Parameters V_{abc} and I_{abc} are the voltages and currents in the boundary nodes of EMT and DP. The TS side can also be replaced by any commercially available transient stability software such as PSS/E.

5.3.1 Data communication Between the Models

In the proposed method, EMT and DP use same integration time-step. Typically in EMT simulations, the time-step vary between 2 μs to 50 μs. In this work, $h_s = 50\,\mu$s is used in both EMT and DP simulations. In TS simulation, $h_t = 5\,$ms is used, which is a value commonly used with large-scale TS simulations. Since

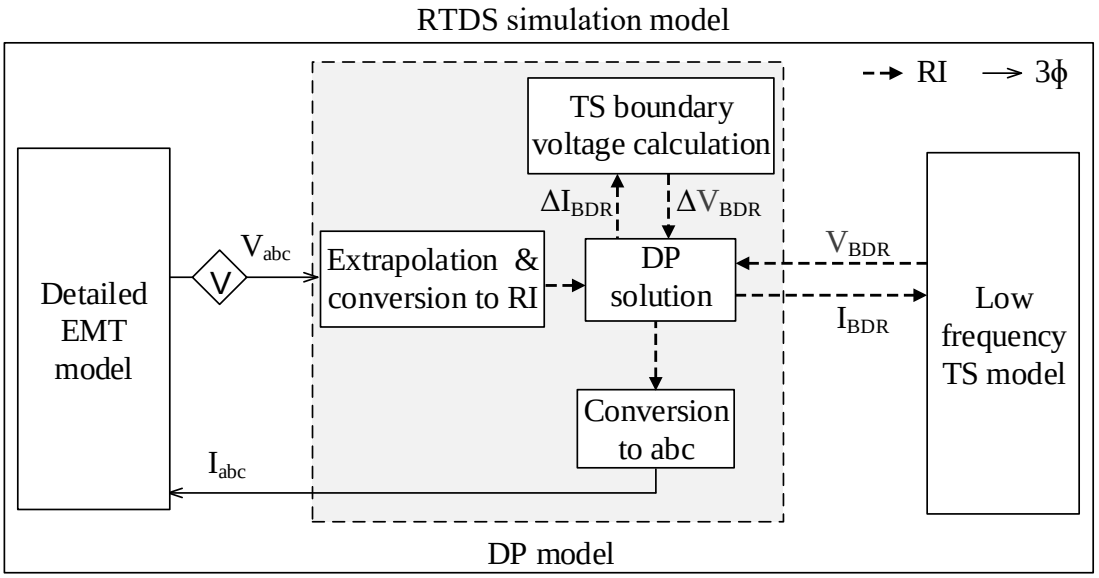

FIGURE 5.5: Block diagram of the proposed EMT-TS co-simulation platform

TS time-step is different from the EMT and DP time-step, the data transfer is performed as described below for proper coordination. The sequence of operations referring to Fig. 5.5:

- Let us say that all simulations start at $t = t_0$. EMT and DP run from t_0 to $t_0 + h_s$ at the first time-step. Both models will solve the nodal equations for the internal and buffer zone respectively. DP will also calculate the boundary voltages of TS boundary using (5.8).

- At the same time, TS model starts its run from t_0 to $t_0 + h_t$. It will solve any state equations in the external system and solve the algebraic equation $V = Y^{-1}I$.

- At the end of every h_s time-step, EMT and DP exchange their solutions. The voltages and currents are updated corresponding to the TS boundary calculation (ΔV_{BDR} and ΔI_{BDR}).

- At the end of every h_t time-step, the TS side will transfer the boundary voltages (V_{BDR}) calculated from the network solution to the DP side. Also, the DP side will transfer the calculated current injections (I_{BDR}) of the boundary to TS side.
- At the end of every integer multiples of h_t, "TS boundary voltage calculation" in the DP side is bypassed, as TS has new values of voltage injections (V_{BDR}).
- These steps are continued until the end of the simulation.

5.4 Summary

The main building blocks of the EMT-TS co-simulation model with a DP buffer zone was presented in this chapter. The network models of EMT, DP and TS were explained. The details of implementing the DP-TS interface in real-time were presented. The validation of the proposed co-simulation model is presented in the next chapter.

Chapter 6

Testing and Validation of the Co-simulation Model

This chapter presents the implementation and testing of the proposed real-time EMT-TS co-simulation model. The proposed model contains a buffer zone of a part of the external system modelled using dynamic phasors connecting the EMT and TS models. The co-simulation model is implemented in RTDS using the New York & New England 68 bus system. An LCC HVDC [57] in-feed is added to the system to analyse the interactions of the HVDC system with the rest of the power system. The results are validated using a complete EMT simulation, which is the best possible benchmark to compare results of the co-simulation model. It is shown that the co-simulation model produces matching results with the EMT simulation results under disturbances applied in the internal system.

6.1 Test System and Simulation Hardware

The New England & New York 68 bus system (Fig. 6.1) used in Chapter 4 is used as the test case for the proposed EMT-TS co-simulation model. The test system data are given in Appendix A.2. The subsystem containing NETS is considered as the internal system and modelled using an EMT model. The NYPS is considered as the external system. The network containing the buses 61, 53, 47, 48, 40, 30, 36, 31 and 32 is simulated using DP (thick red color lines). These buses define the buffer zone connecting the external system to the internal system. The Rest of the NYPS is modelled using the TS model. Buses 61 and 53 are the interface buses between EMT and DP. Buses 36, 32, 31 and 40 are the interface buses between DP and TS. Generators 1 to 8 except the generator 6 are modelled using a detailed machine model with the stator winding dynamics [1]. Generator 6 in the internal system is replaced by a voltage source to fix the base frequency of the system to 60 Hz. Transmission lines in the EMT model are modelled using the Bergeron line model. Generators 10 to 16 in the TS part of the network are modelled using the simplified machine models neglecting the stator winding dynamics. These machines operate using a constant field voltage (E_{fd}) and a constant mechanical torque (T_m). The transmission lines in the DP and TS models are modelled using π-section models. In DP, the transmission lines are modelled incorporating network dynamics whereas, in TS, constant admittances are used to model the capacitors and inductors. The modelling steps and interfacing methods were discussed in the previous chapter.

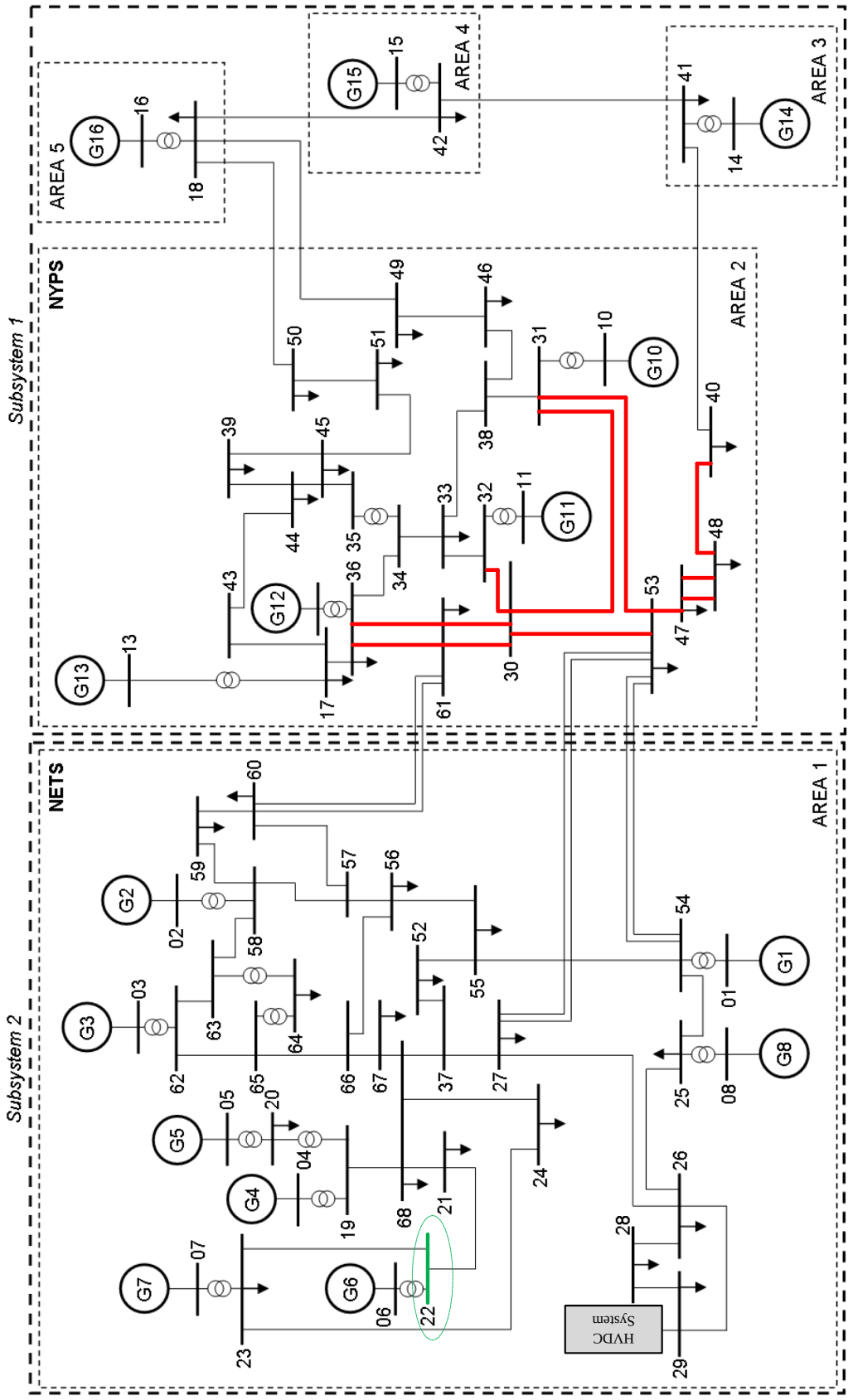

FIGURE 6.1: New England & New York 68 bus system

Let us assume that there is a plan to replace the generation at bus 29 in NETS using an LCC HVDC in-feed. The objective of the study would be to analyse the performance of the HVDC system. One of the many applications of an EMT-TS co-simulation is to analyse HVDC interactions on the power system. Evaluation of the impact on the AC system and the testing HVDC control performance during Factory Accepting Tests (FAT) are some of the examples. Considering the fast dynamics and harmonics associated with the HVDC, it is more appropriate to model the system around the HVDC in an EMT environment. The HVDC in-feed is modelled using the CIGRE HVDC benchmark with a rating of 1000MW. The single line diagram and the network data are given in Appendix A.3. A small number of filters are added at the rectifier and the inverter terminals. In a typical power system, the Total Harmonic Distortion (THD) at the terminal is kept below 1.5% [58]. In the test system, it is kept at around 3.4% purposely to have a significant amount of harmonics injected to the system. This is done by removing the filters at the inverter end. This will allow us to analyse the performance of the co-simulation model in the presence of harmonics in the system.

The co-simulation model is implemented in RTDS from existing library components and user-written components. A description of RTDS hardware and software was given in Chapter 4 Section 4.3.1. The dynamic phasor model of the buffer zone was implemented as a power system component and the TS model containing the rest of the external system is modelled as a control system component in RTDS. The user-written DP and TS models are shown in Fig. 6.2. The connections from the DP model to the network are also shown in the same figure.

The box in colour red shown in Fig. 6.2 is the user-written transient stability model. Since it is a control system component it is not directly connected to the power system network. It takes the currents of the DP-TS interface buses

from the DP side and after every time-step, it updates voltages of the same buses in the DP model. The computations in this block are done in every 5 ms.

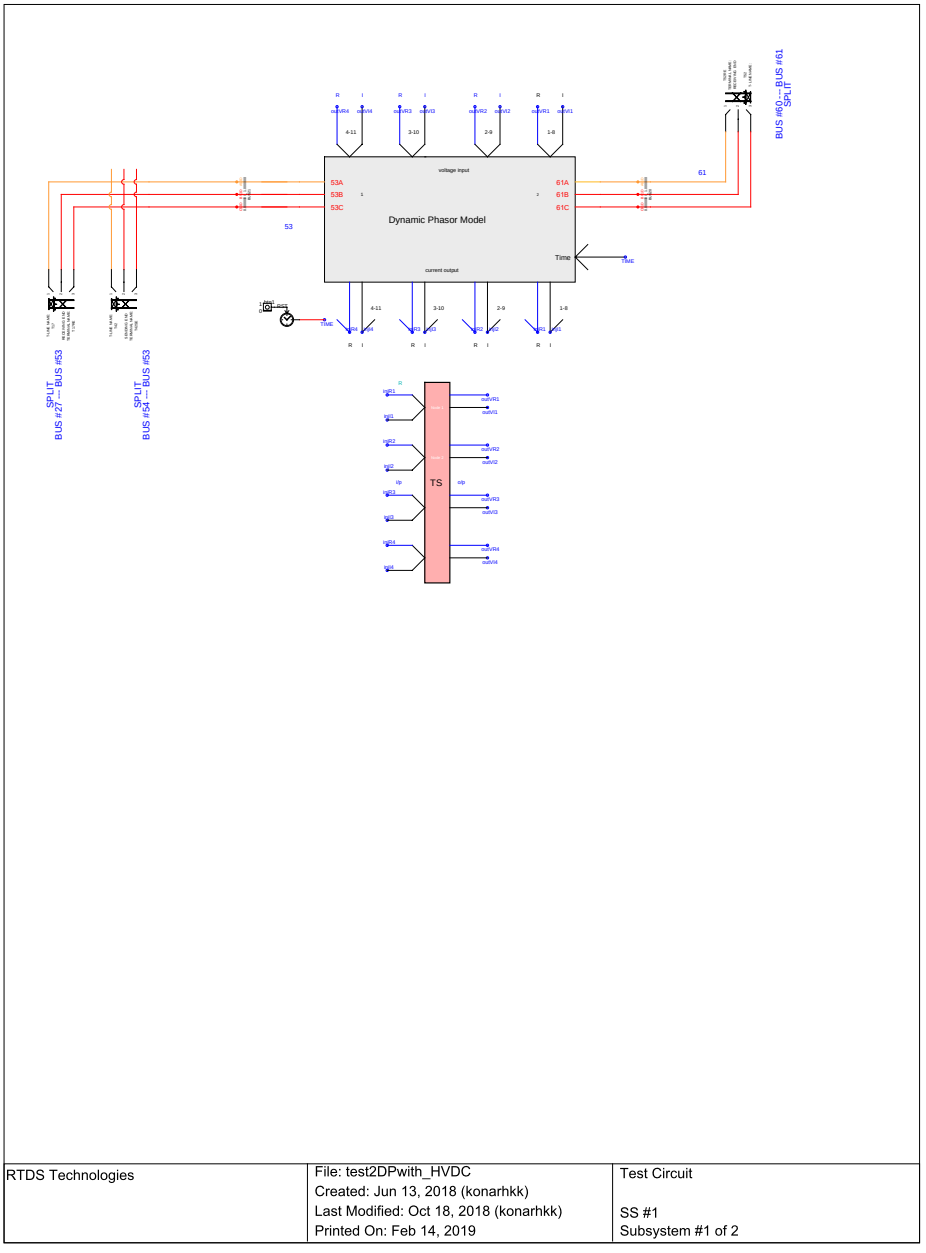

FIGURE 6.2: Part of the RSCAD draft containing the user-written DP and TS models

6.2 Validation of the Proposed Co-simulation Model

The validation of the co-simulation model is presented in this section. An EMT model is used to simulate the entire New England & New York 68 bus system to be used to validate the co-simulation model. The objective of the study is to analyse the dynamics in NETS around the node where the LCC HVDC is connected to. Therefore, the faults are applied in NETS and the dynamics in NETS are analysed.

Balanced three-phase faults are applied at different locations of the internal system of the New England & New York 68 bus system to check the performance of the proposed model. Three simulation cases are generated by applying faults at the following locations:

1. Fault at the HVDC terminal
2. Fault at a bus next to an interface bus of internal and external models
3. Fault at a interface bus

The accuracy of the proposed co-simulation model is examined by how well it's results match the results obtained from the EMT model.

6.2.1 Case 1: Three Phase Fault at the Converter Bus

In this case, the performance of the co-simulation model is evaluated for a fault at the AC bus of the HVDC converter. The results are validated against a fully EMT simulated 68 bus system. A three-phase fault with a duration of 5 cycles is applied at bus 29 (HVDC converter bus) at $t = 10\,\text{s}$. The current through the DC line and converter AC side voltage (bus 29) are shown in Fig. 6.3. The voltage

at bus 54 and current in the branch connecting buses 54 and 53 are shown in Fig. 6.4. Fig. 6.5 shows the speed of generator 8, which is the closest generator to the faulted bus. The results match very well with the EMT simulation results.

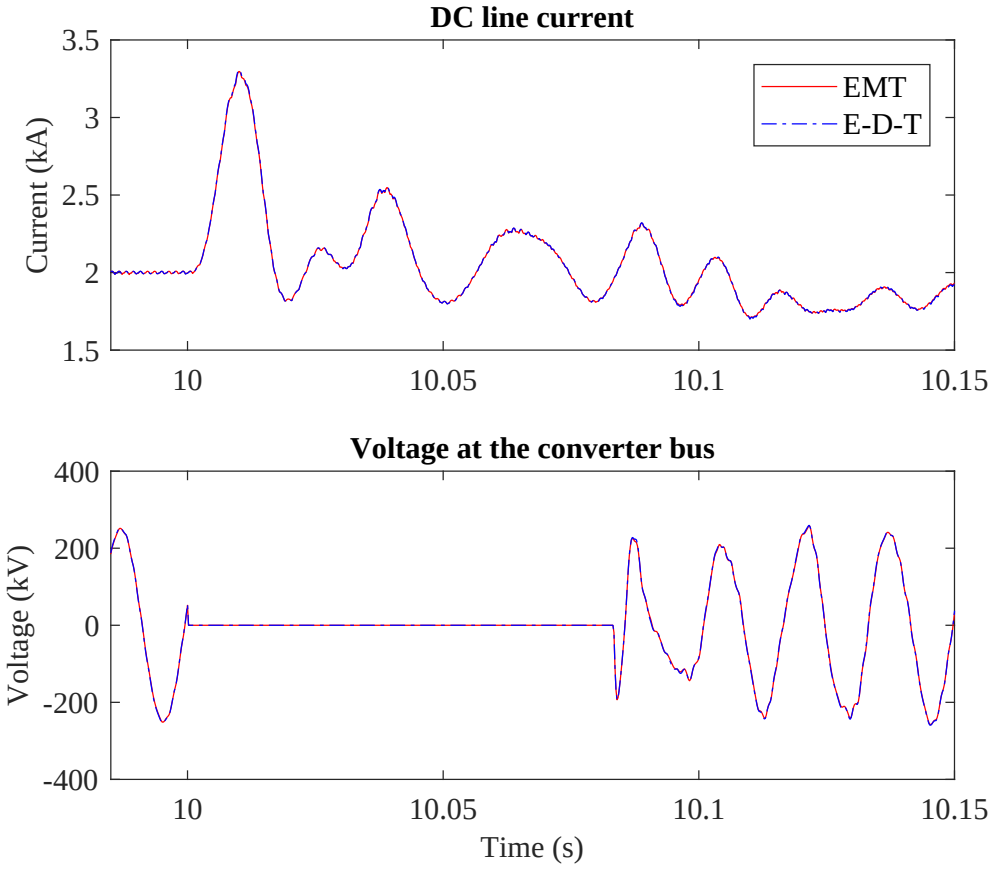

FIGURE 6.3: Converter parameters for a three-phase fault at bus 29

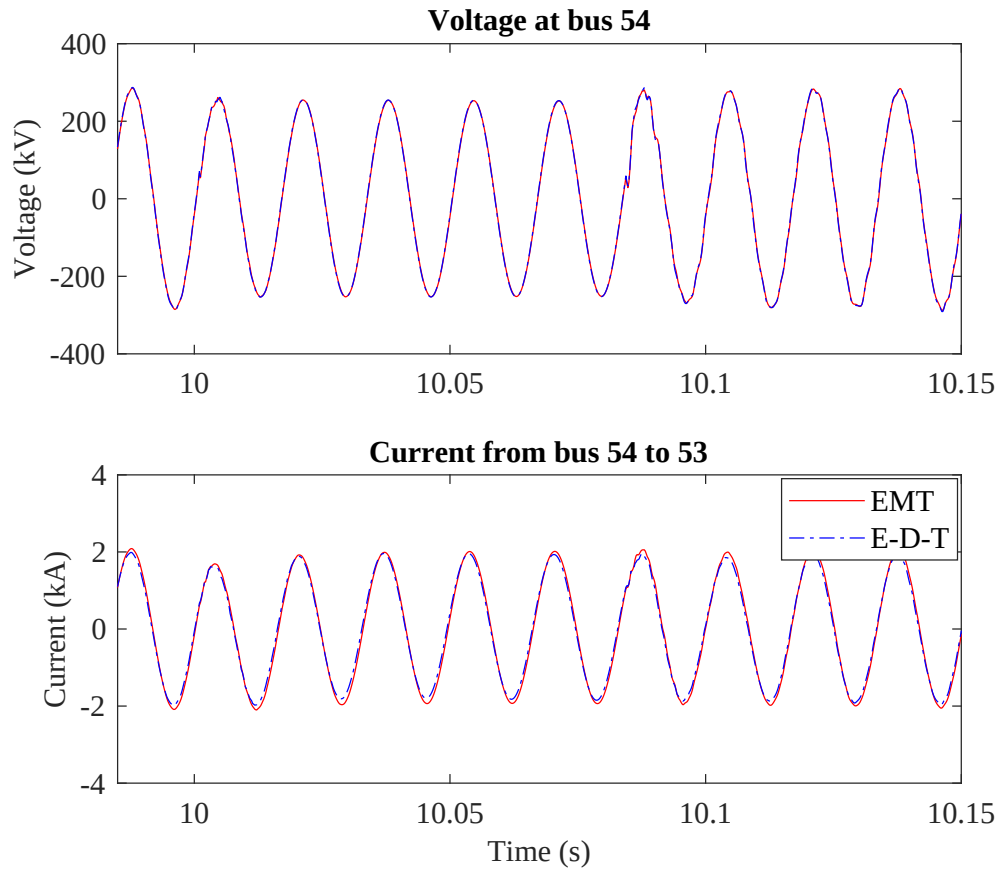

FIGURE 6.4: Voltages and currents for a three-phase fault at bus 29

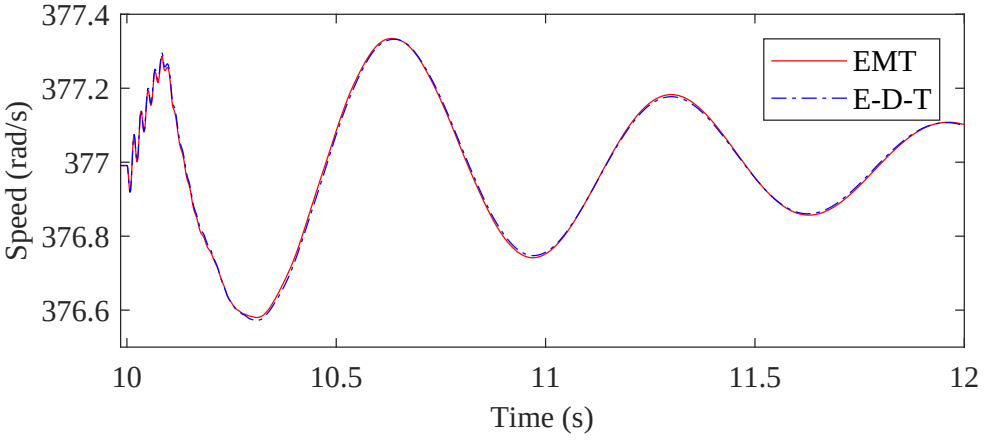

FIGURE 6.5: Speed of generator 8 for a three-phase fault at bus 29

6.2.2 Case 2: Three-Phase Fault at a Bus Next to one of the EMT-DP Interface Buses

In EMT side, the buses connected to boundary buses (bus 53 and 61) are 60, 54 and 27. A three-phase fault with a fault duration of 5 cycles is applied at bus 54 at $t = 10$ s. Fig. 6.6 shows voltage at bus 54 and current in the line connecting buses 54 and 53. The current through the DC line and phase 'A' voltage at the converter (bus 29) are shown in Fig. 6.7. Fig. 6.8 shows the speed and the electric torque of the generator 1. The results of the co-simulation model match well with the EMT results except for some discrepancy in the current in Fig. 6.6 during the fault.

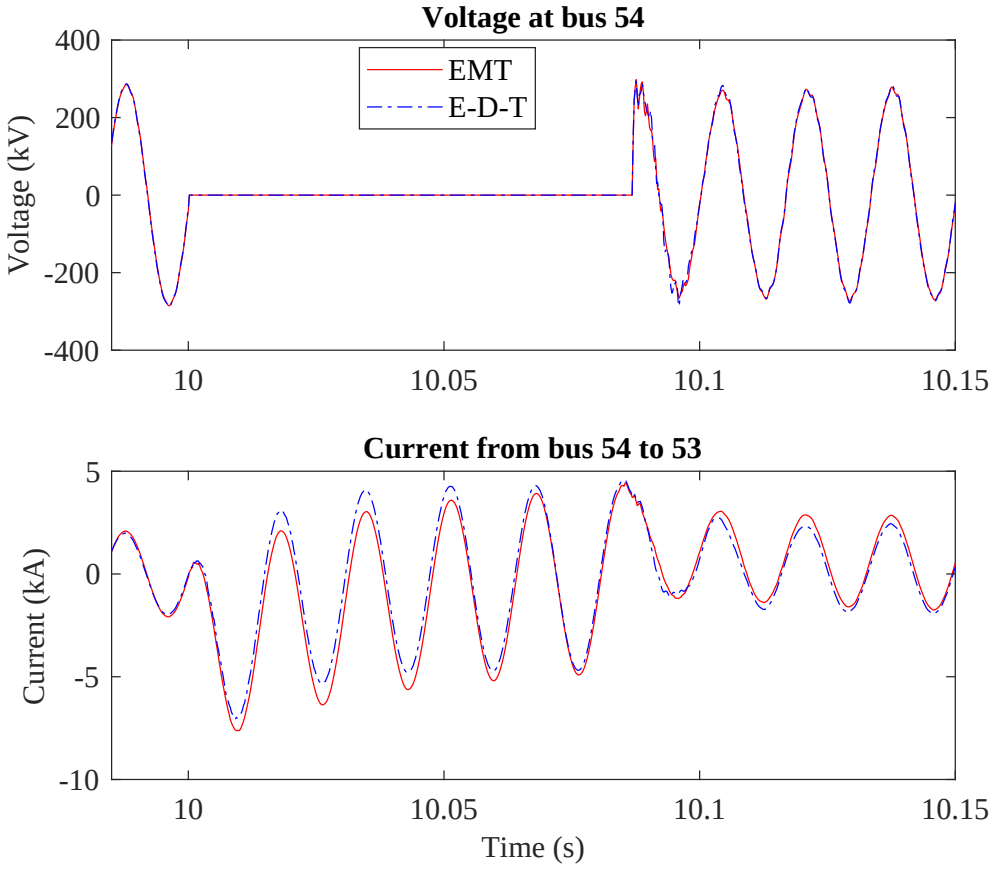

FIGURE 6.6: Voltage and currents for a three-phase fault at bus 54

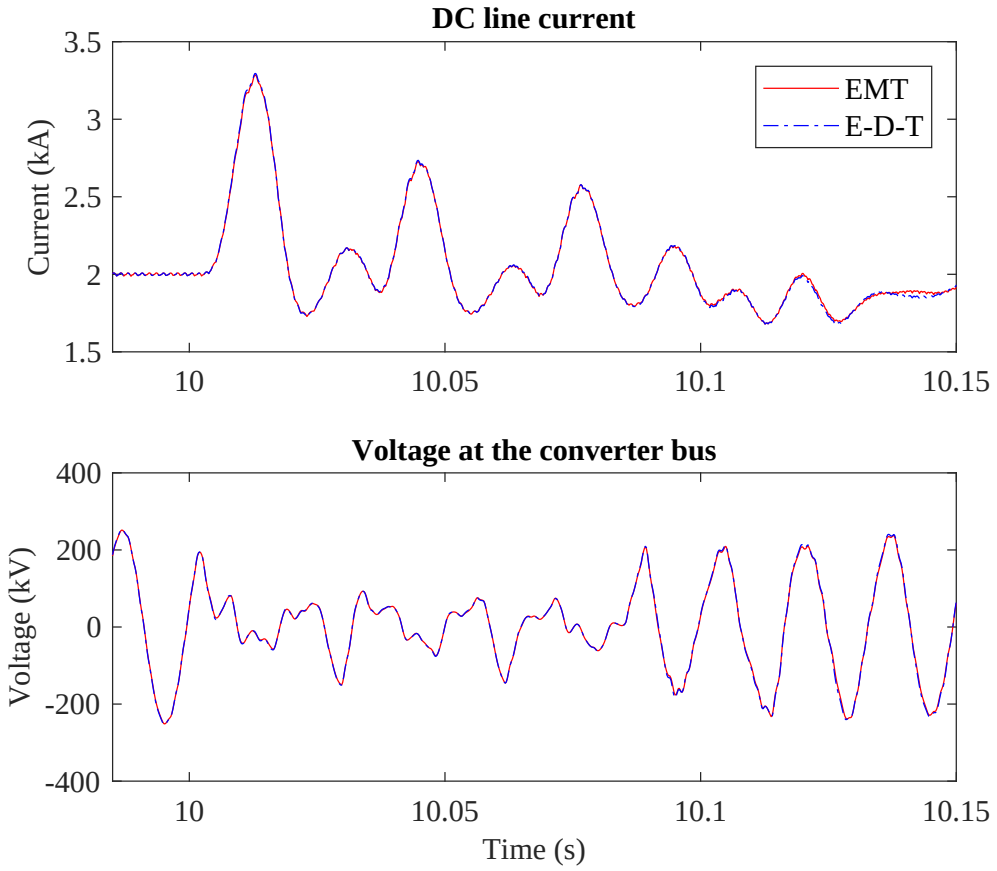

FIGURE 6.7: Converter voltage and DC current for a three-phase fault at bus 54

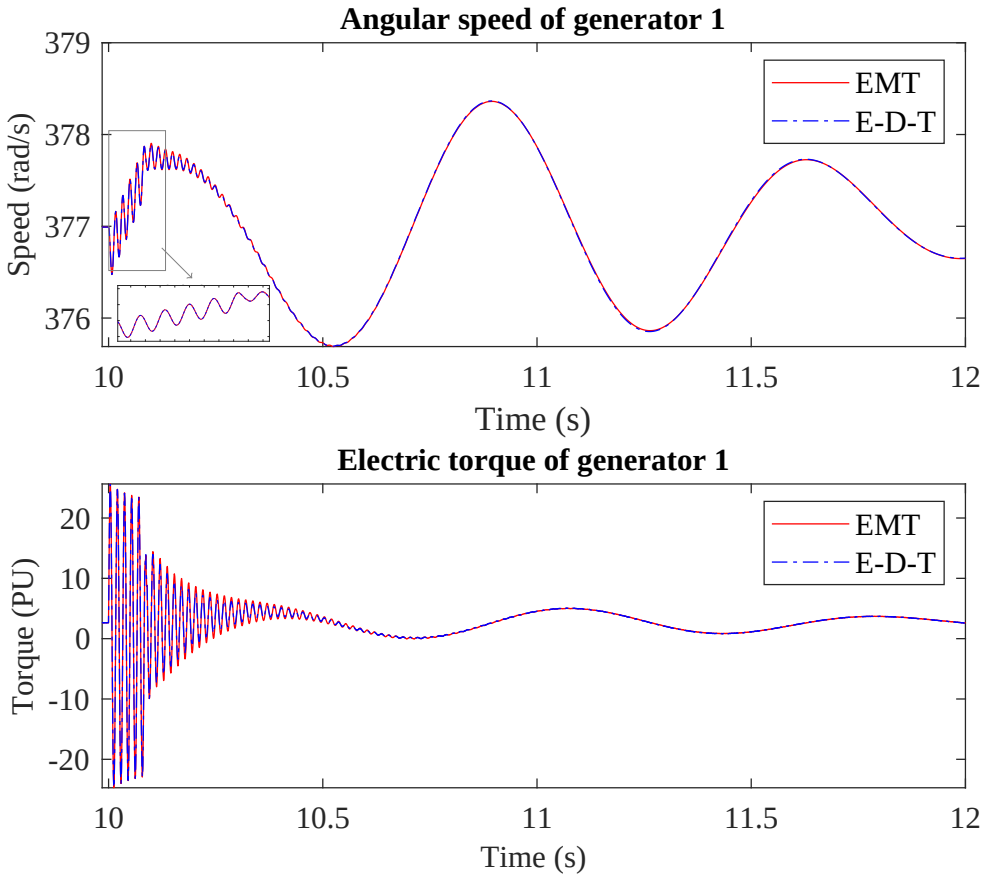

FIGURE 6.8: Generator 1 parameters for a three-phase fault at bus 54

6.2.3 Case 3: Three-Phase Fault at a Bus Right at the EMT-DP Interface

In typical studies, faults are applied in the EMT side. In this study, faults are applied right at the interface buses to check the performance of the co-simulation model. Applying faults at the interface buses is not recommended. However, for the purpose of testing the numerical stability and robustness, a three phase-fault is applied at one of the interface buses, bus 53. Fig. 6.9 shows voltages at buses 53 and 29 and current in the branch connecting 27 to 53 for the three-phase fault at bus 53. Fig. 6.10 shows the generator 16 speed, which is inside the TS model.

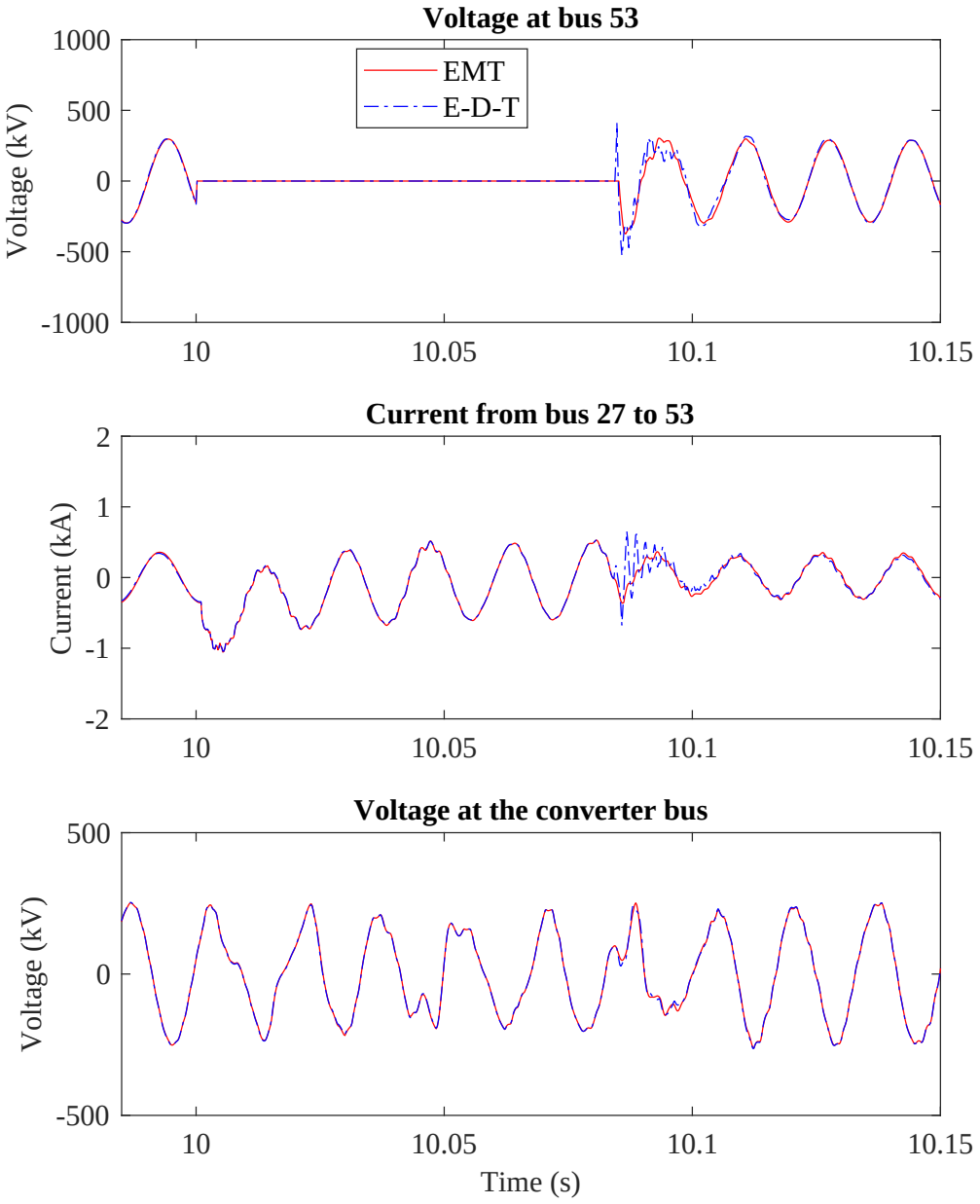

FIGURE 6.9: Voltages and currents for a three-phase fault at bus 53

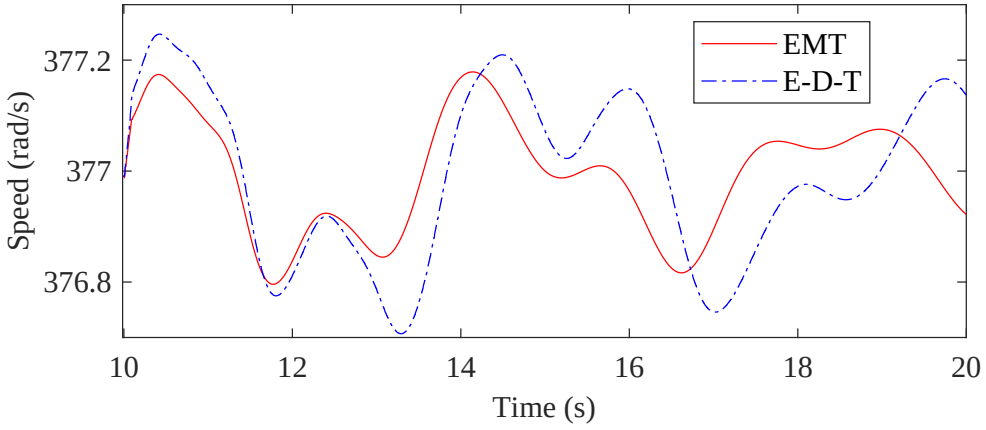

FIGURE 6.10: Speed of generator 16 for a three-phase fault at bus 53

It can be seen from the figures that there are some inaccuracies but the simulation is numerically stable. Even at the interface bus, the comparisons are good except in the first 2-3 cycles. Speeds of generators in the TS side is shown to demonstrate the reliability of the co-simulation. In the TS portion of the network, the generators are modelled without the dynamics of stator winding flux. In addition, the integration time step is 5 ms. Therefore, the two simulations are not expected to give identical results.

6.3 Discussion

The proposed DP buffer zone for EMT-TS co-simulation is a convenient alternative compared to the methods proposed in the literature. Faults were applied at different locations to test the robustness of the proposed approach and compared against an EMT simulation. Without any exceptions, all simulations produced results similar to that is presented above. The HVDC link is also simulated in different locations in the internal system and the same level of accuracy in the results was observed.

6.3.1 Identification of the Interface Nodes

The boundary between the internal and external system should be selected carefully. The boundary should be away from the interested part (i.e. HVDC system) of the internal system. Some of the limitations of selecting the boundary in already existing EMT-TS co-simulations are summarized below.

- EMT-TS Boundary must be few buses away from the interested part of the network. Faults applied close to the boundary cause numerical instability [59].
- Assumed EMT system is well damped around the boundaries containing only electromechanical oscillations. High-frequency components and fast transients in the boundary can cause instabilities due to the large time-step used in TS model [59].
- Having multiple boundary buses can make the simulation numerically unstable [23].
- Boundary buses should be electrically far away from each other. Electrically close boundary buses could cause numerical instability due to the large time-step used in TS model [59].

The boundary between EMT and DP models of the proposed EMT-TS co-simulation must be at least two buses away from the interested part of the network. The simulation is numerically stable even at a fault in an interface bus but as shown in Section 6.2.3 however the waveforms contain some inaccuracies. There is no restriction on selecting the DP-TS boundary. According to [32], buffer zone could contain only a single transmission line. However, a buffer zone with at least two buses depth will increase the accuracy of the co-simulation model.

Since the TS model in the proposed co-simulation model updates the voltages at DP-TS boundary buses at every DP time-step many numerical issues discussed in previous work can be avoided.

6.3.2 Computational Efficiency of the Proposed Co-simulation Model

The computational advantage is gained in the proposed model by using a large time-step at the TS side of the co-simulation. In the proposed model a time-step of $5ms$ is used to simulate the external system. Compared to a typical EMT simulation time-step this is 100 times larger. Also, the use of simplified models of power system components in the TS model further reduce the computational burden.

6.3.3 Limitations/Drawbacks of the Proposed Co-Simulation Model

One of the drawbacks of the proposed platform is that there are two interfaces (i.e. EMT-DP and DP-TS) instead of one. And the user will also have to specify the buffer zone. Dynamic phasor buffer zone allows smoother integration of EMT and TS. The buffer zone can be one bus or more buses in depth. Having at least two buses of depth buffer zone will improve the accuracy of the co-simulation model. However, the user should keep in mind that the computational burden of DP is higher compared to TS. The DP Buffer zone could include Transmission Lines, Loads, Synchronous machines and Transformers. The proposed synchronous machine model in Section 3.3 can be used to model the synchronous machines

inside the DP buffer zone. There is no restriction on selecting the interfacing buses between DP and TS.

The faults applied in the previous section was balanced three-phase faults. Section 6.3.3.1 added to examine the performance of the co-simulation model under unbalanced faults.

Another limitation of the proposed model is its performance under a change of system frequency. The test cases used for validating the co-simulation model has a constant steady-state system frequency of 60 Hz. However, in the absence of proper governor models, the system frequency can deviate from 60 Hz. For the conversion between the EMT three-phase voltages to phasor values, a constant system frequency was assumed. Any deviation of frequency results in an error in the phase angle of the calculated phasor. If the frequency deviation is considerable, there will be errors in the results of the co-simulation model.

6.3.3.1 Performance of the Co-Simulation Model Under Unbalanced Faults

One limitation of the proposed interface is performance under an unbalanced fault. In the approach presented in this thesis, both DP and TS parts are modelled using positive sequence voltages and currents. In order to handle unbalances, the negative and zero sequence components should be considered in DP and TS side. A phase 'A' to ground fault is applied at bus 60 to analyse the performance of the co-simulation model under an unbalanced fault. The phase 'A' and 'B' voltages of bus 60 and current in the branch connecting buses 61 to 60 are shown in Fig. 6.11. For this particular case, the difference in the results is negligible however, the error would be case dependent.

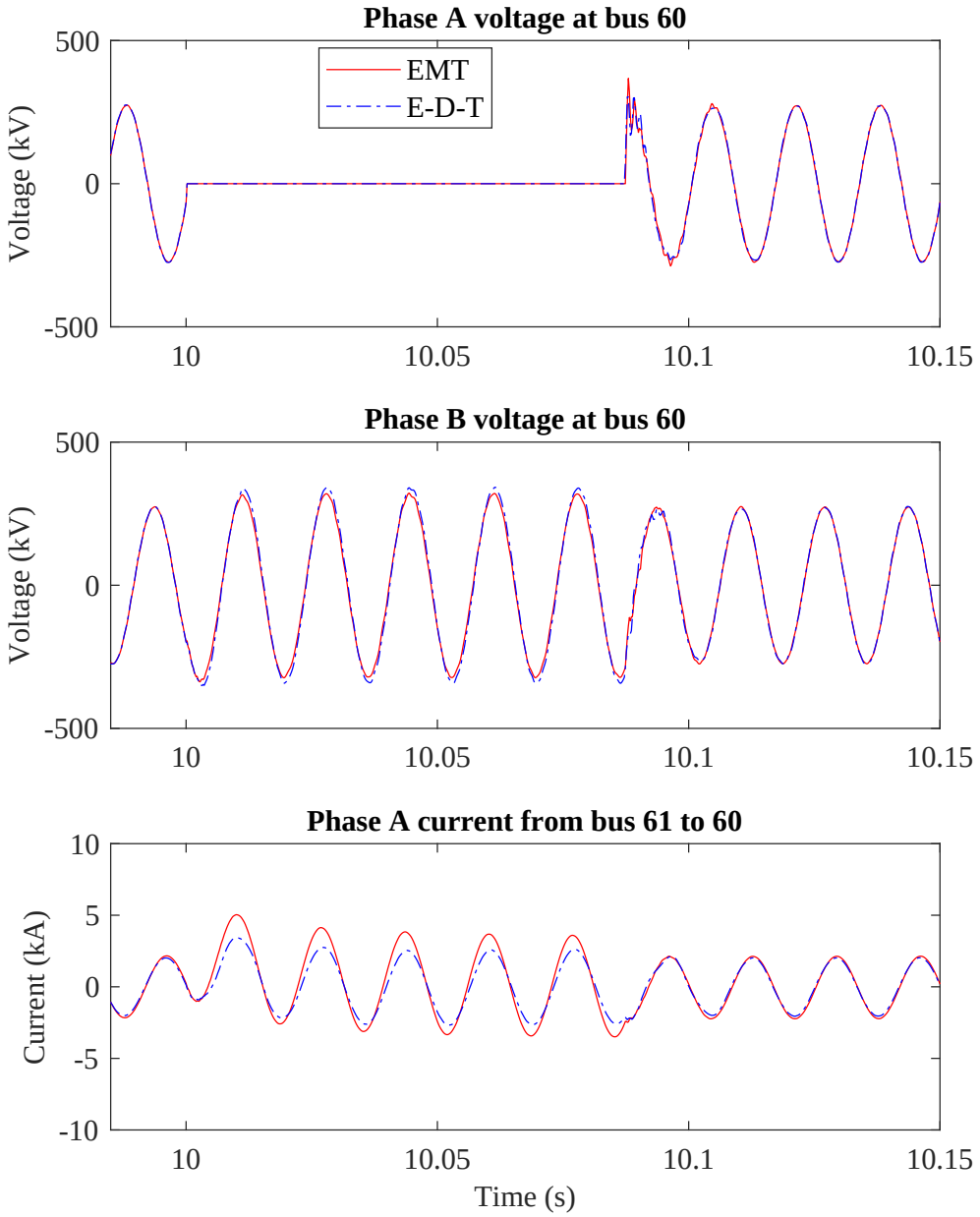

FIGURE 6.11: Voltages and currents for a phase A to ground fault

6.3.4 Performance of the System Under Worst Electromagnetic Transients

The worst scenario for the proposed co-simulation model is applying a fault at one of the interface buses. As it was shown in Section 6.2.3, the simulation results

have some errors however the simulation was numerically stable.

The proposed model was also tested under an unstable fault. A three-phase fault was applied at bus 60 for a period of 450 ms to create an unstable system. The results of the co-simulation model are compared with the EMT simulation results and the line current through bus 61 to 60 and the speed of generator 2 are shown in Figures 6.12 and 6.13 respectively. The results confirm that the co-simulation works well under an unstable scenario.

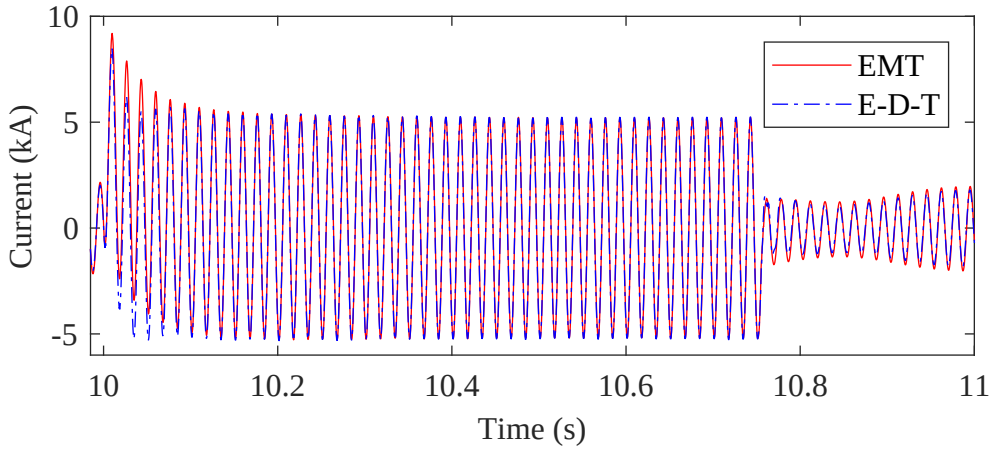

FIGURE 6.12: Line current for a fault at bus 60

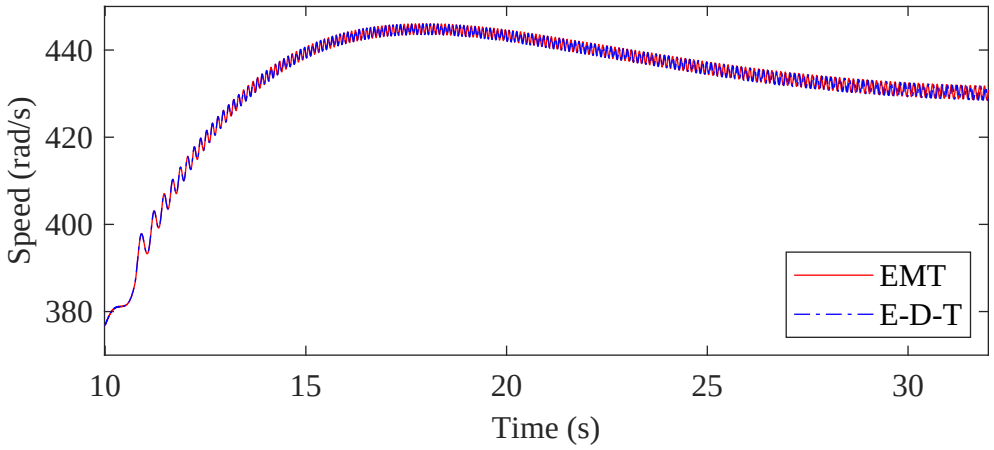

FIGURE 6.13: Speed of the generator 2 for a fault at bus 60

The proposed model is tested for a line energization case. Figure 6.14 shows the line current for energization of line connecting buses 58 and 59.

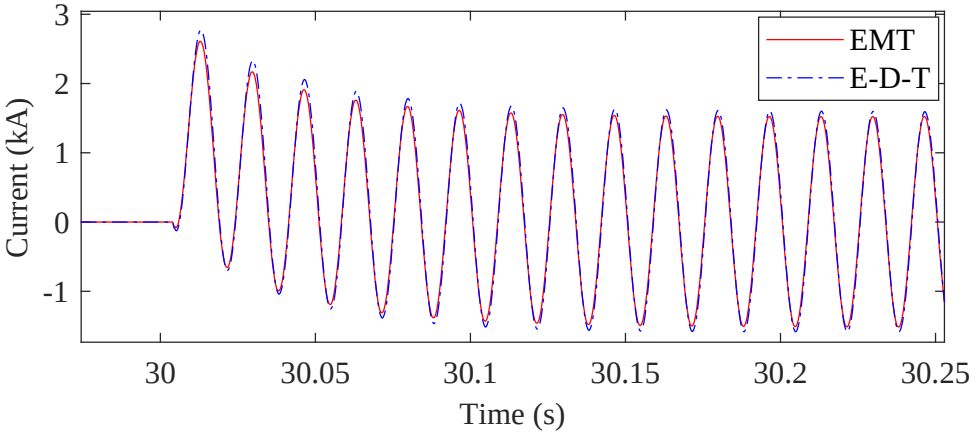

FIGURE 6.14: Breaker current for a line energization between bus 58 and bus 59

Harmonic frequencies were presented in the internal system due to the HVDC in-feed in the system. Under that amount of harmonics, the co-simulation model has produced accurate results. Section 6.3.4.1 is added to check the performances of the co-simulation model with the presence of a large amount of high-frequency signals in the system.

6.3.4.1 Performance of the Co-Simulation Model in Presence of High Frequencies

The proposed co-simulation can perform well at sufficiently high frequencies applicable to typical planning studies. It was shown using simulations (Section 6.2) that even with a THD of 3.4 the simulation results show a good agreement. To test this further, a source with $1kHz$ and a magnitude equal to 20% of the bus voltage is added to bus 22 (the bus circled in green in Fig. 6.1). The voltage at bus 22 and current from bus 27 to 53 are shown in Fig. 6.15. It can be seen that the 1 kHz component is well captured in the co-simulation model. The goal of the co-simulation model is to capture electromechanical oscillations and controller interactions with the external system. For this purpose, 1 kHz is sufficient.

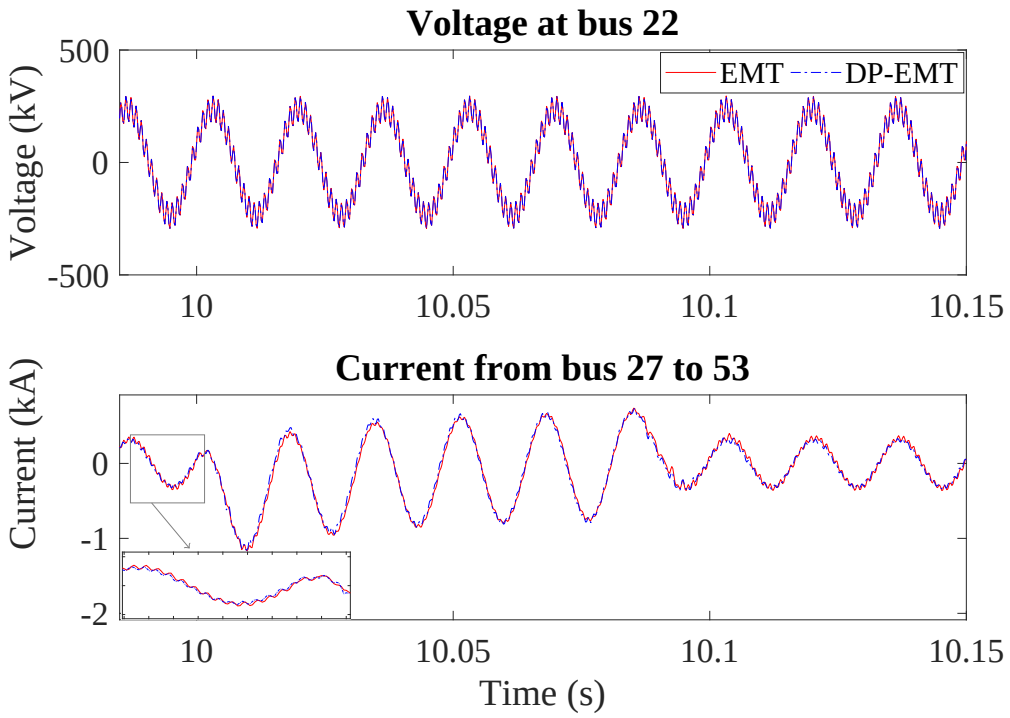

FIGURE 6.15: Voltages and currents in a presence of 1000 Hz signal

6.4 Summary

The implementation and testing of the proposed EMT-TS co-simulation model were presented in this chapter. The co-simulation model has produced promising results under disturbances applied in the internal system. Therefore, it can be concluded that the dynamic phasor buffer zone is a simple alternative for using an FDNE in an EMT-TS co-simulation model.

Chapter 7

Conclusions, Contributions and Future Work

7.1 Conclusions

The objective of the thesis was to develop a co-simulation model suitable to analyse electromagnetic transients in a large power system. EMT-TS co-simulation models proposed in the literature have limitations due to the use of FDNEs. The EMT-TS co-simulations require an FDNE at the boundary between the EMT and TS models. The main concern with FDNE is that it is not convenient for the user to tune FDNE for a particular network. This thesis has addressed this problem using two approaches. In the first approach, dynamic phasors are used to model the external system of a large power system. The internal system, which is the study area, was modelled using an EMT simulation. In the second approach, dynamic phasors are used to model a part of the external system as a buffer zone connecting the internal and external systems. The internal system was modelled using EMT and the external system, excluding the buffer zone, was modelled

using TS. This is a simple alternative to FDNE based EMT-TS co-simulations. The conclusions of this thesis can be summarized as below.

A stability criterion for interfacing two different network models with a time-step delay was introduced. It was concluded from this study that when there is an interface between two models involving a time-step delay, if the simulation is unstable when one part of the network is modelled as a voltage source, then it is going to be stable when it is modelled as a current source, or vice versa. If this steady-state stability criterion is not satisfied, the dynamic simulation will be numerically unstable. A synchronous machine model used in transient stability studies was used for validation of the stability criterion. It was shown that depending on the network parameters, the equivalent synchronous machine model can only be numerically stable either as a current source or as a voltage source. This principle was used to interface a synchronous machine model into the DP model. It was also pointed out that the stability criterion is equally valid for any interface involving a time-step delay (e.g. co-simulations).

An efficient, numerically robust voltage source type synchronous machine model was proposed to interface to a DP model. The proposed model is an EMT compatible model where the dynamics of flux in the stator winding are included. The robustness of the model was achieved by splitting the stator inductance into two components. The constant part was included in the network and the remaining part was updated at each time-step and included in the transient boundary voltage. The proposed methodology results in a constant admittance bus matrix, therefore, it is computationally efficient. The proposed synchronous machine model was validated by using the machine model in the RTDS simulator. The computational efficiency and the numerical robustness of the model were discussed against the existing synchronous machine models.

In this thesis, a DP model was interfaced to a real-time EMT model. Numerical instability due to time-step delay in EMT-DP co-simulation was successfully overcome by using a data prediction technique. The test system of New England & New York 68 bus system with an HVDC in-feed in the New England side was used to demonstrate the performance of the co-simulation model. The simulation results showed that the results of the co-simulation model closely reproduce the results of a complete EMT simulation. It was shown that unlike an EMT-TS co-simulation, the proposed EMT-DP co-simulation does not require an FDNE model at the interface bus. It was concluded that a TS model is more appropriate to simulate a large power system and DP can be used to model a buffer zone between the EMT and the TS models.

A real-time EMT-TS co-simulation using a multi-port DP buffer zone was presented in the thesis. The interface between EMT and TS models has been achieved by using DP to model a multi-port buffer zone between the EMT and TS models. This was a simple alternative to the existing FDNE models proposed in the literature. The methods of achieving numerical stability and accuracy of DP-TS interface has been discussed. The New England & New York 68 bus system with an HVDC in-feed was used as the test system. The New England system was selected as the internal system and it was simulated using an EMT model and the New York power system was selected as the external system. The accuracy and stability of the proposed co-simulation model were validated against a complete EMT simulation model. The co-simulation model shows promising results under disturbances applied in the internal system.

Testing of both EMT-DP and EMT-TS co-simulation models (Chapter 4 and 6) included applying three-phase faults at the boundary bus (i.e. EMT and DP boundary), which is the most severe in terms of numerical stability

7.2 Contributions

The key contributions of the thesis are listed below:

- A stability criterion for interfacing two network models with a time step delay was presented [38].
- A study of existing synchronous machine models was performed in order to find a suitable synchronous machine model for a DP simulation [60].
- A novel numerically robust and an efficient voltage source type synchronous machine model with the dynamics of stator winding flux was presented [39].
- A numerically stable real-time EMT-DP co-simulation model to analyse a power system was implemented and validated [48].
- A real-time EMT-TS co-simulation was implemented to analyse a large power system. The interface between the EMT and TS models was accomplished by using dynamic phasors to model a multi-port buffer zone between the EMT and TS models [61].

7.3 Future Work

The necessary building blocks for a real-time EMT-DP co-simulation and an EMT-TS co-simulation using DP were presented. The future work of the thesis is identified as follows.

- The scope of this research was limited to studying balanced three-phase systems. One of the future extensions to this work is to enable the co-simulation model to handle unbalances in internal network that was modelled

using the EMT simulation. In order to do this, the voltages at the EMT-DP interface has to be fed through a positive, negative and zero sequence filter before the phasor conversion. The positive sequence voltages can be used to solve the buffer zone as presented in Chapter 5. The negative and zero sequence impedances of the external system can be used to calculate the negative and zero sequence current injections to the internal system.

- In this thesis, the disturbances were applied only in the internal system. However, in some studies, the system response to disturbances in the external system is needed. Applying faults in the external system requires further research since the proposed models generate numerical oscillations under a fault at the external system. This can be considered as another area of future work for this thesis.

- In the proposed method, the three-phase voltages are converted to the phasor domain assuming a fixed centre frequency (i.e. 60 Hz). In some power system studies, system frequency settles on a different frequency from the base frequency. A frequency measuring technique is needed inside the DP model to accurately convert the three-phase voltages to the phasor domain in such cases. This can be considered as another future work of the thesis.

- In this work, a simple linear extrapolation method is used to interface EMT and DP models. During a disturbance, extrapolation methods add inaccuracies to the simulation since the voltages for next time-step are predicted using the previous data. Therefore, improving the extrapolation algorithm to mitigate errors under a disturbance is another extension to the work of this thesis.

- The TS part of the EMT-TS co-simulation model can be partitioned to simulate even larger power systems. This can be considered as another future work of the thesis.

Appendix A

Test System Data

A.1 Single Machine to Infinite Bus System

The SMIB model used in Chapter 3 is shown in Fig. A.1 below.

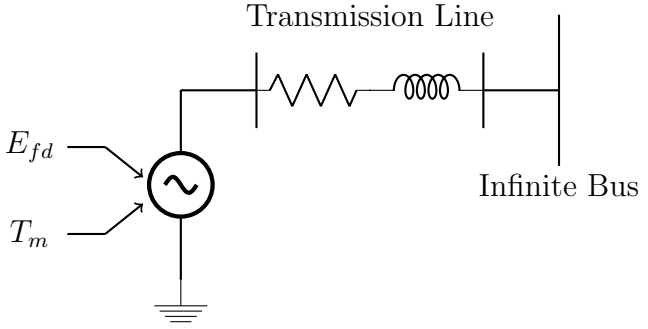

FIGURE A.1: SMIB system

The data of the network model of SMIB system used to validate the stability criterion are given in Table A.1 and the data used to validate the novel synchronous machine model are given in Table A.2. The data of the synchronous machine model are given in Table A.3.

TABLE A.1: SMIB system data used for the validation of the stability criterion

Constant	**Value**
Infinite bus voltage	24 kV
E_{fd}	1.1321 pu
T_{mech}	0.1838 pu
Line resistance	0.1 Ω
Line inductance	5.46 mH

TABLE A.2: SMIB system data used for the validation of the novel synchronous machine model

Constants	**Value**
Infinite bus voltage	24 kV
E_{fd}	1.6569 pu
T_{mech}	0.5753 pu
Line resistance	0.075 Ω
Line inductance	3.855 mH

TABLE A.3: Synchronous machine data for SMIB system

Machine constant	**Value**
R_a	0.00125 pu
X_d	1.536 pu
X_q	1.494 pu
$X_d^{'}$	0.3 pu
$X_q^{'}$	0.65 pu
$X_d^{''}$	0.23 pu
$X_q^{''}$	0.23 pu
X_l	0.15 pu
$T_{do}^{'}$	8 s
$T_{qo}^{'}$	1 s
$T_{do}^{''}$	0.03 s
$T_{qo}^{''}$	0.07 s
H	3.5
Machine MVA base	555 MVA
Machine voltage base	24 kV
D	5

A.2 New England and New York 68 Bus System

The New England & New York 68 bus system is the interconnected New England Test System (NETS) and New York Power System (NYPS). The system contains five areas as shown in Fig. A.2. The data used for the system are taken from [33]. NETS accommodates the area 1 and NYPS accommodates areas 2, 3, 4 and 5. The generator data are converted to base of 4000 MVA. Generator dynamic data are give in Table A.4 and A.5. Here, the impedance data are given in pu and the time constants are given in seconds.

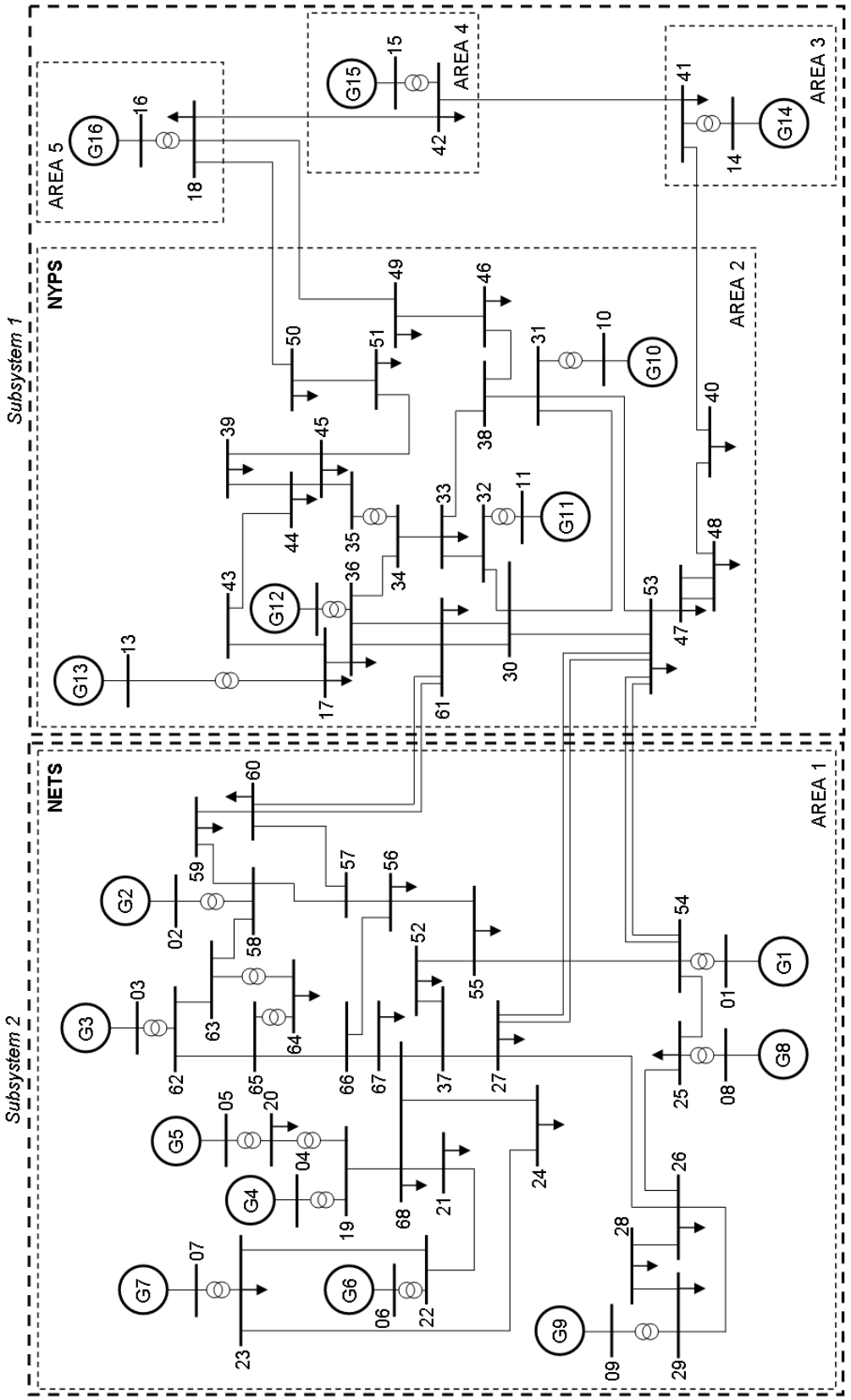

FIGURE A.2: New England & New York 68 bus system

TABLE A.4: Generator dynamic data

Gen	**Bus**	X_a	X_d	X'_d	X''_d	X_q	X'_q	X''_q
1	1	0.5	4	1.24	1	2.76	1.12	1
2	2	1.4	11.8	2.788	2	11.28	2.4	2
3	3	1.216	9.98	2.124	1.8	9.48	2	1.8
4	4	1.18	10.48	1.744	1.4	10.32	1.6	1.4
5	5	1.08	13.2	2.64	2	12.4	2.4	2
6	6	0.896	10.16	2	1.6	9.64	1.8	1.6
7	7	1.288	11.8	1.96	1.6	11.68	1.8	1.6
8	8	1.12	11.6	2.28	1.8	11.2	21.8	1.8
9	9	1.192	8.424	2.28	1.8	8.2	2	1.8
10	10	0.796	6.76	1.828	1.6	4.6	1.8	1.6
11	11	0.412	5.12	0.72	0.48	4.92	0.6	0.48
12	12	0.88	4.04	1.24	1	3.8	1.12	1
13	13	0.06	0.592	0.11	0.08	0.572	0.1	0.08
14	14	0.068	0.72	0.114	0.096	0.692	0.1	0.092
15	15	0.068	0.72	0.114	0.092	0.692	0.1	0.092
16	16	0.082	0.712	0.142	0.11	0.668	0.152	0.11

TABLE A.5: Generator dynamic data II

Gen	**Bus**	Ra	T'_{do}	T''_{do}	T'_{qo}	T''_{qo}	H	D
1	1	0.00125	10.2	0.05	1.5	0.035	1.05	0.1
2	2	0.00125	6.56	0.05	1.5	0.035	0.755	0.24375
3	3	0.00125	5.7	0.05	1.5	0.035	0.895	0.25
4	4	0.00125	5.69	0.05	0.05	0.035	0.715	0.25
5	5	0.00125	5.4	0.05	0.44	0.035	0.65	0.075
6	6	0.00125	7.3	0.05	0.4	0.035	0.87	0.25
7	7	0.00125	5.66	0.05	1.5	0.035	0.66	0.2
8	8	0.00125	6.7	0.05	0.41	0.035	0.6075	0.225
9	9	0.00125	4.79	0.05	1.96	0.035	0.8625	0.35
10	10	0.00125	9.37	0.05	1.5	0.035	0.705	0.139
11	11	0.00125	4.1	0.05	1.5	0.035	0.705	0.3375
12	12	0.00125	7.4	0.05	1.5	0.035	2.3075	0.3375
13	13	0.00125	5.9	0.05	1.5	0.035	12.4	0.825
14	14	0.00125	4.1	0.05	1.5	0.035	7.5	2.5
15	15	0.00125	4.1	0.05	1.5	0.035	7.5	2.5
16	16	0.00125	7.8	0.05	1.5	0.035	11.25	1.25

Generator voltages and scheduled power are given in Table A.6. The voltage and the MVA bases are 13.8 kV and 100 MVA respectively.

TABLE A.6: Generator PV setting

Bus	**Voltage (pu)**	**Power (pu)**
1	1.0450	2.50
2	0.9800	5.45
3	0.9830	6.50
4	0.9970	6.32
5	1.0110	5.05
6	1.0500	7.00
7	1.0630	5.60
8	1.0300	5.40
9	1.0250	8.00
10	1.0100	5.00
11	1.0000	10.00
12	1.0156	13.05
13	1.0110	35.91
14	1.0000	17.85
15	1.0000	10.00
16	1.0000	40.00

All the generators except generator 9 consist of IEEE type AC4 excitation systems. Generator 9 consist of IEEE type ST1 excitation system. Excitation system data are given in Table A.7 and A.8. All the generators consist of TGOV1 type steam governors. Turbine data are given in Table A.9. Generators 1 to 5 consist of IEEE PSS1A Power System Stabilizers (PSS). PSS data are given in Table A.10.

TABLE A.7: IEEE type AC4 excitation system data

T_r (sec)	T_c (sec)	T_b (sec)	K_a	T_a (sec)	Kc
0.01	1.0	10	100	10	0

TABLE A.8: IEEE type ST1 excitation system data

T_r (sec)	T_c (sec)	T_b (sec)	K_a	T_a (sec)	K_f	T_f (sec)	Kc
0.01	0.1	0.1	200	0	0	0	0

TABLE A.9: Governor system data

R	T_1 (sec)	T_2 (sec)	T_3 (sec)	D
0.05	0.05	2.1	7.0	0

TABLE A.10: PSS data

Ks	T_1 (sec)	T_2 (sec)	T_3 (sec)	T_3 (sec)	T_4 (sec)	T_5 (sec)	T_6 (sec)
10	0.01	0.01	0.01	0.01	0.01	10	0.01

The transmission line data of the power system are given in Table A.11. The transformer data and load data are given in Table A.12 and A.13 respectively. The voltage and the MVA bases of the transmission network are $345kV$ and $100MVA$ respectively.

TABLE A.11: Transmission line data

From bus	To bus	R (pu)	X (pu)	B (pu)	Travel time (ms)
36	17	0.0005	0.0045	0.32	0.100658
49	18	0.0076	0.1141	1.16	0.96503

TABLE A.11: Transmission line data

From bus	**To bus**	**R (pu)**	**X (pu)**	**B (pu)**	**Travel time (ms)**
68	19	0.0016	0.0195	0.304	0.204232
68	21	0.0008	0.0135	0.2548	0.155573
21	22	0.0008	0.014	0.2565	0.158956
22	23	0.0006	0.0096	0.1846	0.111666
68	24	0.0003	0.0059	0.068	0.053131
54	25	0.007	0.0086	0.146	0.093993
25	26	0.0032	0.0323	0.531	0.34739
37	27	0.0013	0.0173	0.3216	0.197856
26	27	0.0014	0.0147	0.2396	0.157424
26	28	0.0043	0.0474	0.7802	0.510107
26	29	0.0057	0.0625	1.029	0.672692
28	29	0.0014	0.0151	0.249	0.960806
53	30	0.0008	0.0074	0.48	0.15809
61	30	0.0019	0.0183	0.29	0.193238
61	30	0.0019	0.0183	0.29	0.193238
30	31	0.0013	0.0187	0.333	0.209321
53	31	0.0016	0.0163	0.25	0.16933
30	32	0.0024	0.0288	0.488	0.314467
32	33	0.0008	0.0099	0.168	0.108179
33	34	0.0011	0.0157	0.202	0.149381
34	36	0.0033	0.0111	1.45	0.336523
61	36	0.0022	0.0196	0.34	0.216539
61	36	0.0022	0.0196	0.34	0.216539

TABLE A.11: Transmission line data

From bus	**To bus**	**R (pu)**	**X (pu)**	**B (pu)**	**Travel time (ms)**
68	37	0.0007	0.0089	0.1342	0.091673
31	38	0.0011	0.0147	0.247	0.159837
33	38	0.0036	0.0444	0.693	0.465293
41	40	0.006	0.084	3.15	1.364469
48	40	0.002	0.022	1.28	0.445128
42	41	0.004	0.06	2.25	0.974621
18	42	0.004	0.06	2.25	0.974621
17	43	0.0005	0.0276	0	R-L Branch
39	44	0	0.0411	0	R-L Branch
43	44	0.0001	0.0011	0	R-L Branch
35	45	0.0007	0.0175	1.39	0.413709
39	45	0	0.0839	0	R-L Branch
44	45	0.0025	0.073	0	R-L Branch
38	46	0.0022	0.0284	0.43	0.293131
53	47	0.0013	0.0188	1.31	0.416278
47	48	0.0025	0.0268	0.4	0.274642
47	48	0.0025	0.0268	0.4	0.274642
46	49	0.0018	0.0274	0.27	0.228153
45	51	0.0004	0.0105	0.72	0.230637
50	51	0.0009	0.0221	1.62	0.501906
37	52	0.0007	0.0082	0.1319	0.087236
55	52	0.0011	0.0133	0.2138	0.141449
53	54	0.0035	0.0411	0.6987	0.449506

TABLE A.11: Transmission line data

From bus	**To bus**	**R (pu)**	**X (pu)**	**B (pu)**	**Travel time (ms)**
54	55	0.0013	0.0151	0.2572	0.165308
55	56	0.0013	0.0213	0.2214	0.182158
56	57	0.0008	0.0128	0.1342	0.109939
57	58	0.0002	0.0026	0.0434	0.028177
58	59	0.0006	0.0092	0.113	0.085527
57	60	0.0008	0.0112	0.1476	0.10785
60	61	0.0023	0.0363	0.3804	0.311704
58	63	0.0007	0.0082	0.1389	0.089521
62	63	0.0004	0.0043	0.0729	0.046964
62	65	0.0004	0.0043	0.0729	0.046964
56	66	0.0008	0.0129	0.1382	0.112
65	66	0.0009	0.0101	0.1723	0.110655
66	67	0.0018	0.0217	0.366	0.236396
67	68	0.0009	0.0094	0.171	0.106348
53	27	0.032	0.32	0.41	0.960806
18	50	0.0012	0.0288	2.06	0.646099

TABLE A.12: Transformer data

From bus	**To bus**	***R* (pu)**	***X* (pu)**	**Tap ratio**
54	1	0	0.0181	1.025
58	2	0	0.025	1.07
62	3	0	0.02	1.07
19	4	0.0007	0.0142	1.07

TABLE A.12: Transformer data

From bus	**To bus**	***R* (pu)**	***X* (pu)**	**Tap ratio**
20	5	0.0009	0.018	1.009
22	6	0	0.0143	1.025
23	7	0.0005	0.0272	1
25	8	0.0006	0.0232	1.025
29	9	0.0008	0.0156	1.025
31	10	0	0.026	1.04
32	11	0	0.013	1.04
36	12	0	0.0075	1.04
17	13	0	0.0033	1.04
41	14	0	0.0015	1
42	15	0	0.0015	1
18	16	0	0.003	1
19	20	0.0007	0.0138	1.06
35	34	0.0001	0.0074	0.946
64	63	0.0016	0.0435	1.06

TABLE A.13: Load PQ data

Bus number	**P (pu)**	**Q (pu)**
17	60	3
18	24.7	1.23
19	0	0
20	6.8	1.03
21	2.74	1.15
22	0	0

TABLE A.13: Load PQ data

Bus number	**P (pu)**	**Q (pu)**
23	2.48	0.85
24	3.09	-0.92
25	2.24	0.47
26	1.39	0.17
27	2.81	0.76
28	2.06	0.28
29	2.84	0.27
30	0	0
31	0	0
32	0	0
33	1.12	0
34	0	0
35	0	0
36	1.02	-0.1946
37	0	0
38	0	0
39	2.67	0.126
40	0.6563	0.2353
41	10	2.5
42	11.5	2.5
43	0	0
44	2.6755	0.0484
45	2.08	0.21
46	1.507	0.285

TABLE A.13: Load PQ data

Bus number	**P (pu)**	**Q (pu)**
47	2.0312	0.3259
48	2.412	0.022
49	1.64	0.29
50	1	-1.47
51	3.37	-1.22
52	1.58	0.3
53	2.527	1.1856
54	0	0
55	3.22	0.02
56	2	0.736
57	0	0
58	0	0
59	2.34	0.84
60	2.088	0.708
62	0	0
63	0	0
64	0.09	0.88
65	0	0
66	0	0
67	3.2	1.53
68	3.29	0.32

A.3 CIGRE HVDC Benchmark System

Fig. A.3 shows the one line diagram of CIGRE HVDC First Benchmark Model [57]. The power system data of the model is given in Table A.14 and Table A.15. The control system data is given in Table A.16.

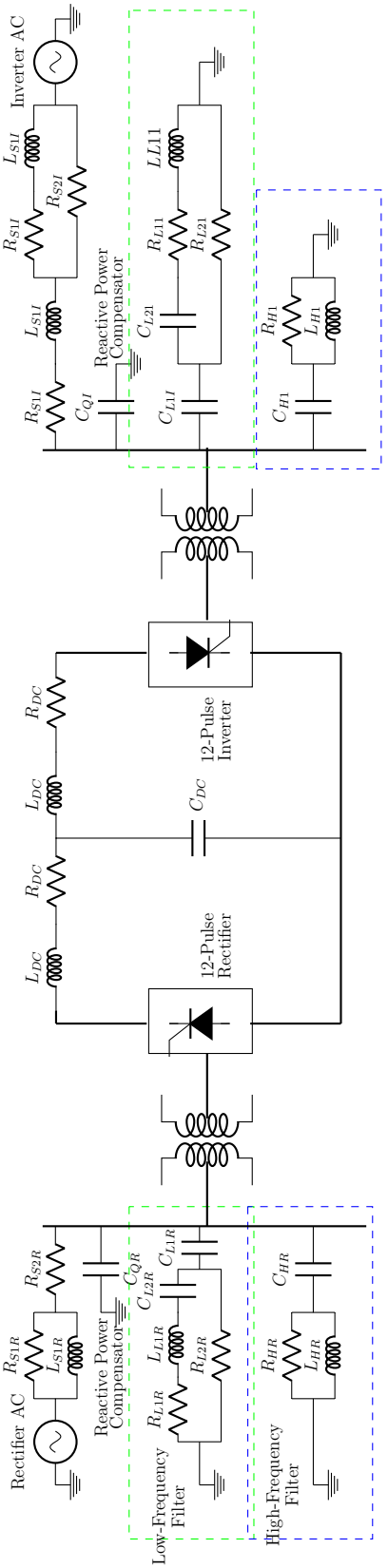

FIGURE A.3: CIGRE HVDC benchmark system

TABLE A.14: System ratings and system base quantities

Parameter	**Rectifier side**	**Inverter side**
AC voltage rating	345 kV	345 kV
System Frequency	60 Hz	60 Hz
AC voltage rating	1000 MVA	1000 MVA
Voltage	$362.47\,\text{kV}/17.95^0$	-
Transformer rating	1196 MVA	1196 MVA
Transformer voltages	213.26 : 345 kV	345 : 209.43 kV
Transformer tap ratio	1.01	0.99
Nominal DC voltage	500 kV	500 kV
Nominal DC current	2 kA	2 kA

TABLE A.15: Impedance data

Parameter	**Rectifier side**	**Inverter side**
Source	$L_{S1R} = 0.151$ H	-
	$R_{S1R} = 3.737\,\Omega$	-
	$R_{S2R} = 2160.633\,\Omega$	-
Reactive power compensator	$C_{QR} = 3.342\,\mu$F	$C_{Q1} = 6.93\,\mu$F
Low frequency filter	$L_{R1R} = 0.1364$ H	$L_{R1I} = 0.0606$ H
	$R_{L1R} = 29.76\,\Omega$	$R_{L1I} = 13.23\,\Omega$
	$R_{L2R} = 261.87\,\Omega$	$R_{L2I} = 116.38\,\Omega$
	$C_{L1R} = 6.685\,\mu$F	$C_{L1I} = 15.04\,\mu$F
	$C_{L2R} = 74.28\,\mu$F	$C_{L2I} = 167.2\,\mu$F
High frequency filter	$R_{HR} = 83.32\,\Omega$	$R_{HI} = 37.03\,\Omega$
	$L_{HR} = 0.0136$ H	$L_{HI} = 0.0061$ H
	$C_{HR} = 6.685\,\mu$F	$C_{HI} = 15.04\,\mu$F
Transformer	$X_{TR} = 0.18$ pu	$X_{TI} = 0.18$ pu
DC line	$R_{DC} = 0.151\,\Omega$, $L_{DC} = 0.5968$ H, $C_{DC} = 26\,\mu$F	

TABLE A.16: Control system data

Controller	**PI gains**
Rectifier current controller	$K_P = 1.0989, T_I = 0.01092$ s
Inverter current controller	$K_P = 2.63, T_I = 0.01524$ s
Gamma controller	$K_P = 0.7506, T_I = 0.0544$ s

Appendix B

Dynamic Phasor Representation of a Transformer

The transformers are modelled using an equivalent circuit derived using the inductance matrix for two mutually coupled circuit (B.1) shown in Fig. B.1. It is derived using the same principles used in EMT simulations [1].

$$\begin{pmatrix} V_1 \\ V_2 \end{pmatrix} = \begin{pmatrix} L_{11} & L_{12} \\ L_{12} & L_{22} \end{pmatrix} \frac{d}{dt} \begin{pmatrix} I_1 \\ I_2 \end{pmatrix} \tag{B.1}$$

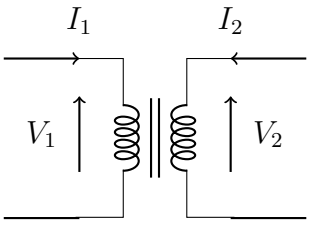

FIGURE B.1: Two mutually coupled coils of the transformer

$$\frac{d}{dt}\begin{pmatrix} I_1 \\ I_2 \end{pmatrix} = \frac{1}{L'}\begin{pmatrix} L_{22} & -L_{12} \\ -L_{12} & L_{11} \end{pmatrix}\begin{pmatrix} V_1 \\ V_2 \end{pmatrix} \tag{B.2}$$

$$L' = L_{11}L_{22} - L_{12}L_{12} \tag{B.3}$$

$$\frac{d}{dt}I_1 = \frac{L_{22}}{L'}V_1 - \frac{L_{12}}{L'}V_2 \tag{B.4}$$

Using the principle of dynamic phasors (B.4) can be written as,

$$\frac{d}{dt}I_1 = -j\omega I_1 + \frac{L_{22}}{L'}V_1 - \frac{L_{12}}{L'}V_2 \tag{B.5}$$

By applying Trapezoidal rule it can be shown that

$$I_1(t) = I_{1h} + k_{11}V_1(t) + k_{12}\left(V_1(t) - V_2(t)\right) \tag{B.6}$$

Where,

$$I_{1h} = \left(\frac{1 - \frac{j\omega_0\Delta t}{2}}{1 + \frac{j\omega_0\Delta t}{2}}\right) I_1(t-1) + k_{11}V_1(t-1) + k_{12}\left(V_1(t-1) - V_2(t-1)\right) \tag{B.7}$$

$$k_{11} = \frac{\frac{L_{22}\Delta t}{2L'} - \frac{L_{12}\Delta t}{2L'}}{1 + \frac{j\omega_0\Delta t}{2}} \tag{B.8}$$

$$k_{12} = \frac{\frac{L_{12}\Delta t}{2L'}}{1 + \frac{j\omega_0\Delta t}{2}} \tag{B.9}$$

Similarly we can derive the equation for the current in the second winding as,

$$I_2(t) = I_{2h} + k_{22}V_2(t) + k_{12}\left(V_2(t) - V_1(t)\right) \tag{B.10}$$

Where,

$$I_{2h} = \left(\frac{1 - \frac{j\omega_0\Delta t}{2}}{1 + \frac{j\omega_0\Delta t}{2}}\right) I_2(t-1) + k_{22}V_2(t-1) + k_{12}\left(V_2(t-1) - V_1(t-1)\right) \tag{B.11}$$

$$k_{22} = \frac{\frac{L_{11}\Delta t}{2L'} - \frac{L_{12}\Delta t}{2L'}}{1 + \frac{j\omega_0 \Delta t}{2}} \tag{B.12}$$

The Nortan equivalent for the transformer is given by Fig. B.2 and the terms k_{11}, k_{12} and k_{22} are the impedances and the terms I_{1h} and I_{2h} are controlled current sources which represent the history terms.

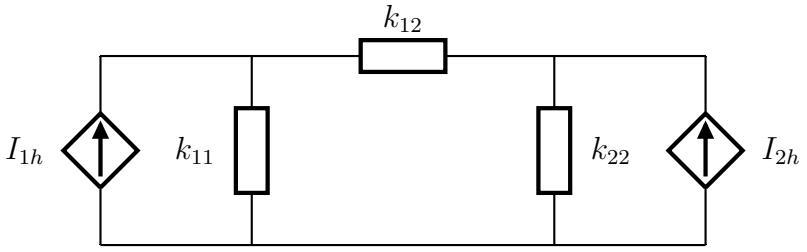

FIGURE B.2: Transfomer equivalent model

References

[1] Neville Watson and Jos Arrillaga. *Power Systems Electromagnetic Transients Simulation*. IET power and energy series 39. Institute of Engineering and Technology, London UK, 2003. ISBN 0852961065.

[2] P. Kundur, J. Paserba, V. Ajjarapu, G. Andersson, A. Bose, C. Canizares, N. Hatziargyriou, D. Hill, A. Stankovic, C. Taylor, T. Van Cutsem, and V. Vittal. Definition and classification of power system stability ieee/cigre joint task force on stability terms and definitions. *IEEE Transactions on Power Systems*, 19(3):1387–1401, Aug 2004. ISSN 0885-8950. doi: 10.1109/TPWRS.2004.825981.

[3] V. Venkatasubramanian, H. Schattler, and J. Zaborszky. Fast time-varying phasor analysis in the balanced three-phase large electric power system. *IEEE Transactions on Automatic Control*, 40(11):1975–1982, Nov 1995. ISSN 0018-9286. doi: 10.1109/9.471228.

[4] H. Schattler J. Zaborszky and V. Venkatasubramanian. Limitations of the quasistationary dynamics and error due to phasor computation in network equations. *in Proc. Power Systems Computations Conf.,*, pages 721–729, France, 1993.

[5] V. Venkatasubramanian, H. Schattler, and J. Zaborsky. Dynamics of large constrained nonlinear systems-a taxonomy theory [power system stability].

Proceedings of the IEEE, 83(11):1530–1561, Nov 1995. ISSN 0018-9219. doi: 10.1109/5.481633.

[6] Sebastian Henschel. *Analysis of electromagnetic and electromechanical power system transients with dynamic phasors*. PhD thesis, 1999. URL `https://open.library.ubc.ca/cIRcle/collections/831/items/1.0065161`.

[7] V. Venkatasubramanian. Tools for dynamic analysis of the general large power system using time-varying phasors. *International Journal of Electrical Power & Energy Systems*, 16(6):365 – 376, 1994. ISSN 0142-0615. doi: https://doi.org/10.1016/0142-0615(94)90023-X. URL `http://www.sciencedirect.com/science/article/pii/014206159490023X`.

[8] Chandana Karawita. *HVDC Interaction Studies Using Small Signal Stability Assessment*. PhD thesis, University of Manitoba, Canada, April 2009.

[9] TURHAN HILMI DEMIRAY. *Simulation of Power System Dynamics using Dynamic Phasor Models*. PhD thesis, SWISS FEDERAL INSTITUTE OF TECHNOLOGY ZURICH, 2008.

[10] S. R. Sanders, J. M. Noworolski, X. Z. Liu, and G. C. Verghese. Generalized averaging method for power conversion circuits. *IEEE Transactions on Power Electronics*, 6(2):251–259, Apr 1991. ISSN 0885-8993. doi: 10.1109/63.76811.

[11] A. M. Stankovic, S. R. Sanders, and T. Aydin. Dynamic phasors in modeling and analysis of unbalanced polyphase ac machines. *IEEE Transactions on Energy Conversion*, 17(1):107–113, Mar 2002. ISSN 0885-8969. doi: 10.1109/60.986446.

[12] A. M. Stankovic and T. Aydin. Analysis of asymmetrical faults in power systems using dynamic phasors. *IEEE Transactions on Power Systems*, 15 (3):1062–1068, Aug 2000. ISSN 0885-8950. doi: 10.1109/59.871734.

[13] J. Mahdavi, A. Emaadi, M. D. Bellar, and M. Ehsani. Analysis of power electronic converters using the generalized state-space averaging approach. *IEEE Transactions on Circuits and Systems I: Fundamental Theory and Applications*, 44(8):767–770, Aug 1997. ISSN 1057-7122. doi: 10.1109/81.611275.

[14] V. A. Caliskan, O. C. Verghese, and A. M. Stankovic. Multifrequency averaging of dc/dc converters. *IEEE Transactions on Power Electronics*, 14(1): 124–133, Jan 1999. ISSN 0885-8993. doi: 10.1109/63.737600.

[15] Matthew Alexander Kulasza. Generalized dynamic phasor-based simulation for power systems. Master's thesis, University of Manitoba, Canada, 2014.

[16] RTDS Technologies. Utilities keep the lights on with large scale power system simulation. 2014. URL `https://www.rtds.com/wp-content/uploads/2015/12/Large-scale-utility-simulators.pdf`.

[17] A. S. Morched, J. H. Ottevangers, and L. Marti. Multi-port frequency dependent network equivalents for the emtp. *IEEE Transactions on Power Delivery*, 8(3):1402–1412, July 1993. ISSN 0885-8977. doi: 10.1109/61.252667.

[18] N. R. Watson and J. Arrillaga. Frequency-dependent ac system equivalents for harmonic studies and transient convertor simulation. *IEEE Transactions on Power Delivery*, 3(3):1196–1203, July 1988. ISSN 0885-8977. doi: 10.1109/61.193903.

[19] V. Jalili-Marandi, V. Dinavahi, K. Strunz, J. A. Martinez, and A. Ramirez. Interfacing techniques for transient stability and electromagnetic transient programs ieee task force on interfacing techniques for simulation tools. *IEEE Transactions on Power Delivery*, 24(4):2385–2395, Oct 2009. ISSN 0885-8977. doi: 10.1109/TPWRD.2008.2002889.

[20] Y. Zhang, A. M. Gole, W. Wu, B. Zhang, and H. Sun. Development and analysis of applicability of a hybrid transient simulation platform combining tsa and emt elements. *IEEE Transactions on Power Systems*, 28(1):357–366, Feb 2013. ISSN 0885-8950. doi: 10.1109/TPWRS.2012.2196450.

[21] Hongtian Su, Ka Wing Chan, L. A. Snider, and Tak Shing Chung. A parallel implementation of electromagnetic electromechanical hybrid simulation protocol. In *2004 IEEE International Conference on Electric Utility Deregulation, Restructuring and Power Technologies. Proceedings*, volume 1, pages 151–155 Vol.1, April 2004. doi: 10.1109/DRPT.2004.1338484.

[22] Y. Zhang, A. M. Gole, W. Wu, B. Zhang, and H. Sun. Development and analysis of applicability of a hybrid transient simulation platform combining tsa and emt elements. *IEEE Transactions on Power Systems*, 28(1):357–366, Feb 2013. ISSN 0885-8950. doi: 10.1109/TPWRS.2012.2196450.

[23] Xi Lin. *System Equivalent for Real Time Digital Simulator*. PhD thesis, University of Manitoba, Canada, 2010.

[24] U.D. Annakkage, N.C. Nair, A.M. Gole, V. Dinavahi, T. Noda, G. Hassan, and A. Monti. Dynamic system equivalents: A survey of available techniques. In *Power Energy Society General Meeting, 2009. PES '09. IEEE*, pages 1–5, July 2009. doi: 10.1109/PES.2009.5275650.

[25] Yuefeng Liang. *An Improved Wide-Band System Equivalent Technique for Real Time Digital Simulators*. PhD thesis, University of Manitoba, Canada, 2011.

[26] Y. Hu, W. Wu, A. M. Gole, and B. Zhang. A guaranteed and efficient method to enforce passivity of frequency-dependent network equivalents. *IEEE Transactions on Power Systems*, 32(3):2455–2463, May 2017. ISSN 0885-8950. doi: 10.1109/TPWRS.2016.2611603.

[27] Y. Hu, W. Wu, and B. Zhang. A semidefinite programming model for passivity enforcement of frequency-dependent network equivalents. *IEEE Transactions on Power Delivery*, 31(1):397–399, Feb 2016. ISSN 0885-8977. doi: 10.1109/TPWRD.2015.2479403.

[28] J. Morales-Rodriguez, J. Mahseredjian, K. Sheshyekani, A. Ramirez, E. Medina, and I. Kocar. Pole-selective residue perturbation technique for passivity enforcement of fdnes. *IEEE Transactions on Power Delivery*, pages 1–1, 2018. ISSN 0885-8977. doi: 10.1109/TPWRD.2018.2810706.

[29] A. Thakallapelli and S. Kamalasadan. Optimization based real-time frequency dependent reduced order modeling of power grid. In *2017 IEEE Power Energy Society General Meeting*, pages 1–5, July 2017. doi: 10.1109/PESGM.2017.8273745.

[30] M. Abdel-Rahman, A. Semlyen, and M. Reza Iravani. Two-layer network equivalent for electromagnetic transients. *IEEE Transactions on Power Delivery*, 18(4):1328–1335, Oct 2003. ISSN 0885-8977. doi: 10.1109/TPWRD.2003.817749.

[31] Xin Nie, Yuan Chen, and Venkata Dinavahi. Real-time transient simulation based on a robust two layer network equivalent. In *2008 IEEE Power and Energy Society General Meeting - Conversion and Delivery of Electrical Energy in the 21st Century*, pages 1–1, July 2008. doi: 10.1109/PES.2008.4595974.

[32] D. Shu, X. Xie, V. Dinavahi, C. Zhang, X. Ye, and Q. Jiang. Dynamic phasor based interface model for emt and transient stability hybrid simulations. *IEEE Transactions on Power Systems*, 33(4):3930–3939, July 2018. ISSN 0885-8950. doi: 10.1109/TPWRS.2017.2766269.

[33] B.C. Pal and B. Chaudhuri. *Robust Control in Power Systems*. New York, Springer-Verlag. 2005.

[34] C L DeMarco and Verghese G C. Bringing phasor dynamics into the power system load flow. *Proc. North American Power Symposium*, 1993. ISSN 0142-0615.

[35] P. Zhang, J. R. Marti, and H. W. Dommel. Synchronous machine modeling based on shifted frequency analysis. *IEEE Transactions on Power Systems*, 22(3):1139–1147, Aug 2007. ISSN 0885-8950. doi: 10.1109/TPWRS.2007.901288.

[36] P. Zhang, J. R. Marti, and H. W. Dommel. Shifted-frequency analysis for emtp simulation of power-system dynamics. *IEEE Transactions on Circuits and Systems I: Regular Papers*, 57(9):2564–2574, Sept 2010. ISSN 1549-8328. doi: 10.1109/TCSI.2010.2043992.

[37] P. Kundur. *Power system stability and control*. EPRI power system engineering series. McGraw-Hill, 1994. ISBN 9780070359581.

[38] H. Konara, U. D. Annakkage, and C. Karawita. Stability criterion for interfacing a transient stability model to a dynamic phasor model. In *2018 IEEE/PES Transmission and Distribution Conference and Exposition (T D)*, pages 1–5, April 2018. doi: 10.1109/TDC.2018.8440345.

[39] H. Konara, U. D. Annakkage, and C. Karawita. Novel voltage source type synchronous machine model for nodal analysis based simulations. In *Accepted to be published in 2019 The International Conference on Power Systems Transients (IPST)*, pages 1–5, June 2019.

[40] A. M. Gole, R. W. Menzies, H. M. Turanli, and D. A. Woodford. Improved interfacing of electrical machine models to electromagnetic transients programs. *IEEE Power Engineering Review*, PER-4(9):56–57, Sept 1984. ISSN 0272-1724. doi: 10.1109/MPER.1984.5525823.

[41] L. Wang and J. Jatskevich. A voltage-behind-reactance synchronous machine model for the emtp-type solution. In *2007 IEEE Power Engineering Society General Meeting*, pages 1–1, June 2007. doi: 10.1109/PES.2007.385684.

[42] M. Rafian and M. A. Laughton. Determination of synchronous-machine phase-co-ordinate parameters. *Electrical Engineers, Proceedings of the Institution of*, 123(8):818–824, August 1976. ISSN 0020-3270. doi: 10.1049/piee.1976.0176.

[43] Vladimir Brandwajn. *Synchronous generator models for the analysis of electromagnetic transients*. PhD thesis, University of British Columbia, Canada, April 1977.

[44] H. K. Lauw and W. S. Meyer. Universal machine modeling for the representation of rotating electric machinery in an electromagnetic transients program. *IEEE Transactions on Power Apparatus and Systems*, PAS-101(6):1342–1351, June 1982. ISSN 0018-9510. doi: 10.1109/TPAS.1982.317181.

[45] P. Subramaniam and O. P. Malik. Digital simulation of a synchronous generator in direct-phase quantities. *Electrical Engineers, Proceedings of the Institution of*, 118(1):153–160, January 1971. ISSN 0020-3270. doi: 10.1049/piee.1971.0024.

[46] M. Chapariha, F. Therrien, J. Jatskevich, and H. Dommel. Explicit formulations for constant-parameter voltage-behind-reactance interfacing of synchronous machine models. In *2014 IEEE PES General Meeting — Conference Exposition*, pages 1–1, July 2014. doi: 10.1109/PESGM.2014.6939340.

[47] Chung Wen Ho, A. Ruehli, and P. Brennan. The modified nodal approach to network analysis. *IEEE Transactions on Circuits and Systems*, 22(6):504–509, June 1975. ISSN 0098-4094. doi: 10.1109/TCS.1975.1084079.

[48] H. Konara, U. D. Annakkage, and C. Karawita. Real-time co-simulation model using electromagnetic transient and dynamic phasor simulations. *CIGRE Science & Engineering (CSE) Journal*, June 2019.

[49] Harshani Konara. Interfacing dynamic phasor based system equivalents to an electromagnetic transient simulation. Master's thesis, University of Manitoba, Canada, 2015.

[50] W. Ren, M. Steurer, and T. L. Baldwin. Improve the stability and the accuracy of power hardware-in-the-loop simulation by selecting appropriate interface algorithms. *IEEE Transactions on Industry Applications*, 44(4):1286–1294, July 2008. ISSN 0093-9994. doi: 10.1109/TIA.2008.926240.

[51] Seaseung Oh and Suyong Chae. A Co-Simulation Framework for Power System Analysis. February 2016. doi: 10.3390/en9030131.

[52] K. Mudunkotuwa, S. Filizadeh, and U. Annakkage. Development of a hybrid simulator by interfacing dynamic phasors with electromagnetic transient simulation. *IET Generation, Transmission Distribution*, 11(12):2991–3001, 2017. ISSN 1751-8687. doi: 10.1049/iet-gtd.2016.1616.

[53] M. Abramowitz and I. A. Stegun. *Handbook of Mathematical Functions with Formulas, Graphs, and Mathematical Tables,*. New York: Dover, 1972.

[54] Carl De Boor. *A Practical Guide to Splines*. New York: Springer-Verlag. New York: Springer-Verlag, 1978. ISBN 978-0387953663.

[55] Xuegong Wang, P. Wilson, and D. Woodford. Interfacing transient stability program to emtdc program. In *Power System Technology, 2002. Proceedings. PowerCon 2002. International Conference on*, volume 2, pages 1264–1269 vol.2, 2002. doi: 10.1109/ICPST.2002.1047605.

[56] L. A. Snider H. Su, K. W. Chan and J-C. Soumagne. Advancements on the integration of electromagnetic transients simulator and transient stability simulator. In *International Conference on Power Systems Transients Montreal*, January 2005.

[57] M. Szechtman, T. Wess, and C. V. Thio. First benchmark model for hvdc control studies. In *Electra*, volume No. 135, pages 154–67, Apr 1991.

[58] IEEE recommended practice and requirements for harmonic control in electric power systems. *IEEE Std 519-2014 (Revision of IEEE Std 519-1992)*, pages 1–29, June 2014. doi: 10.1109/IEEESTD.2014.6826459.

[59] P. Zadkhast, Xi Lin, B. Ko, and K. Hur. Practical challenges of hybrid interfacing with real-time digital simulators. In *The International Conference on Power Systems Transients (IPST)*, pages 1–5, June 2019.

[60] Harshani Konara, U. D. Annakkage, and C. Karawita. Synchronous machine models for dynamic phasor simulations. In *CIGRE Canada Conference*, October 2018.

[61] H. Konara, U. D. Annakkage, and C. Karawita. Interfacing electromagnetic transient simulation to transient stability model using a multi-port dynamic phasor buffer zone. *CIGRE Science & Engineering (CSE) Journal*, October 2019.